GLOBAL DECONVOLUTION OF HETEROTROPIC COOPERATIVITY IN CYTOCHROME P450 3A4

BY

DANIEL JACOB FRANK

DISSERTATION

Submitted in partial fulfillment of the requirements
for the degree of Doctor of Philosophy in Biochemistry
in the Graduate College of the
University of Illinois at Urbana-Champaign, 2011

Urbana, Illinois

Doctoral Committee:

Professor Stephen Sligar, Chair
Professor Robert Clegg
Professor Rutilio Fratti
Professor John Gerlt

ABSTRACT

Cytochrome P450 3A4 (CYP3A4) plays a central role in xenobiotic metabolism, and is of critical importance to both human health and the pharmaceutical industry. Its ability to interact with multiple molecules of the same substrate, or multiple substrates, leads to complex non-Michaelis kinetics, called “homotropic” and “heterotropic” cooperativity respectively. Significant progress has been made towards understanding the enzyme’s complex kinetics by work in our laboratory to isolate the enzyme in Nanodiscs. This provides a homogenous, monodisperse, native-like environment, where the monomeric enzyme is biophysically characterized in the absence of detergent micellar mixtures or liposomal systems which are reported to lead to enzyme heterogeneity and obfuscate its kinetic behavior.

Three distinct observable properties which CYP3A4 displays as a result of its reaction cycle are: heme iron spin state, NADPH oxidation rate, and product formation rate. Measuring these three observables as a function of substrate concentration and simultaneously fitting the data sets to a model results in a global analysis of the enzyme’s properties. It reveals the source of homotropic atypical kinetics is not due to any binding cooperativity between the substrates, but rather differences in magnitude of the functional properties from the various enzyme-substrate complexes in solution.

To extend this analysis to better understand heterotropic interactions in the system, we generate an interaction surface based upon the linear combination of two substrates kinetic profiles, which corresponds to the absence of any specific heterotropic interactions between them. By comparing the observed behavior of the

mixed substrate system to that of the model, we show how two commonly reported heterotropic substrates of CYP3A4 are actually not cooperative, and the observed cooperativity is due to differences in the amplitudes of the functional properties from the various binding intermediates in the system which give rise to the overall observed behavior of the enzyme.

To Mom and Dad

ACKNOWLEDGEMENTS

The work represented in this thesis would not have been possible without the support of many individuals. It begins with my advisor, Dr. Stephen Sligar, who is an inspirational scientist and team leader, and fosters a collaborative and friendly environment in his laboratory. The “hemeteam” as we have come to call ourselves includes Dr. Ilia Denisov, whose intellectual curiosity is the driving force behind a brilliant and dedicated scientist, Drs. Mark McLean, Tim Bayburt and Aditi Das, whose years of experience helped me to overcome numerous scientific obstacles, and Yelena Grinkova, one of the most skilled experimentalists I have ever had the pleasure of working with, and whose attention to detail is unsurpassed. Former graduate students in the lab, Dr. Andrew Shaw, Dr. Na Ke, Dr. Amy Shih, and most importantly Dr. Brad Baas helped pave the way for my work, while my current peers, especially Mike Gregory and Abhinav Luthra, have made the laboratory a fun and exciting place to be. Many thanks go to Aretta Weber and Shawna Smith for all of their help and guidance, as well as Dr. Keith Westcott.

My interest in science was launched by Dr. Thomas and Mr. Ward, the two science teachers at my high school who ran the original science research program. Without them I doubt I would have ever followed this path, which took me through several laboratories before I ended up with Drs. Anne Davidson and Betty Diamond in New York. It was in their laboratories that I honed the research skills, primarily under the tutelage of Dr. Davidson and her talented postdoc Dr. Meera Ramanujam, which helped me to be successful here in graduate school.

This experience would not have been as enriching without my friends in Champaign and Chicago. Paul and An made me feel like Chicago was a home away from home, while countless friends here (Aidas and Daina, Beth and Nick, Amy and George, Kieran, Brian, Quinn, Fiona and Poe, John and Jessica, McKay, Bill, Jennifer, Daiva, Ben and many others) joined me in brewing, poker nights, a marrow drive, a softball team, and journal club. Thank you to my friends at The Point Fencing Club who kept me 'on guard.' While my friends away from here, particularly Tim, Damien, Levy, Fred, T, and Korak, were always there to pick me up when I was down (and knock me down a peg when I got too high).

Most importantly, I need to thank my family, for without their love and support I would not be anywhere close to where I am today. Thanks go to my Nana and Grandpa, whose doors are always open in Milwaukee (and whose chocolate chip cookies fueled all nighters), and to my loving sister, Rachel, and brother, Adam. I could not have had better siblings to share my life with. Mom and Dad, I cannot thank you enough for everything you have given me. Your patience and guidance has served me well, and I am so grateful to have had grown up with your love and care.

Lastly, to anyone I have not specifically named thank you for your help and support as well.

TABLE OF CONTENTS

CHAPTER ONE: INTRODUCTION

1.1 Cytochrome P450 Monoxygenases: Discovery and Nomenclature

Cytochrome P450 monoxygenases represent a diverse superfamily of heme enzymes observed in all kingdoms of life. Discovered by Garfinkel and Klingeneberg in 1958 (*1-2*) who isolated a novel pigment with a large absorbance peak at 450 nm when reduced with sodium hydrosulfite and saturated with carbon monoxide while studying rat and pig liver pigments. The pigment was further isolated and quantitatively characterized by Omura and Sato (*3-4*), leading to the discovery of a new superfamily of enzymes now known as the cytochromes P450. The cytochrome P450 mechanism utilizes atmospheric oxygen two electrons from NAD(P)H and two protons from the solvent water to from the active ferryl-oxo intermediate, termed compound I.

The number of cytochromes P450 has grown exponentially as genome sequencing has become more common. As of Febrauary 2011 over 12,500 sequences have been identified encompassing over 950 families and over 2500 subfamilies. Cytochromes P450 are divided into families and subfamilies based on primary amino acid sequence identity (*5-10*). Families share 40% amino acid identity denoted by the first number. The following letter denotes the subfamily designation and a 55% amino acid identity between members. The subfamilies are then broken down into individual loci represented by a second number (*5-6*).

The number of cytochromes P450 identified in various organisms' genomes varies widely. In the single-celled photosynthetic organism *Chlamydomonas* there are 41 putative cytochrome P450 genes, 20 in the microbe *Mycobacterium tuberculosis*, 57 in *Homo sapiens* (human), 90 in *Drosophilia meloganster* (fruit fly), 103 in *Mus musculus* (mouse), and 83 in *Caenorhabditis elegans* (roundworm) (*11-13*). Higher plants generally have a larger number of cytochrome P450 genes – for example, there are 289 identified P450 genes in *Arabidopsis thaliana* and 182 in *Carica papaya* (papaya) (*8, 14 , 15*).

1.2 General Structure and Function of Cytochromes P450

All cytochromes P450, whether soluble or membrane associated, contain one heme b (protoporphyrin IX) buried within protein globule which is coordinated with the thiolate sulfur atom of cysteine as the fifth axial ligand. The protein globule, which ranges between 45-60 kDa and shares a common P450 fold across the members of the superfamily (*16*). The helices are labeled A through L, though some isozymes have the additional B', F', G', J' and K' helices, see figure 1.1. The loop at the N-terminus of the L-helix contains the absolutely conserved cysteine which serves as the ligand for the heme iron. Amide groups from three highly conserved neighboring residues serve to form hydrogen bonds with the sulfur atom, which raise the redox potential of the cytochrome P450 into the accessible physiological range for the NAD(P)H reductant. This leads to the most characteristic P450 consensus sequence, Phe-X-XGly-X-Arg-X-Cys-X-Gly, in the heme binding loop (*17*). The other conserved sequence in the I helix,

Ala/Gly-Gly-X-Asp/Glu-Thr-Thr/Ser, forms a kink in the helical structure which is believed to position side-chains to stabilize water molecules that are involved in proton delivery during the formation of Compound 0 and Compound I (*18*). The other conserved Glu-X-X-Arg motif located in the K helix likely helps form the core structure (*17*). Helices B, B', F, F', G' and G, along with their connecting loops are involved in substrate binding and are generally more flexible, and vary in length depending upon the isozyme. Comparison of X-ray structures with and without substrate bound have shown these helices undergo large scale conformational changes to accommodate substrate binding, as first observed using a modified substrate in CYP101 to trap the (P450cam) 'open' state (*19*).

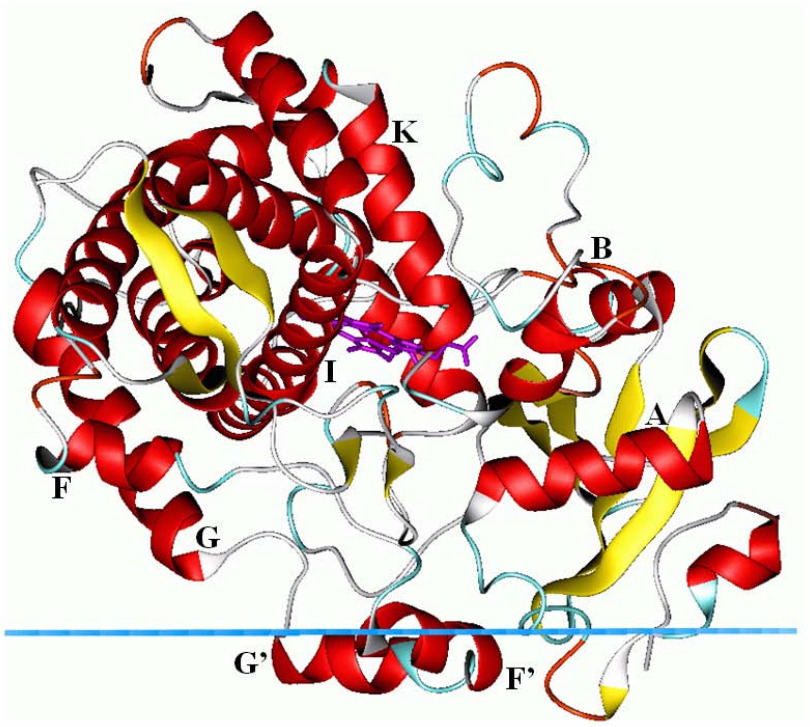

Figure 1.1 Crystal Structure of CYP3A4. The heme is shown in purple, the helices in red, and the membrane bilayer is represented by the blue line.

Cytochromes P450 can generally be divided into performing one of two physiological roles: metabolic synthesis of important biological molecules and the catabolic breakdown of xenobiotics. Single celled microbes such as bacteria and archaea use the cytochromes P450 to adapt to their environment and to manufacture signaling molecules. Most multicellular organisms use them for cellular signaling and some for manufacturing toxins as a defense (*14, 20*), while some use them to metabolize these toxins, and other toxins encountered in the environment (*14, 21-22*).

Cytochromes P450 are ubiquitous because they are able to catalyze many diverse reactions, diagramed in figure 1.2. Secondary structural elements with a common protein fold facilitate a diverse set of chemical reactions on a wide range of substrates by changing the substrate recognition event (*16*). The most commonly studied reaction of cytochromes P450 is substrate hydroxylation, which was been studied extensively in CYP101A1 (*23-25*). Other reactions performed by the superfamily include dealkylation, epoxidation, dehydrogenation, carbon-carbon (C-C) bond cleavage (*26-27*).

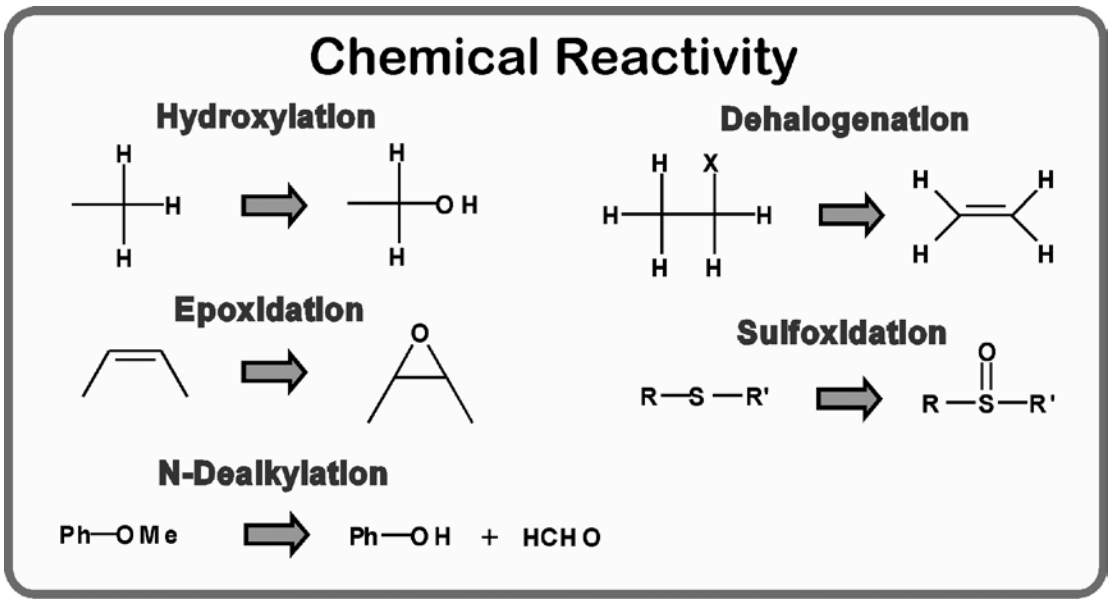

Figure 1.2 Chemical Reactions of Cytochromes P450. Adapted from Makris et al. 2004

1.3 Cytochrome P450 Reduction Mechanism

There are two main classes of cytochromes P450, the first accepts electrons from an iron-sulfur protein, which in turn receives the electrons from a partnering flavin-containing reductase protein. The reductase protein utilizes NAD(P)H to receive two electrons and transfer them to the ferrodoxin in two one electron transfers. The second class of cytochromes P450 consist of a single diflavin-containing reductase protein that contains both an FMN and a FAD domain, which can shuttle electrons between NADPH and the heme iron of the P450 for substrate metabolism through a cyclical quinone and semi-quinone transfer (*28-29*). These cytochromes P450 are usually membrane associated, as are their reductase redox partners.

There are several cytochromes P450 that do not fit into either class using reducing equivalents from NADPH, NADH or pyruvic acid. CYP102 (P450 BM-3) is a soluble isozyme from *Bacillus megaterium* which catalyzes a hydroxylation of fatty acids at several non-terminal positions (*30*-*33*). This P450 has been shown to catalyze fatty acid hydroxylations at a rate up to 15000 min^{-1} (*34*). The enzyme contains both a heme domain similar to those found in other cytochromes P450, and a reductase domain that is similar to an FMN and FAD containing reductase, utilized by the second class enzymes. These two domains are fused together though a small peptide linker (*35*). Recent studies have shown that the reductase domain by itself, expressed recombinantly, retains its ability to interact with and reduce other class 2 enzymes such CYP3A4, although more slowly than their native reductase redox partner (*36*-*37*).

Several other cytochrome P450 classes exist catalyzing a variety of reactions using an assortment of reducing equivalents. Cytochrome P450 RhF from *Rhodococcus sphaeroides* is an example of a class comprised of a fusion of three domains, an iron sulfur protein (similar to class 1) and an FMN reductase domain that utilizes NADH for its electrons (*38*-*39*). In another class the enzyme can directly utilize reducing equivalents from NADH in solution, without the need for accessory proteins. An example is cytochrome P450nor from *Fusarium oxysporum*, which catalyzes the conversion of nitric oxide to nitrous oxide (*40*). Another example is cytochrome P450 119A2, from a thermoacidophilic crenarchaeon, which can catalyze styrene epoxidation using NADH or NADPH as an electron donor in the absence of a redox partner (*41*). Additionally, CYP119 has been isolated from *Sulfolobus solfataricus*, and this enzyme can use pyruvic acid as the reducing equivalents, which are shuttled through the redox

partner and metabolizing substrate such as lauric acid (*42*). It was using this isozyme that the highly reactive Compound I state of the reactive cycle was first observed (*43-44*), which will be discussed in the following section.

Additionally, a reconstituted *in vitro* system has been developed to perform light driven P450 reactions using photosystem I to generate reducing equivalents and ferredoxin as the electron carrier to cytochrome P450 79A1 (*45*). Although this is not a naturally occurring system, the use of light to substitute for NAD(P)H offers an alternative approach for the *in vitro* synthesis of bioactive compounds.

1.4 The P450 Reaction Cycle

Cytochromes P450 progress through a common catalytic cycle to activate molecular oxygen and incorporate a single oxygen atom into their substrates, as detailed in the figure 1.3 below (*46*). Beginning in the resting state at the top of the figure the enzyme has a water molecule bound at the sixth coordination position, and the ferric heme is in the low spin state (the five d-shell electrons in the S=1/2 configuration). Binding of the substrate perturbs the ligand field, displacing the water molecule, and results in a re-configuration of the d-shell electrons to a high spin (S=5/2) state. This produces the observable Type-I spectral change. This is followed by the delivery of an electron, causing the reduction of the heme iron to the ferrous state, through one of mechanisms described in section 1.3. Next, oxygen binds to the ferrous heme forming the ferrous-dioxygen adduct. This intermediate may autoxidize releasing superoxide and regenerating the ferric protein. Otherwise, a second electron is

delivered forming a heme bound peroxo anion, and is followed by the delivery of a proton forming the hydroperoxo intermediate. "Compound 0" (Cpd 0) may refer to either the protonated or unprotonated iron-peroxo complex. This intermediate serves as a branch point for either the non-productive release of peroxide or the delivery of a second proton to the distal oxygen. The delivery of the second proton causes O-O bond scission and results in the release of water and the formation of the higher valent ferryl-oxy complex, with a pi-cation radical on the porphyrin; referred to as "Compound I" (Cpd I) or the ferryl-oxo state. Cpd I can transfer the oxygen atom to the bound substrate, or undergo a further two electron reduction, leading to the formation of a second water molecule. Dissociation of the product returns the enzyme to the ferric resting state completing the cycle.

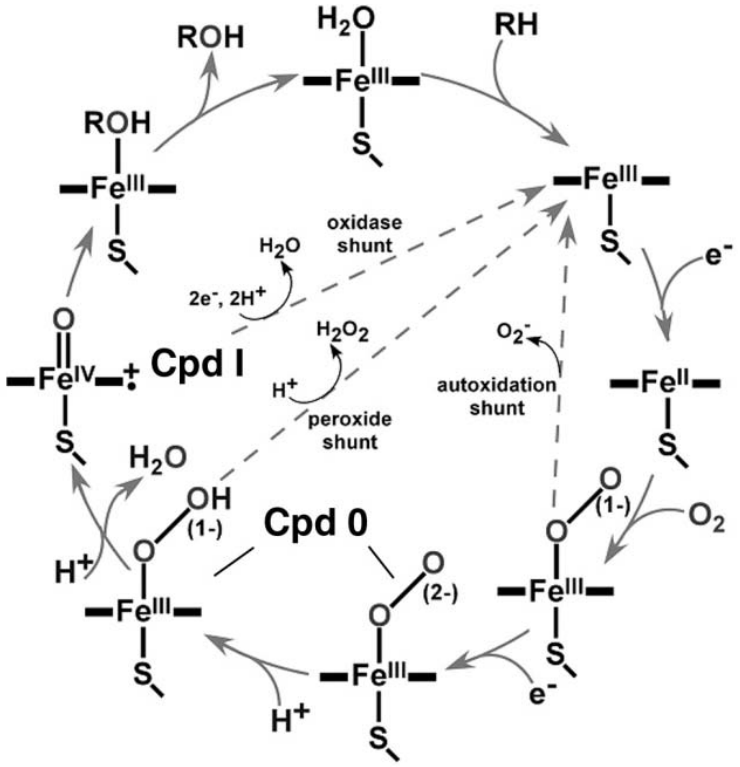

Figure 1.3 The Cytochrome P450 Reaction Cycle. Adapted from Denisov et al. 2005.

1.5 Human Cytochromes P450

There are 57 known cytochromes P450 in the human, though others may be present due to alternate splicing events (*11, 21*). Cytochromes P450 are responsible for several key aspects of human homeostasis including both anabolic and catabolic metabolism. The metabolism of drugs, vitamin A, steroids, fatty acids, and prostaglandins, are all pathways which include cytochromes P450. Human cytochromes P450 are usually located in the endoplasmic reticulum or the mitochondria of the target tissue, such as the liver, lungs, brain, or reproductive tissues (*21*).

1.5.1 Drug Metabolizing Cytochromes P450

There are eleven major drug metabolizing cytochromes P450 in the adult human body. All are promiscuous enzymes with broad substrate specificity which leads to some overlap in substrates between the isozymes (*47*). Their prominent role in drug metabolism leads to several different considerations during pharmaceutical development. The expression levels of cytochromes P450 in the liver vary dramatically among populations. For the main hepatic drug metabolizing enzymes, which include 1A2, 2A6, 2B6, 2C9 2D6, 2E1, and 3A4, the difference can be as much as 0.43 nmol of P450 per mg of liver protein in Caucasians versus 0.26 nmol of P450 per mg of liver protein in the Japanese potentially resulting in these populations having different metabolic profiles for specific drugs (*48*).

Another aspect of human drug clearance is the differential hepatic cytochromes P450 allelic variation and genetic polymorphisms. In the late 1950s and early 1960s clinicians coined terms for individuals who were out of the norm for metabolizing the

pharmaceuticals: poor, extensive, and ultra metabolizers (*49-51*). As the drug metabolizing cytochromes P450 became better understood, it was discovered that these categories stem mostly from genetic variation in cytochrome P450 genes. The common problems found in Poor Metabolizers include frame shifts, single nucleotide deletions, and mRNA misplicing events (*50, 52-53*). Among Northern Europeans, 97% of Poor Metabolizers can be traced to four allelic variations in different classes of cytochromes P450 (*54-57*). The Ultra Metabolizer category is due mostly to gene duplication of specific cytochromes P450 (*58*), but it may also be caused by defective regulatory control of gene transcription (*21*).

Other aspects of human cytochromes P450 are the toxicology and cancer risks associated with the bioactivation of potentially harmful compounds and their precursors. Acetaminophen and the insecticide parathion have been shown to be bioactivated by cytochromes P450 (*59-61*), which leads to liver toxicity and poisoning.

There is a well-established link between glaucoma and a truncated form of CYP1B1 (*62*), though the reason is still uncertain. Other links between hepatic P450s and disease, such as CYP1A2 and colon cancer (*63*) and between CYP2A6 and lung cancer (*64*). Some of these are simply the bioactivation of environmental chemicals that lead to cytotoxicity and DNA damage. The differential expression of P450s can lead to individual sensitivity to different chemicals and environmental factors, providing a further level of complexity to the toxicological role played by these enzymes (*65*).

An important factor in the role of the human drug metabolizing cytochromes P450 is the broad substrate set that they may recognize and metabolize. This lack of

substrate specificity allows for a variety of substrates to bind and be metabolized by any given cytochrome P450, and the same substrate can be metabolized by multiple isozymes of cytochrome P450 (*47, 66*). Drug metabolizing enzymes, which reside mainly in the liver and kidney, can be responsible for drug-drug interactions or other side effects, sometimes to leading the removal of an efficacious compound from the market due to toxic metabolites (*67-69*). These enzymes are of critical importance to pharmaceutical companies, as an understanding of the complex metabolites of these enzymes can mean the difference between the success and failure of a given drug, and millions of dollars. The study of drug metabolizing enzymes and how they function was in part of the motivation behind the work described in this thesis.

1.5.2 Cytochrome P450 3A4

CYP3A4 is the key drug metabolizing enzyme in the human liver, although it is also found in the small intestine, lungs, brain, stomach and colon (*21*). CYP3A4 accounts for as much as 25-30% of the total cytochrome P450 in the liver (*70*), and in specific cases can increase to as much as 60% of the total P450 population (*71*). In other tissues, such as the small intestine, CYP3A4 can account for around 60% of the P450 population (*71-72*). CYP3A4 is expressed primarily in adults, while in fetal tissues the isozyme CYP3A7 predominates and little CYP3A4 is expressed (*73*). The expression of CYP3A4 is 50% compared to that of adults within 6 to 12 months after birth. There are also no known gender differences in the expression of CYP3A4 (*48*).

The *CYP3A4* gene is located on chromosome 7q22.1 (*74*) and was originally found to be inducible by multiple different classes of pharmaceuticals, including barbiturates and macrolide antibiotics (*75*); but there was limited direct correlation of

action (*76-78*). More recently studies have linked *CYP3A4* expression to PXR, a steroid family receptor. This receptor has been shown to activate *CYP3A4* transcription and the production of *CYP3A4* mRNA (*79-80*). The vitamin D receptor class has been shown to downregulate the transcription of *CYP3A4* (*81*), as has ketoconazole, a common antifungal drug (*82*). It is interesting to note that ketoconazole also specifically inhibits CYP3A4 protein by ligating the heme iron, leading to several competing mechanisms for ketoconazole inhibition (*83*). Other pharmaceuticals that inhibit the transcription of *CYP3A4* include erythromycin and other amine antibiotics (*84*).

Once CYP3A4 is translated and has metabolized substrates, it is targeted for destruction by specific phosphorylations at Thr264 and Ser420 by protein kinase C (*85*). The first step to the ubiqutination pathway and final destruction of the enzyme, and is thought to target CYP3A4 to a proteasome for degradation (*86*). However, this pathway remains to be fully elucidated.

CYP3A4 is known to metabolize almost 50% of the pharmaceuticals on the market today (*87*). The diversity of substrate specificity for CYP3A4 is so great that it has not only substrates, but also classes of known inducers and inhibitors (*88*). Examples of inducers include St. John's wort, barbiturates, rifampin, and carbamazepine, all of which stimulate the metabolic rates of other substrates (*88*). Inhibitors of CYP3A4 include indinavir, saquinavir, ciprofloxacin, erythromycin, gestodene, verapamil, and fluconazole (*78, 88*). For a comprehensive list of CYP3A4 substrates, inhibitors, and inducers (a list which includes >1000 substrates and chemical reactivities for CYP3A4, as well as the other xenobiotic metabolizing cytochromes P450) refer to Rendic's 2002 review (*88*). These classes of drugs include

HIV anti-retrovirals, cholesterol lowering drugs (statins), antifungals (azoles), antibiotics (erythromycin), and dietary supplements (St. John 's wort). From the number of potential interactions it is clear why a detailed understanding of this enzyme is important (*78, 89*).

CYP3A4 was first studied as a mixture with other cytochromes P450 using liver microsomes, which were known to metabolize many endogenous and xenobiotic compounds (*90-94*). When studying the pharmacological effects of CYP3A4 from liver tissue *in vitro*, there is always the concern that the effects seen could be caused by one of the other ten P450 isozymes in the liver. While CYP3A4 is the major enzyme in liver tissue, studies have also shown these enzymes to be cross reactive (*95-97*). For any given substrate, there are often two or possibly three isozymes that can metabolize it at various positions (*98*). While liver microsomes yield insights about metabolism on a physiological level, it only provides a limited understanding of the function of any individual P450. The advent of recombinant DNA technologies has allowed for the expression of a single cytochrome P450 in an organism for study. With CYP3A4, this was first accomplished with a full-length CYP3A4 gene expressed in *Saccharomyces cerevisiae* (*99*). This led to the expression of a truncated but fully functional version of CYP3A4 and many other P450s in *Escherichia coli* (*100*).

Some of the greatest hindrances to the biophysical characterization of recombinantly expressed CYP3A4 arise from the variability in reconstitution conditions. Imaoka and colleagues first showed that catalytic rates of testosterone hydroxylation change as a function of phospholipid constituents (*101*). This was further complicated by the work of several laboratories, including Guengerich, Estabrook, and Halpert,

which showed drastically different catalytic rates depending on several variables: the buffer used (HEPES, KPi, Tris-HCl), the salts (divalent metal ions) and phospholipids added (phosphatidylcholine versus phosphatidylserine), the saturation of the phospholipids (saturated, single unsaturated, or double unsaturated), the detergents used (CHAPS, cholate, Emulgen 911 or 913), the presence or absence of auxiliary proteins (cytochrome b_5) and the order in which the reconstitution components are added (*102-116*). This is still a problem with the biophysical characterization of CYP3A4 as there is no standardized optimal set of conditions under which this enzyme is usually studied.

CYP3A4's *in vitro* parameters have widely been examined including many detailed studies of individual reaction steps in the catalytic cycle (*70, 117-120*) and shown to be complex (*118, 121-123*). It demonstrates both heterotropic and homotropic cooperativity, which can manifest as both positive and negative cooperativity (*78*). Differing metabolic profiles have been shown with varying substrate pairs, such as testosterone or progesterone in the presence of α-naphthoflavone (*124*). The testosterone and progesterone change the metabolic profile, altering the ratio of the main metabolite to minor metabolites when α-naphthoflavone is added to the reaction mixture. This is thought to be due to the differential binding of multiple substrates in one large active site and a different presentation of the substrate to the reactive oxygen intermediate (*124*). Studies of active site accommodation by several methods, including X-ray crystal structures (*125-126*), NMR relaxation (*127-128*), eximer fluorescence (*129*), and the simultaneous analysis of multiple data sets (*130-131*) show that the CYP3A4 active site can accommodate at least two, and possibly three, substrates at

any given time. However, the use of non-homogeneous systems may lead to some of these complex behaviors. Multiple sources claim there are several nonequivalent populations of CYP3A4 in a reconstituted system (*121, 132-133*).

1.6 Methods for the Characterization of Membrane Associated Proteins

Appropriate experimental methods are necessary in the biophysical and biochemical studies of a membrane associated enzyme, especially to ease the spectroscopic analysis of measured thermodynamic and catalytic parameters, and prevent aggregation. In order to increase the signal to noise ratio, the sample is rendered soluble for study. Options include membrane preparations, detergent solubilization liposomal systems, and Nanodiscs (*134-136*). Each of these methods has its own advantages and drawbacks and have helped to elucidate the behavior of CYP3A4.

A whole cell membrane suspension may be used when first trying to biophysically characterize a target protein. This furnishes a phospholipid bilayer with unknown lipid constituents to aid in the stabilization of the enzyme under study. Studies performed on whole cell membrane suspensions yield knowledge about the reactions that can be catalyzed by the enzyme of interest and limit the use of detergents, which may disrupt the molecular recognition events that are critical for proper enzyme function. The membrane suspensions are of particular use if it is not necessary to examine the fully purified protein. This methodology can lead to cross-reactivity of the measured catalytic reaction, making this type of measurement possibly unreliable, as

another enzyme or cross-reactivity may be present. Many studies of CYP3A4 performed using liver microsomes have led to novel insights into the catalytic mechanism of CYP3A4 (*90, 137*). The downside to this type of investigation lies in the presence of multiple cytochrome P450 isoforms in these tissue samples (*48, 138-139*). Another complicating factor is the size of these microsomes, as well as the complications for spectroscopic analysis that are associated with light scattering.

Detergent solubilization systems have been very useful in the biophysical characterization of cytochromes P450. Detergents that have been commonly used to study CYP3A4 include CHAPS, Emulgen 911 and 913, Triton X-100, and cholate. When using detergents in the solubilization of cytochromes P450, care must be taken to ensure that the detergent used does not change the activity of the enzyme. It has been shown that several of the detergents commonly used in the study of substrate binding and catabolic reactions are themselves substrates of CYP3A4 (*140*). In spite of these drawbacks, the use of detergents as a solubilization system has several advantages, such as the ease of enzyme preparation and the ability to study a purified sample that has decreased light scattering due to the smaller particle size. However, the actual size of the particles is usually in question, as the detergents form unknown micellar structures around the target enzyme, so the actual enzyme structure may not be the same as in a natural phospholipid bilayer. This can lead to complications in the understanding of the chemical mechanism or biophysical characterization of membrane associated proteins (*78, 102, 108, 141*). There are also concerns that there may be unknown oligomeric structures of enzymes that may play a role in conformational heterogeneity (*132-133*).

Unilamellar vesicle systems has been of great use in the study of cytochromes P450, for they have been shown to greatly enhance the metabolic rates of P450s when complexed with their redox partner (*141*). Unilamellar vesicles consist of a single phospholipid bilayer into which the enzyme is incorporated through vesicle extrusion, sonication, or detergent dialysis (*141-142*). Large unilamellar vesicles (LUVs) are 100 nm or more in diameter, and are produced by vesicle extrusion or detergent dialysis, while sonication produces small unilamellar vesicles (SUVs), which are 25 - 50 nm in diameter. The difficulty with these systems arises when attempting to understand the higher-order structures of the enzyme components, or when there is any domain formation or domain capping of these enzymes in the unilamellar vesicles. Due to their size, the vesicle systems usually give rise to light scattering events that can obstruct the measured spectroscopic parameters. A further complication that arises when incorporating a protein into vesicle systems is the statistical chance that the enzyme may be incorporated into the lumenal side of the vesicle, thus obstructing it from bulk solvent and interaction with an analyte molecule. This may also change the measured parameters of the enzyme, because the expected substrate concentration or analyte that is presented to the enzyme in the lumen may be different then in bulk solvent.

Nanoscale phospholipid bilayer systems, named “Nanodiscs,” have been in development since 1998 (*143-144*). These particles were invented from an interesting observation, namely that there is a transient structure of the HDL that forms small discrete discoidal phospholipid bilayers. The HDL functions *in vivo* to transport lipid and cholesterol around the body by complexing an amphipathic, mostly alpha helical protein Apo A1, with phospholipids and cholesterol (*143, 145-148*). At a specific protein to lipid

ratio, the ApoA1 forms discoidal phospholipid bilayers. A gene was designed to enhance the expression of this protein in *E. coli*, to remove any mRNA secondary structure, remove the LCAT signaling and molecular recognition domains, and to optimize the production of this protein via optimal codon usage (*149*). This new genetically engineered amphipathic alpha helical protein was termed Membrane Scaffold Protein, MSP. Since its inception and initial publication, there have been 50 or so variants made, changing the Nanodisc size and the amino acid sequence for chemical modification, and multiple cleavage sequences and affinity tags have been incorporated for different applications (*149-153*). These Nanodiscs are a soluble, monodisperse phospholipid bilayer of a discrete size ranging from 9.7 nm to 17 nm in diameter (*153-154*). This system has allowed for incorporation of monomeric CYP3A4 for a variety of biophysical studies including cryo-spectroscopy, stopped-flow, and solid state NMR (*134, 155-157*).

1.7 Cooperative Behavior of Cytochromes P450

Many cytochromes P450, such as CYP3A4, have large flexible substrate binding pockets capable of accommodating relatively large substrates, >1000 Da, or two or three smaller organic substrates. Binding of multiple substrates and their interactions gives rise to deviations from the simple hyperbolic dependence of functional enzyme properties on the concentration of substrate. This is often referred to as homotropic cooperativity in the case of multiple molecules of the same substrate, or heterotropic cooperativity in the case of different substrates. Cooperativity is typically defined as the

interaction between the binding sites on a macromolecule (*158*). Positive cooperativity is present if the binding of a substrate to one site increases the affinity of other binding sites, and it is negative in the opposite case. If the site is not involved in catalytic action, this effect is often termed allosteric. Upon binding an allosteric effector molecule, the catalytic activity of the enzyme towards the substrate may be enhanced, in which case the effector is an activator, or reduced, in the case of an inhibitor.

Sigmoidal kinetics of 6β-hydroxylation of androstenedione by purified cytochromes P450 was observed over 30 years ago for rabbit P450 isozymes reconstituted in phospholipid vesicles (*159*). Heterotropic effects of ANF and progesterone on the activity of rabbit P450 isozymes were described shortly later (*160-161*). Cooperativity has been reported in numerous systems, *in vivo* (*162*), in liver microsomes (*163-166*), and in purified enzyme reconstituted systems (*78, 167-169*). In addition to CYP3A4, several isozymes have been reported to show cooperative behavior. It has been well documented with CYP107 (*170-171*), CYP2C9 (*172-174*), and others include the xenobiotic metabolizing enzymes CYP1A2 (*175*), CYP2A6 (*176*), CYP2B1 (*177*), CYP2B6, and CYP2E1 (*178*), bacterial enzymes CYP102 (*179*), CYP130 (*180*), CYP158A2 (*181*), P450 crpE (*182*), and even chloroperoxidase (*183-184*).

1.7.1 Cooperativity of Cytochrome P450 3A4

Positive cooperativity has been observed in CYP3A4 binding experiments where heme iron spin shift was monitored by changes in the optical absorption using several substrates including testosterone (TST) (*116, 118, 127, 155, 185-187*), progesterone

(*116*), pyrene butanol (*131, 188*), 7-benzyloxy-4-(trifluoromethyl)coumarin (*188*), ANF (*187, 189-190*), 7-benzyloxyquinoline (*191*), flavone (*118*), and Nile Red (*192*). These sigmoidal spin shift curves generally fit with low Hill coefficients ($n < 2.0$), consistent with two or three substrate molecules binding simultaneously. However, other substrates and inhibitors such as bromocriptine (*118*), erythromycin (*185*), ketoconazole, midazolam (*118*), and acetaminophen (*128*) bind with no apparent cooperativity. The list of substrates for which sigmoidal kinetics has been observed in microsomes includes aflatoxin B1, amitriptyline, carbamazepine, diazepam, estradiol, nifedipine, progesterone, and testosterone (*193*).

The first systematic study of heterotropic effects in CYP3A4 showed that phenanthrene metabolism was activated by ANF and that both of these compounds were substrates for the enzyme (*137*), indicating both could access the active site since neither could competitively inhibit the other substrate. Heterotropic interactions were recently compiled in a comprehensive list by Niwa et al. (*163*). ANF is one of the most commonly studied effectors (although it is also a substrate as previously noted), and exhibits seemingly contradictory effects on CYP3A4 metabolism. It has been shown to activate a number of reactions including TST hydroxylation, aflatoxin B1 epoxidation, 17β–estradiol hydroxylation, while also inhibiting aflatoxin B1 hydroxylation (*194*). It also activates progesterone hydroxylation (*189*), diazepam hydroxylation and demethylation (*195*), carbamazepine expoxidation (*196*), and nifedipine oxidation (*197*). ANF simultaneously activates carboxylic acid formation and inhibits hydroxylation of losartan, while losartan inhibits ANF epoxidation (*198*). Interestingly, ANF stimulates

midazolam 1'-hydroxylation and inhibits 4-hydroxylation, TST has the opposite effect on the two midazolam products (*199*).

Several models have been proposed to account for these cooperative observations including a single large binding pocket which can accommodate different combinations of substrates and/or effectors, a model with distinct allosteric peripheral binding sites that exert influence through conformational changes in the enzyme, and a model with distinct populations of enzyme in various oligomeric states (*121, 200-201*).

1.7.2 Modeling Cooperative Ligand Binding

Understanding drug clearance *in vivo* based on *in vitro* studies requires applying the in vitro derived parameters as a basis for intrinsic clearance (*202-203*):

$$\text{Rate of metabolism} = CLint \bullet [S] = (V_{max} \bullet [S]) / (K_m + [S])$$

Where CLint is the intrinsic clearance, [S] is the drug concentration, V_{max} is the maximal velocity and K_m is the concentration at which half-maximal velocity is observed. This assumes the drug's metabolism follows Michaelis-Menten type kinetics.

If $K_m >> [S]$ then:

$$CLint = (V_{max} \bullet [S]) / K_m$$

By substituting back into the prior equation:

$$CLint = V_{max} / K_m$$

and:

CLint = Rate of metabolism / [S]

This relation allows one to use Michaelis-Menten parameters to estimate *in vitro* clearance (*204*). However, cooperative interactions typically involve more complex non-Michaelis type kinetics, and utilizing the Michaelis-Menten parameters, such as K_m and V_{max}, to model these observed phenomena will cause misleading conclusions regarding the drug clearance. It is necessary to develop better models of cooperative interactions to more accurately predict drug clearance from *in vitro* data.

Definitions of cooperativity are, in general, based either on the purely phenomenological approach to the analysis of experimental data, or on an *a priori* model of two or more identical binding sites with interactions between them. The first approach relies on the non-Michaelis (or non-Langmuir) shape of the plot of the enzyme property as a function of the substrate concentration (*205*). The simple hyperbolic binding isotherm is characteristic for the ensemble of macromolecules each having one or several identical binding sites with dissociation constant K. For one binding site on each macromolecule, the binding scheme consists of only one step:

$$E + S \underset{}{\overset{K}{\rightleftharpoons}} ES$$

The equation for the binding isotherm is a hyperbolic Langmuir isotherm:

$$Y = \frac{[ES]}{[E_0] + [ES]} = \frac{[S]}{K + [S]} = \frac{\frac{[S]}{K}}{1 + \frac{[S]}{K}}$$

For two binding sites, which are not identical, there are four site-specific (microscopic) equilibrium dissociation constants, k_{11}, k_{21}, k_{12}, k_{22}, three of which are independent, because the relation $k_{11} \bullet k_{12} = k_{21} \bullet k_{22}$ always holds in equilibrium due to thermodynamic energy conservation.

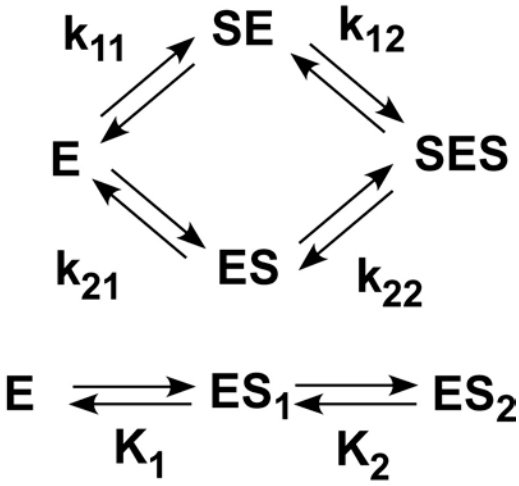

The corresponding stoichiometric (macroscopic) dissociation constants K_1 and K_2 can be expressed as $K_1 = (k_{11}+k_{21})$, $K_2 = k_{11} \bullet k_{12}/(k_{11}+k_{21})$. Concentrations of the binding intermediates $[E_0]$, $[ES_1]$, and $[ES_2]$, and the relative populations of the enzyme with zero, one, and two substrate molecule bound, y_0, y_1, and y_2, can be calculated from the stoichiometric equilibrium:

$$[ES_1] = [E_0] \bullet [S] / K_1$$

$$[ES_2] = [ES_1] \bullet [S] / K_2 = [E_0] \bullet [S]^2 / K_1 \bullet K_2,$$

$$[E_{total}] = [E_0] + [ES_1] + [ES_2] = [E_0] (1 + [S] / K_1 + [S]^2 / K_1 \bullet K_2)$$

The overall binding isotherm is expressed as the following equation:

$$Y = \frac{\frac{[S]}{K_1} + \frac{2[S]^2}{K_1 K_2}}{2\left(1 + \frac{[S]}{K_1} + \frac{[S]^2}{K_1 K_2}\right)} = \frac{1}{2} y_1 + y_2$$

Here y_1 and y_2 are fractions of the binding intermediates [ES_1] and [ES_2], *i.e.* the relative populations of the enzyme with one or two ligand molecules bound, and Y is the fraction of binding sites occupied by ligands.

For identical non-interacting binding sites (no cooperativity), $k_{11} = k_{21} = k_{12} = k_{22} = k$, the shape of binding isotherm is the same as for the single site model, with k as a binding constant, but the stepwise (stoichiometric) binding constants become:

$K_1 = 2k$,

$K_2 = k/2 = K_1/4$.

If the two sites are distinct and independent:

$k_{11} = k_{22} = k_1$

$k_{21} = k_{12} = k_2$

and

$K_1 = (k_1+k_2)$

$K_2 = k_1 \bullet k_2/(k_1+k_2)$

Using these relations, it is easy to show that $K_2 < K_1/4$, if $k_1 \neq k_2$. Therefore, for two-site binding with intrinsically different sites, the binding isotherm is indistinguishable from the presence of negative cooperativity in the system with identical sites.

In the presence of a positive cooperative interaction between sites, the second binding step occurs with higher affinity than it would have had the first site been unoccupied, meaning that $k_{12} > k_{21}$, and $k_{22} > k_{11}$. For the two-site system one can define a cooperativity coefficient $\alpha = k_{12}/k_{21} = k_{22}/k_{11}$, where $\alpha > 1$ corresponds to positive cooperativity, and $\alpha < 1$ to negative cooperativity. Then the site-specific binding constants are:

$k_{11} = k_1$, $k_{22} = \alpha \bullet k_1$,

$k_{21} = k_2$, $k_{12} = \alpha \bullet k_2$,

The stoichiometric binding constants:

$K_1 = (k_1 + k_2)$

$K_2 = \alpha \bullet k_1 \bullet k_2/(k_1 + k_2)$

Note that the same cooperativity coefficient α appears as the measure of cooperativity for the stoichiometric stepwise binding constants K_1 and K_2, and for the microscopic site-specific binding constants k_{ij}. If the site-specific microscopic binding constants differ by factor p, so that $k_1 = pk_2$, then $K_1 = (p+1)k_2$ and $K_2 = k_2\, \alpha p/(p+1)$, there is a positive cooperative interaction between these sites with $\alpha = (p+1)^2/4p$. Then $K_2 = K_1/4$ and the binding isotherm will be hyperbolic, with no apparent cooperativity. Thus, for the system with intrinsically different sites, the presence of site-specific cooperativity has to be evaluated through additional independent measurements of site-specific binding constants. Only overall apparent cooperative or non-cooperative behavior of the system is indicated by the shape of binding isotherm.

These equations help one to understand and evaluate cooperativity in terms of experimentally derived quantities (the equilibrium binding constants) which can be measured directly using various methods (*206-207*). Typically, the stepwise stoichiometric binding constants K_i can be derived from experimental data in more straightforward manner than microscopic site-specific constants k_{ij}. The stoichiometric binding scheme, or sequential binding model, does not rely on any specific model assumptions about the nature and mutual influence of binding sites, but rather assumes an overall binding stoichiometry. For the systems with more than two binding sites the complete resolution of all site-specific constants from analysis of the binding isotherm is, in general, impossible because of the number of independent parameters to fit: seven for three sites, fifteen for four sites; for further analysis see (*208-209*).

For three binding sites, the binding isotherm can also be expressed through stoichiometric binding constants:

$$\mathbf{E} \underset{\mathbf{K_1}}{\rightleftharpoons} \mathbf{ES} \underset{\mathbf{K_2}}{\rightleftharpoons} \mathbf{ES_2} \underset{\mathbf{K_3}}{\rightleftharpoons} \mathbf{ES_3}$$

$$Y = \frac{\frac{[S]}{K_1} + \frac{2[S]^2}{K_1 K_2} + \frac{3[S]^3}{K_1 K_2 K_3}}{3\left(1 + \frac{[S]}{K_1} + \frac{[S]^2}{K_1 K_2} + \frac{[S]^3}{K_1 K_2 K_3}\right)} = \frac{1}{3} y_1 + \frac{2}{3} y_2 + y_3$$

The multipliers 1/3, 2/3, and 3/3 at the right side of the equation yield the fractional contributions to the binding isotherm from each binding intermediates, corresponding to the fraction of binding sites occupied by ligand. However, if the

measured signal is not directly proportional to the fraction of occupied binding sites, this equation will look different:

$$Y_a = \frac{a_0 + a_1\frac{[S]}{K_1} + a_2\frac{[S]^2}{K_1K_2} + a_3\frac{[S]^3}{K_1K_2K_3}}{1 + \frac{[S]}{K_1} + \frac{[S]^2}{K_1K_2} + \frac{[S]^3}{K_1K_2K_3}} = a_0y_0 + a_1y_1 + a_2y_2 + a_3y_3$$

This form provides a useful representation of binding isotherm as a sum of contributions of binding intermediates and will be used further in analysis of functional cooperativity operating in the cytochromes P450, in chapter four.

If the number of binding sites and binding stoichiometry is unknown, the Hill equation is commonly used to characterize the binding cooperativity with one averaged parameter, the Hill coefficient. Originally, this equation was derived to describe the cooperative binding of oxygen and carbon monoxide to hemoglobin, assuming that the protein is composed of several subunits, which bind ligands simultaneously (*210-212*), or with infinite cooperativity:

$$E + nS \underset{}{\overset{K^n}{\rightleftharpoons}} ES_n$$

The binding isotherm for this binding scheme is described by the Hill equation:

$$Y = \frac{[ES_n]}{[E_0] + [ES_n]} = \frac{[S]^n}{K^n + [S]^n}$$

K is the dissociation constant for binding of one ligand, so that the Nth order reaction of simultaneous binding of n ligands is defined by the Nth power of K. By definition, Hill coefficient n_H represents the number of subunits acting simultaneously which is

unrealistic. However, fitting of experimental data with the Hill equation is widely used as a simplest two-parameter approximation without additional knowledge of the binding stoichiometry. The position of the midpoint of the binding isotherm $S_{50} = K$ characterizes averaged affinity, and the Hill coefficient n_H, being a quantitative measure of apparent cooperativity, defines the sigmoid shape of binding isotherm. Physically, the interpretation of the Hill coefficient is equivalent to the average size of cooperative domain in the studies of thermotropic phase transitions in lipid bilayers, which is calculated as a ratio of van't Hoff and calorimetric enthalpies (*213*), or the similar mean size of cooperative unit for the helix-coil transition point in the Zimm-Bragg model calculated as an average length of the helical segment undergoing conformational transition (*214-215*). All these representations provide a useful quantitative measure of cooperativity by comparison of the real experimental system to the simple model of the small but infinitely cooperative system, which has the same shape of the transition curve. However, the Hill coefficient is not equal to the number of binding sites or subunits of the real macromolecule. It indicates only the minimal number of binding sites, which cannot be lower than n_H. The value of S_{50} is also not a binding constant by itself, but a composite of the real binding constants (*216*).

Bardsley and Wyman (*217*) provided a useful, general analysis of the shape of binding isotherm as an indicator of cooperative interactions in the system. It shows that, in general, the sign of Hessian of the binding polynomial at the given substrate concentration defines the curvature of the binding isotherm and thus the presence and sign of cooperativity at the given point. In the case of more than two binding sites, the sign of cooperativity may be different as the interactions between binding sites can be

favorable or unfavorable (*158, 218-220*). The unambiguous conclusion of the presence of cooperativity in the system based solely on the shape of binding isotherm can be reached only in case of positive cooperativity, while the presence of apparent negative cooperativity may be due to the heterogeneity of the binding sites. The application and validity of the Hill plot and equation to the analysis of cooperative binding to dimers and tetramers have been analyzed by Cornish-Bowden and Koshland (*221*) and Bardsley (*222*) for heterogeneous three-site binding.

Another approach to define cooperativity is based on the explicit theoretical model of several binding sites on the macromolecule. Detailed analysis can be found in several excellent books (*219-220, 223*). If these multiple sites are independent and binding of the ligand at any one does not depend on the occupation of other, the system is non-cooperative. However, if the affinity of the site changes as a result of the presence of ligands at another site, then there is a cooperative interaction between them, often called site-specific cooperativity (*158*). This definition requires knowledge of the binding stoichiometry, and the separate measurement of the site-specific binding constants which are unperturbed by their cooperative interactions. The measurement of these constants can be achieved using site-specific mutations (*224-225*), but such experiments rely on the detailed structural information which is unavailable in most cases.

In the case of different functional response from two binding sites, for example different spin shift caused by the first and the second ligand binding, the substrate concentration dependence of this property may appear cooperative even without binding cooperativity. If the first binding is “functionally silent” the second provides most

of the signal and generates an apparently cooperative response. This is the most relevant case with respect to the several mammalian cytochromes P450, including human CYP3A4 (*130*), human CYP2C9 (*226*), rabbit CYP1A2 (*175*), and several others, like CYP107 (*171, 227*), in which the catalytically competent enzyme-substrate complex was only formed upon the second, lower affinity binding event.

1.7.3 Heterotropic Cooperativity

Heterotropic cooperativity, when ligands of two different types can interact simultaneously with one enzyme, has been reported for several cytochromes P450 including CYP3A4, CYP3A5, and CYP2D6, (*163*), CYP2C9 (*228*), CYP1A2 (*229*), CYP107(*230*), and CYP102 (*231*). The ability of one ligand (effector) to enhance the metabolism of another (substrate) is often called positive heterotropic cooperativity, even if there is no information on the enhancement of binding of the substrate in the presence of the effector. Heterotropic effectors may be substrates themselves and can seemingly abolish homotropic cooperativity of the other substrate, as is the case for ANF and its effect on TST hydroxylation (*194*) and progesterone hydroxylation (*116*) in CYP3A4. Heterotropic cooperativity is typically treated as positive cooperativity, since observed inhibition is commonly explained by competitive, noncompetitive or uncompetitive models (*162-163*).

Korzekwa et al. (*201*) developed a complete and simplified kinetic schemes for a binding model with either two catalytic sites, or one catalytic and one effector site. Others have developed similar schemes (*198, 232*). This model involves six different binding intermediates and three catalytic rate constants and is too complex to analyze

for the behavior of two catalytic sites. Using the rapid equilibrium assumption (*233*) it is possible to simplify the model and derive an equation for positive heterotropic cooperativity in the model with one effector and one catalytic site:

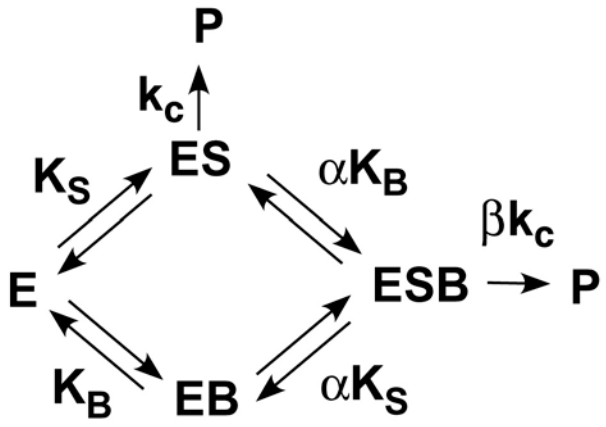

$$v = V_{\max} \frac{[S]}{K_m\left(1+\frac{[B]}{K_B}\right)\left(1+\frac{\beta[B]}{\alpha K_B}\right)^{-1} + [S]\left(1+\frac{[B]}{\alpha K_B}\right)\left(1+\frac{\beta[B]}{\alpha K_B}\right)^{-1}}$$

Here K_m is the apparent Michaelis constant from the ES binding intermediate, and α and β represent cooperativity coefficients induced by the effector, B. This analysis, like others which include the simultaneous binding of two substrates and one effector, allows for the estimation of kinetic and cooperative parameters for the substrate, but only a binding constant for the effector (*167*). In the case where both interacting molecules are enzymatic substrates, these methods do not take into account the full extent of the landscape of heterotropic interactions, instead dividing the two substrates into two substrate-effector pairs for individual analysis.

Other more complex models have been developed for cases where three substrates are in the active site simultaneously, or where the effector activates at lower

concentrations and inhibits at higher concentrations (*234-236*). However, because of the number of parameters involved in these models a large number of data points must be collected in order to accurately describe the system (*216*).

In order to expand upon the understanding of heterotropic interactions in cytochromes P450 and their potential role in deleterious drug-drug interactions, this work describes the development of a model for a complete description of the heterotropic interactions of the ANF and TST substrate pair, using a homogenous monodisperse population of CYP3A4 embedded into Nanodiscs. By monitoring multiple observable properties and simultaneously fitting the data sets to the model the individual state properties of the various enzyme-substrate complexes, along with the step wise binding constants are deconvoluted for the individual substrates and the mixed substrate system. By varying the ratio of the two substrates and comparing the observed kinetic data to a corresponding linear combination of the two substrates' individual kinetic profiles, which represents the absence of heterotropic interactions, conclusions about the presence or absence of heterotropic cooperativity can be made using a limited number of parameters.

CHAPTER TWO: HETEROTROPIC COOPERATIVITY OF HEME IRON SPIN STATE IN CYTOCHROME P450 3A4 NANODISCS PROBED WITH TESTOSTERONE AND α-NAPHTHOFLAVONE

2.1 Introduction

Both testosterone (TST) and α-naphthoflavone (ANF) (figure 2.1) bind to CYP3A4 inducing a Type I spin conversion by displacing water as the axial heme ligand, and cause a shift from the low spin ferric state to the high spin ferric state observable by a change in the position of Soret band in UV-vis absorbance spectra from 416 nm to 393 nm. The correlation between the spin state and the ligation state of the heme iron and the redox potential has been established for soluble P450s (*237-239*), and recent work has shown that this also holds true for monomeric CYP3A4 embedded Nanodiscs (*240*), implicating the spin state (and ligation state of the heme iron) as an universal regulator of metabolic control. Titrations of either substrate monitored by UV-vis spectroscopy deviate from a standard Langmuir curve suggesting that multiple binding events occur and that these events are apparently cooperative. Previously reported parameters from fitting these titrations to the Hill equation yield ranges of, S_{50} = 28 – 58 μM, n = 1.3 – 2.2 (*116, 118, 130, 155*) for TST, and, S_{50} = 3.7 – 50 μM, n = 1.2 – 2.2 (*118, 185, 187, 189, 241*) for ANF. However, it should be noted that the experiments reported by Roberts et al. (*241*) were performed at a concentration of 5 μM CYP3A4, and resulted in significant difference from the other experiments reported. The variation in these numbers is likely due to the variety of systems (liposomes,

Nanodiscs, or detergent solubilized), and conditions such as temperature (ambient, 25° C, or 37° C), and CYP3A4 concentration (0.5 – 5 μM) which may affect the enzyme oligomerization state.

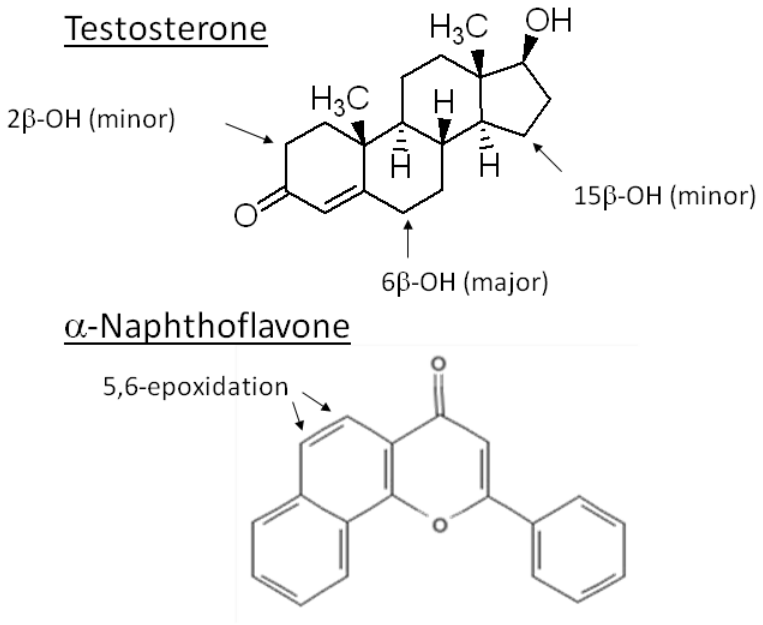

Figure 2.1 Substrates and Major Metabolite Products.

In order to avoid the effects of CYP3A4 oligomerization, and to elucidate the mechanism of heterotropic cooperativity of monomeric CYP3A4, the enzyme was solubilized in Nanodiscs (*130, 155-156*). Nanodiscs are ~10 nm diameter phospholipid bilayer membrane patches stabilized by MSP, which allow for the incorporation of a single membrane protein into native like environment. This creates a homogenous, monodisperse, and stable protein sample suitable for the study of many integral membrane proteins (*190, 242*). Homotropic spectral titrations of TST to CYP3A4 in Nanodiscs was studied in detail previously (*155*), along with a rigorous characterization of the incorporation of the enzyme into the Nanodisc lipid bilayer by size exclusion

chromatography (SEC) and small angle x-ray scattering (SAXS). In this study the high Hill coefficient (n > 2.2) is indicative of at least three TST binding events, with the first event only contributing a minor portion of the high spin signal. Similarly, multiple molecules of ANF can bind to CYP3A4, and the first binding event also appears to be silent with respect to the spin shift (*118, 187, 190, 241*).

ANF is one of the most widely studied effectors of CYP3A4 and it has been shown to stimulate a number of CYP3A4's catalytic reactions (*160, 194-195, 197-199, 243*) as well as eliminate the positive homotropic cooperativity typically observed for binding and/or metabolism of TST and progesterone (*116, 194*). However, the origin of these effects remains unclear and seemingly contradictory in the literature, since it is studied in concert with a variety of other CYP3A4 substrates, and is sometimes treated solely as an effector while other times as an independent substrate. In some cases ANF is reported to act as an inhibitor for CYP3A catalyzed reactions, including the 6β-hydroxylation of testosterone by CYP3A4 (*194*) and CYP3A6 (*244*), but sometimes as an activator (*160, 195, 197, 199*). ANF is itself a substrate for CYP3A4 (*198, 245*), and as such may serve as a competitive inhibitor. However, it is also one of the most well documented effectors for CYP3A4 heterotropic cooperativity, particularly in combination with TST (*21, 121-122, 163, 246*). Results of a recent study (*241*) suggested a moderate positive cooperative interaction between ANF and TST, as estimated by the spin shift of CYP3A4.

Type I spin state changes of CYP3A4 have been measured as a function of ANF and TST concentrations as individual substrates, and compared to the Type I spectral changes induced in mixed titration experiments with fixed molar ratios of the two

ligands. This method of deconvolution of the additive and heterotropic cooperative effects allows for analysis of changes in the spectral dissociation constant, S_{50}, as the concentrations of both substrates were simultaneously altered, revealing changes in the enzyme's overall spectral transition for both substrates as a function of their molar ratio. In the absence of specific heterotropic cooperativity the overall affinity of a given substrate ratio in the system for the enzyme is represented by a linear combination of the affinities of the two individual substrates while deviations from this behavior represent additional positive or negative cooperative interactions which give rise to the non-additive effects (*247-248*). Analysis of the mixed titrations at different molar ratios of the substrates, as compared to the single substrate titrations, showed that the stimulatory effect observed in the presence of the second substrate was entirely due to its additive effect and revealed the absence of any specific heterotropic cooperative interactions between ANF and TST in the monomeric CYP3A4.

2.2 Materials and Methods

2.2.1 Expression and Purification of CYP3A4

The clone of CYP3A4his NF-14 in pCW Ori+ was graciously provided by F. P. Guengerich (Vanderbilt University Nashville, TN). The heterologous expression of CYP3A4his in *E. coli* has been described (*185*) and the growth and purification procedure has been modified to improve both the expression yield and ease of purification (*156*). The CYP3A4his has an N-terminal truncation of 10 amino acids at positions 3-12 and a single point mutation S18F to create the construct CYP3A4his NF-

14 pCW Ori+ which helps in the expression of this protein in *E. coli* and aids in the formation of the holo enzyme over either the apo or the P420 form. The CYP3A4his has a pentahistidine affinity tag engineered at the C-terminus. The expression of CYP3A4his was accomplished by first transforming the clone into *E. coli* DH5α f' Max IQ supercompetent cells using the manufacturer's protocol. The transformed *E. coli* were plated on LB agar plates containing 50 µg/ml ampicillin and incubated at 37° C overnight. A single colony was added to 10 ml of LB media containing 100 µg/ml ampicillin and shaken at 220 RPM at 37°C, and grown overnight. This was used as the starter culture for growth in TB enhanced with BactoPeptone (2 g /L) and 250 µL trace minerals (100 mM $FeCl_3$●6 H_2O, 10 mM $ZnCl_2$●4 H_2O, 10 mM $CaCL_2$●6 H_2O, 8.0 mM Na_2MoO_4, 7.5 mM $CuCl_2$, 8.0 mM H_3BO_3, and 1.0 mM thiamine). The media was inoculated with 10 ml of starter culture and grown at 37˚C with shaking at 200 RPM until OD_{600} was 0.8. The cells were then induced with a final concentration of 1 mM IPTG, 4 g of L-arabinose and 1 mM δ-Aminolevulinic acid to help promote holoenzyme formation. This induced cell culture was grown for an additional 48 hours at 30° C with shaking at 200 RPM. The cells were harvested using a J2-21 Beckman-Coulter centrifuge with a JA-10 rotor. They were isolated from the growth media by spinning at 8000 x G for 10 minutes and stored at -80° C until the purification was performed.

The cells were resuspended in 50 mM potassium phosphate buffer pH = 7.4, 0.5 M sodium acetate, 20% glycerol, 5 mM beta-mercaptoethanol, 1 mM PMSF. 1% CHAPS was added and then the cell suspension was sonicated using a Branson Sonifier 450 set to a duty cycle of 80% and an output of 7 for 1 minute and then allowed to rest on ice for three minutes, for four cycles. The cells were centrifuged using a

Beckman-Coulter L8-55m preparative ultracentrifuge with a Ti-45 rotor for 30 min at 30,000 RPM to clarify the lysate. The lysate was loaded onto a 25 ml Hi-Trap Metal Chelating resin, charged with 0.1 M nickel sulfate and equilibrated with 50 mM potassium phosphate buffer pH = 7.4, 0.25 M sodium acetate, 20% glycerol, 1% CHAPS, followed by ten column volumes of: the equilibration buffer, the buffer supplemented with 15 mM imidazole; the buffer supplemented with 15 mM imidazole, 0.1% Emulgen 913 and without CHAPS; and eluted with 50 mM potassium phosphate buffer pH = 7.4, 0.25 M sodium acetate, 20% glycerol, 0.1% Emulgen 913, 0.3 M imidazole. The fractions were pooled and dialyzed three times against 1000 x volume of 50 mM potassium phosphate pH = 7.4, 20% glycerol (v/v). The dialyzed samples were then aliquoted and flash frozen in liquid nitrogen and stored at -80° C until use. Purified CYP3A4 was quantitated using carbonmonoxy bound ferrous difference spectra using an extinction coefficient of 91 mM^{-1} cm^{-1} (*3*).

2.2.2 Expression and Purification of Membrane Scaffold Protein MSP1D1

The Membrane Scaffold Protein 1D1 (MSP1D1) expression and purification has been previously described (*149, 153*) synthetic gene was cloned into a pET 28 vector and transformed and expressed in BL21 (DE3) Gold *E. coli*. The transformed *E. coli* were plated on an LB agar plate containing 30 µg/ml kanamycin and incubated overnight at 37˚C. A single colony was selected and added to a 5 ml LB culture supplemented with kanamycin, and was incubated at 37˚C with shaking at 220 RPM until the culture reached an OD_{600} of 1.5. 1 ml of the culture was added to 50 ml of culture media and incubated at 37˚C with shaking at 220 RPM until the OD_{600} was 3.0. The culture was added to a Bio-Flow III fermentor containing 2.5 L of TB, and growth at

37˚C with agitation of 500 RPM and air flow of 3.0 L/min was monitored until the OD_{600} reached 2.5 at which point target protein synthesis was induced by addition of IPTG to a final concentration of 1 mM, and growth was continued for an additional hour at 37˚C, and then four more hours at 28˚C. The cells were harvested in a Beckman J2-21 centrifuge using a JA-10 rotor at 8000 x G for 10 minutes. The cell pellet was stored at -80˚C until purification.

The cells were resuspended in 15 mM potassium phosphate pH = 7.4, 50 mM NaCl buffer with a final concentration of 1.0% Trition X-100 (w/v). They were incubated for 30 minutes on ice and sonicated with a Branson Sonifier 450 set to a duty cycle of 60% and output of 7, for 30 seconds followed by a 90 second rest six times. The cell suspension was spun at 25,000 x G in a Beckman Ti-45 rotor for 30 minutes, and purified over a Hi-Trap Metal Chelating resin 2.5 x 5 cm column, charged with 0.1 M nickel sulfate and equilibrated with three column volumes of the resuspension buffer, washing with three column volumes of the following buffers: 40 mM Tris-HCl pH 8.0 0.3 M NaCl 0.1% Triton X-100, 40 mM Tris-HCl pH 8.0 300 mM NaCl 50 mM cholate, 40 mM Tris-HCl pH 8.0 0.3 M NaCl, 40 mM Tris-HCl pH 8.0 0.3 M NaCl 50 mM imidazole. The protein was eluted with 40 mM Tris-HCl pH 8.0 0.3 M NaCl 250 mM imidazole.

2.2.3 Expression and Purification of TEV Protease

TEV protease expression and purification followed a previously described procedure (*249*). The transformed *E. coli* were plated on an LB agar plate containing 100 µg/ml ampicillin 30 µg/ml chloramphenicol and incubated overnight at 37˚C. A single colony was selected and added to a 50 ml LB culture supplemented with

ampicillin and chloramphenicol, and was incubated at 37˚C with shaking at 220 RPM until the culture reached an OD_{600} of 0.8. 10 ml of the culture was added to 1 L of culture media and incubated at 37˚C with shaking at 220 RPM until the OD_{600} was 0.8 at which point target protein synthesis was induced by addition of IPTG to a final concentration of 1 mM, and growth was continued for four additional hours at 30˚C. The cells were harvested in a Beckman J2-21 centrifuge using a JA-10 rotor at 8000 x G for 10 minutes. The cell pellet was stored at -80˚C until purification.

The cell pellet was resuspended in 60 ml of lysis buffer, 50 mM Tris-HCl pH 8.0, 10 mM BME, 0.1% Triton X-100, 5% glycerol, and sonicated with a Branson Sonifier 450 set to a duty cycle of 60% and output of 7, for 30 seconds followed by a 90 second rest four times. The cell suspension was spun at 30,000 x g in a Beckman Ti-45 rotor for 30 minutes, and purified over a 25 ml Hi-Trap Metal Chelating resin 2.5 x 5, charged with 0.1 M nickel sulfate and equilibrated with three column volumes of the lysis buffer, washed with 5 column volumes of lysis buffer plus 0.3 M NaCl, 50 mM imidazole, and eluted with lysis buffer plus 0.3 M NaCl, 0.5 M imidazole. The elution was assayed by a colorimetric change using Coomassie Plus Protein Assay Reagent. 100 µL of assay reagent was added to 5 µL of protein solution in a 96 well microtiter plate, and the concentration was estimated by comparison to a BSA standard. The fractions that contained protein were pooled and dialyzed twice overnight against 4 L 100 mM Tris-HCl pH 7.5, 2 mM EDTA, 10 mM DTT, 0.2% Triton X-100, diluted 1:1 with 100% glycerol and stored at -80˚C until used.

2.2.4 Cleavage of Histidine Tag from MSP1D1

MSP1D1 is genetically engineered to include a hexahistidine affinity tag that that can be cleaved using the TEV Protease from the Tobacco Etch Virus. This protease site has a cleavage consensus sequence of Glu-X-X-Tyr-X-Gln/Ser. Cleavage was carried out using a 1:100 TEV protease:MSP1D1 molar ratio in 50 mM Tris-HCl buffer pH = 8.0, 1.0 mM DTT, and 0.5 mM EDTA (*153, 155*). This solution was incubated for 12 hours at ambient temperature on an orbital shaker. This was followed by dialysis against 4 L of 20 mM Tris-HCl pH = 7.4, 0.3 M NaCl, 50 mM imidazole three times to remove DTT. The protein was loaded onto a 5 mL Hi-Trap Metal Chelating column, charged with 0.1 M nickel sulfate and equilibrated with the dialysis buffer. The flow through was assayed by a colorimetric change using Coomassie Plus Protein Assay Reagent. 100 µL of assay reagent was added to 5 µL of protein solution in a 96 well microtiter plate. The fractions that contained protein were pooled and dialyzed against 4 L of 20 mM Tris-HCl pH = 7.4, 0.1 M NaCl, 0.5 mM EDTA three times, and checked by SDS page to determine cleavage efficiency. The final concentration of cleaved MSP1D1 was calculated using the absorbance at 280 nm, and the corresponding extinction coefficient of 18.2 mM^{-1} cm^{-1} (*153*).

2.2.5 Assembly of Plain Nanodiscs

Assembly of plain Nanodiscs was accomplished using the scaffold protein MSP1D1 after removal of its histidine tag by cleavage with TEV protease, following a modified procedure (*149, 153*). A disc reconstitution mixture was prepared containing MSP1D1, POPC, and sodium cholate present in a 1:65:120 molar ratios. Detergents were removed by treatment with Amberlite beads (1g/ml of disc reconstitution mixture), initiating a self-assembly process which forms discoidal POPC bilayer ~10 nm in

diameter stabilized by the encircling amphipathic MSP1D1 belt. The discs were purified injected onto a Sephadex G-200 size exclusion column at a flow rate of 0.5 ml/min, equilibrated in 0.1 M HEPES buffer pH = 7.5, 15 mM $MgCl_2$, 0.1 mM DTT, to remove any partially formed discs or aggregated MSP1D1.

2.2.6 Incorporation of CYP3A4 into Nanodiscs

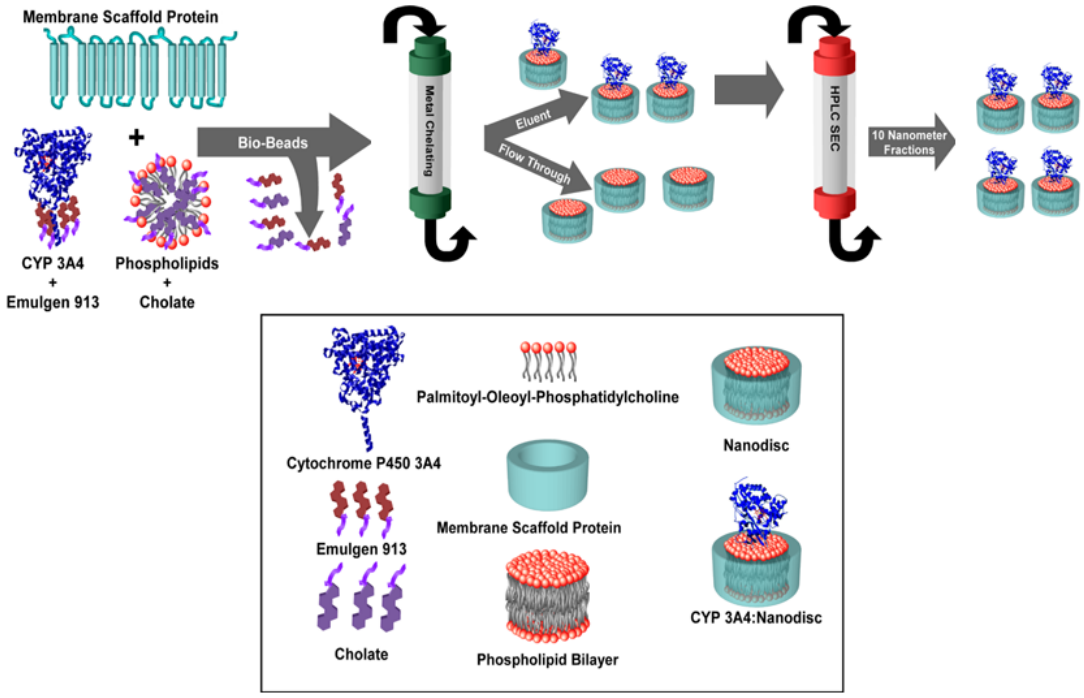

Figure 2.2 Schematic for Incorporation of CYP3A4 into Nanodiscs. Adapted from Baas et al. 2004.

Assembly of CYP3A4 in Nanodiscs (Figure 2.2) was accomplished using the scaffold protein MSP1D1 after removal of its histidine tag by cleavage with TEV protease, following a modified procedure (*153, 155*). Purified CYP3A4 from the *E. coli* expression system was solubilized by 0.1% Emulgen 913 and mixed with a disc

reconstitution mixture containing MSP1D1, POPC, and sodium cholate present in 1:10:650:1300 molar ratios respectively yielding an average final ratio of one CYP3A4 per five Nanodiscs. Detergents were removed by treatment with Amberlite beads (1g/ml of disc reconstitution mixture), initiating a self-assembly process which incorporates monomer of CYP3A4 into a discoidal POPC bilayer ~10 nm in diameter stabilized by the encircling amphipathic MSP1D1 belt. The discs were purified over a 5 mL Ni-NTA agarose column, equilibrated in 50 mM potassium phosphate buffer pH = 7.4, 0.3 M NaCl, washed with equilibration buffer plus 15 mM imidazole, and eluted with equilibration buffer plus 250 mM imidazole. This removes any empty Nanodiscs, as the histidine tag resides on the P450. Red fractions were pooled and concentrated and injected onto a Sephadex G-200 size exclusion column, at a flow rate of 0.5 ml/min, equilibrated in 0.1 M HEPES buffer pH = 7.5, 15 mM $MgCl_2$, 0.1 mM DTT, to remove aggregated CYP3A4. Fractions were individually examined for bromocriptine binding, and those which did not show a ≥85% spin conversion at a saturating concentration were discarded. The remaining pooled fractions showed a minimum 90% spin conversion.

2.2.7 UV-Vis Spectroscopy

Substrate binding was studied at 3 µM CYP3A4 in Nanodiscs using a Carey 300 spectrophotometer. Absorption spectra have been measured at 37°C, in 100mM HEPES buffer pH 7.4, containing 7.5mM $MgCl_2$ and 0.1mM DTT. The substrates, TST and ANF, were added from stock solutions prepared at the desired molar ratio in methanol, with the final concentration of methanol never more than 1%.

2.2.8 Substrate Membrane Partitioning

Partitioning of hydrophobic substrates ANF and TST into the lipid phase of Nanodiscs was taken into account by using the corresponding partition coefficients K_p = 3000 and 500 respectively (*190, 250*).

Considering all binding events as an equilibrium distribution of substrate between aqueous phase, lipid phase, and CYP3A4, the binding polynomial for the CYP3A4 in Nanodiscs will include an additional term to take into account partitioning of the ligand into bilayer. Two simultaneous equilibria are to be considered ((*207*), p. 118):

$$[S_f] \leftrightarrows [S_l] \quad \text{and} \quad [S_f] \leftrightarrows [ES].$$

Here $[S_f]$ and $[S_l]$ are concentrations of the substrate in the aqueous phase and lipid phase, and [ES] is concentration of the enzyme-substrate complex. Because of partitioning of the substrate between aqueous phase and lipid bilayer, concentration of the free substrate in aqueous phase will be lower than that in the absence of partitioning, $[S_f]_0$ by the constant factor determined by partition coefficient K_p and the volume fraction of the lipid phase, v_l, $v_l = V_l/(V_l+V_w)$, where V_l and V_w are the total volumes of the lipid and aqueous phases respectively (Figure 2.3). If $V_l << V_w$, and $(V_w+V_l)/ (V_w+ K_p \bullet V_l) \approx 1 / (1 + K_p \bullet v_l)$, then $[S_f] = [S_f]_0/ (1 + K_p \bullet v_l)$. Thus, the value of observed S_{50}, or the midpoint of titration curve, will be reached at the concentration of unbound substrate, which is higher by the factor $(1+ K_p \bullet v_l)$ than the true S_f, and the true dissociation constants or S_{50} can be found after correction of apparent dissociation constants S_{app} by this factor: $S = S_{app}/(1+ K_p \bullet v_l)$. This correction can be negligible, if $K_p \bullet v_l << 1$, as is the case when the volume fraction of the lipid phase is small. However,

at a 3 µM concentration of Nanodiscs $v_l = 3.3 \times 10^{-4}$, and for ANF $(1+ K_p \bullet v_l) = 2$, while for TST $(1+ K_p \bullet v_l) = 1.15$.

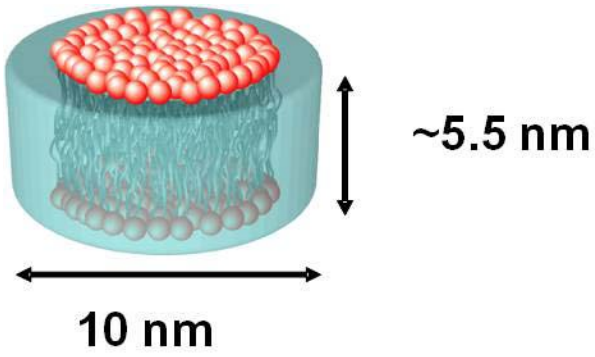

Figure 2.3 Dimensions of a Nanodisc. Adapted from Baas et al. 2004.

2.2.9 Data Analysis

Analysis of the spectral titration of CYP3A4 in Nanodiscs was performed using singular value decomposition as described (*130, 155*). For each substrate ratio, all absorption spectra of CYP3A4 measured between 360 and 500 nm in the presence of different substrate concentrations were corrected for the dilution factor and combined into the matrix. For experiments using ANF, the absorption spectrum for the corresponding concentration of ANF in 3 µM empty Nanodiscs was subtracted from the signal to eliminate interference with the CYP3A4 signal in this region. Singular value decomposition of this spectral matrix revealed that the data are described by two spectral components, with the second one corresponding to the difference spectrum of low and high ferric CYP3A4. The third singular value was always less than 5%. The resulting singular concentration vector corresponding to the transition of CYP3A4 from low to high spin as a function of substrate concentration was fitted to the Hill equation:

$$aF = S^n/(S_{50}{}^n+S^n)$$

where a is the spectroscopic amplitude, F is the fraction of high-spin shift caused by substrate binding, S is the substrate concentration, S_{50} is the spectral dissociation constant, and n is the Hill coefficient. The fitting program was written in MATLAB using the Nelder-Mead simplex minimization algorithm implemented in the subroutine "fminsearch.m."

To detect the presence of heterotropic interaction between two substrates, it is necessary to compare the system with the similar reference system where no heterotropic cooperativity is present. In this case, the response of the system does not change when one ligand is replaced with another while keeping the total equivalent amount of ligands the same. To account for the difference in absolute affinities of two substrates their concentrations are normalized by dividing by the corresponding spectral dissociation constants, S_{50}, the concentration corresponding to the midpoint of the dose-response function. This allows for the direct comparison of the two substrate concentrations in equivalent units in terms of their abilities to independently bind and induce a spin transition in the enzyme.

Using the normalized concentrations of substrates A and B, $[A] = A/S_{A,50}$ and $[B] = B/S_{B,50}$, the total normalized concentration can be defined as $[S] = [A] + [B]$, and the normalized fractions of each substrate as $\alpha = [A]/[S]$, and $\beta = 1-\alpha = [B]/[S]$. Such normalized coordinates allow for deconvolution of the total response of the system into two parts, the first is caused by additive action of two substrates, and the second is due to their synergistic cooperative interaction, if present. The first part may be defined as

the linear combination of the fractional contributions of two substrates, R(A,B) = R([S]) = αR(A,0) + (1-α)R(0,B). This response function can be constructed and calculated based on two homotropic response functions measured in two separate titration experiments with only one substrate at a time, A and B, and used as a reference for experimental evaluation of the presence of specific heterotropic cooperativity. The results of mixed substrate titration experiments can be compared with the response calculated for the case where there is no synergistic interaction between substrates. By definition the presence of positive heterotropic interactions is manifested in the increase of the system response to the simultaneous action of both substrates, as compared to the linear combination of responses to their separate actions. Since the responses of the individual substrates include homotropic cooperativity, the linear combination of the two responses measured in titration experiments with one substrate at a time will also take into account the linear combination of the two homotropic cooperative interactions, and thus serve as a reference system for the case of no specific heterotropic cooperativity. The non-specific heterotropic cooperativity is indicative of heterotropic interaction between two substrates which is equivalent to their averaged respective homotropic interactions and thus does not make sequential binding of different substrates more or less favorable than would be expected from their corresponding homotropic binding constants. A binding isotherm in the mixed titration experiment for this system will have the midpoint substrate concentration:

$$s_{50} = S_{50} /(\alpha A + (1-\alpha)B) = 1$$

In the case of specific positive heterotropic cooperativity, the simultaneous binding of different substrates will be more favorable than would be expected from the

simple linear combination of separate binding events of those two, and the experimentally observed s_{50} will be less than the corresponding reference value with no heterotropic cooperativity, $s_{50} = 1$. Analogously, negative interactions will result in the inhibition of the response function, as compared to the reference system with non-interacting substrates, and experimentally determined $s_{50} > 1$.

An illustration of such an approach is presented here for the binding of two different ligands to a protein molecule with two binding sites. In the general case, the overall occupation of the two sites is represented by the following binding isotherm, Y, (*209*):

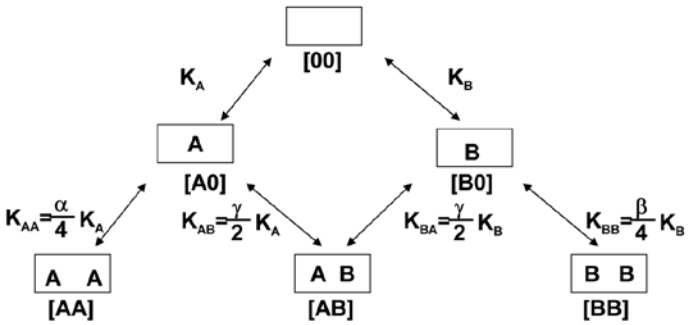

$$C_{tot} = C_{00}+C_{A0}+C_{B0}+C_{AA}+C_{AB}+C_{BB}=$$

$$=C_{00}\,(1+K_A\,[A]_0\,+K_B[B]_0+K_AK_{AA}[A]_0^2+K_AK_{AB}[A]_0[B]_0+K_BK_{BB}[B]_0^2)$$

$$Y=\frac{(C_{A0}+C_{B0})+2(C_{AA}+C_{AB}+C_{BB})}{2(C_{00}+C_{A0}+C_{B0}+C_{AA}+C_{AB}+C_{BB})}$$

Here c_{tot} is the total concentration of the enzyme, represented as the sum of all binding intermediates shown in the scheme. The total fractions of occupied binding sites at different concentrations of both substrates are presented in Figure 2.4, as calculated for three possible heterotropic interactions between two bound substrates, neutral (A), unfavorable (B), and favorable (C). Calculations have been made for the model which

includes homotropic cooperativity for the substrate A (1.2 kcal/mol, corresponding to the 7.3-fold higher binding constant for the second binding event, $\alpha = 7.3$) and no cooperativity for the substrate B ($\beta=1$). In the first case (Figure 2.4A), a 0.6 kcal/mol heterotropic interaction is present between two substrates ($\gamma = 2.7$), which is equal to the mean arithmetic value of two homotropic interactions (0 and 1.2 kcal/mol). In this case, the population of the mixed intermediate [AB] is equal to the mean geometric value of [AA] and [BB], which corresponds to the binding characteristic at the absence of specific heterotropic interactions. Here, where the heterotropic interaction between two substrates in [AB] is equal to the geometric mean of the two homotropic interactions in [AA] and [BB], the cooperativity in the system may be termed non-specific, because the response of the system is identical to the reference system with no heterotropic cooperativity. In such a case, the contour lines of equal height, or isoboles, are straight (*247-248*). If heterotropic interaction between two substrates is less favorable than 0.6 kcal/mole (Figure 2.4B), the population of the mixed binding intermediate [AB] is lower than statistically expected, and the projections of isoboles are convex, indicating that interaction between substrates is unfavorable, or the presence of negative heterotropic cooperativity. For favorable heterotropic interaction greater than 0.6 kcal/mole between the substrates (Figure 2.4C), the contour lines are concave as the population of the mixed binding intermediate [AB] is higher than is statistically expected, meaning the presence of synergistic binding of two substrates, or the presence of positive cooperativity.

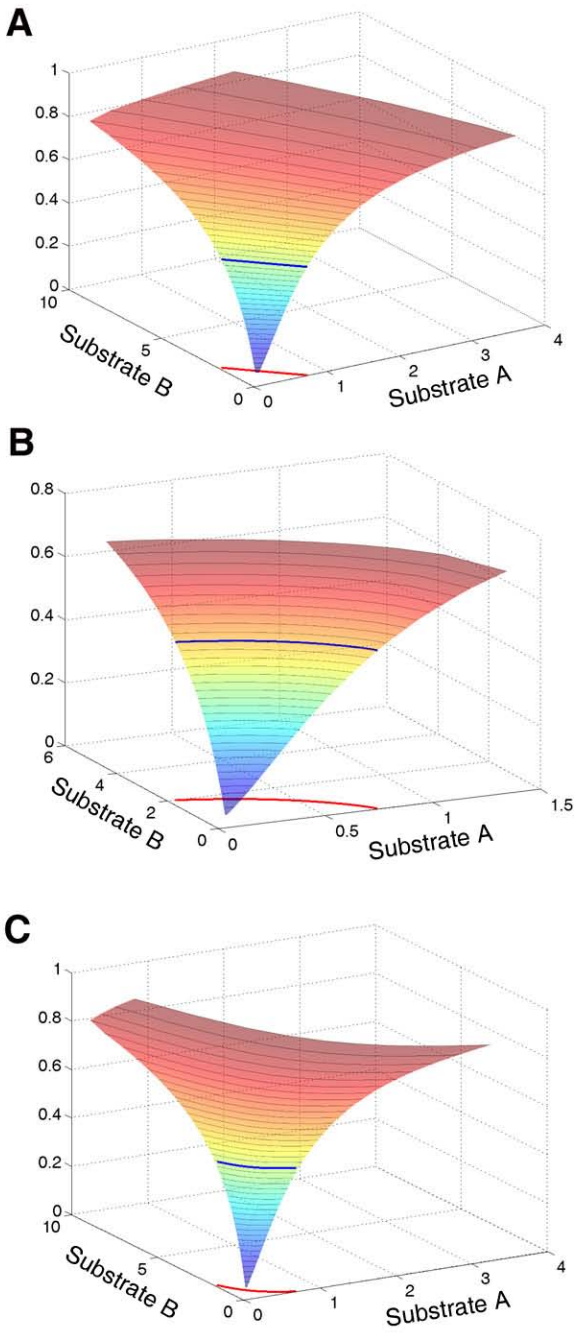

Figure 2.4 Model Binding Surfaces. In the absence (A), and the presence of negative (B) and positive (C) heterotropic cooperativity. Adapted from Frank et al. 2009.

For the mixed substrate titrations at fixed substrate ratio [A]/[T] = α/(1-α), the total concentration of the enzyme with one substrate molecule bound (ANF, or TST) is given by:

$$c_1 = c_A + c_T = c_o K_A[A] + c_o K_T[T] = c_o K_1([A] + [T]) = c_o K_1[A] + c_o K_1[T]$$

$$\text{where: } K_A[A] + K_T[T] = K_1([A] + [T]) \text{ and } K_1 = (\alpha K_A + (1-\alpha)K_T)$$

Here c_0 is concentration of substrate free CYP3A4, K_A and K_T are the binding constants of ANF and TST respectively to CYP3A4. K_1 represents the apparent overall association constant for both substrates in the mixed system at the given ratio of concentrations of two substrates. K_1 is a function of the relative fractions of the two substrates determined by the value of α, $0 < \alpha < 1$, and their respective association constants K_A and K_T, derived from single substrate binding experiments. Thus for any mixed substrate titration designated as S, the mixture of substrates can be treated as a single substrate, as long as their ratio remains constant. The mixed dissociation constant, K_1, is represented as a function of concentration ratio of the two substrates. In order to account for the different affinities of two substrates, the normalized concentration [S] can be defined as:

$$[S]/K_1 = [A]/K_A + [T]/K_T$$

Similarly for the Hill model with two substrates the mixed affinity can be expressed approximately as a function of the individual substrate affinities and their ratio (*247*) utilizing the mixed dissociation constant and accounting for the different Hill coefficients of each substrate,

$$Y = \alpha S^n/(S_{50}{}^n + S^n) + (1 - \alpha)\, S^m/(S_{50}{}^m + S^m)$$

allowing one to analyze the titration with a mixture of multiple substrates as long as their molar ratios remain constant. To generate the three dimensional spin shift surface from the data obtained in mixed titration experiments, the Hill equation fits for TST, ANF, and the mixed 1:1, 1:3, 1:5, and 1:10, ANF to TST molar ratios were plotted as a function of two variables, namely the normalized concentrations of each substrate, $[A]/S_{50,A}$ and $[T]/S_{50,T}$. If the observed S_{50} values for the mixed substrate system remain a linear combination of the two single substrate S_{50} values and the fractions of the substrates:

$$S_{50,S} = (\alpha S_{50,A} + (1 - \alpha) S_{50,T})$$

and the normalized spectral dissociation constant is:

$$[S]/S_{50,S} = (\alpha([A]/S_{50,A}) + (1 - \alpha)\, ([T]/S_{50,T}))$$

then the spectral dissociation constant for the total substrate in the system will remain unchanged as the ratio is varied, indicating the absence of specific interactions. These half saturation points plotted along the normalized axes will form a straight line, since the normalized $S_{50} = 1$ for any substrate ratio, indicating no change in spectral dissociation constant.

If, however, true purely heterotropic cooperativity is observed, the normalized S_{50} will not remain constant as the substrate ratio is varied leading to curvature of the half saturation contour.

2.3 Results

2.3.1 Single Substrate Titrations

One complicating factor of studying ANF spectroscopically with CYP3A4 is that the molecule's absorbance spectrum overlaps with that of the enzyme in the Soret region. One recent attempt to minimize this effect attempted to fix the spectrum at a specific wavelength, 390 nm, and measure changes over the rest of the region (*241*). However, this makes the assumption that the spectrum of CYP3A4 is fixed at this wavelength, which is not valid. In the current studies the signal from ANF over the Soret region was measured by titrations of ANF into Nanodiscs which contained only phospholipids and no CYP3A4. This signal was then subtracted from the overall absorbance spectrum of the titrations of the CYP3A4 Nanodiscs at corresponding substrate concentrations as shown in figure 2.5.

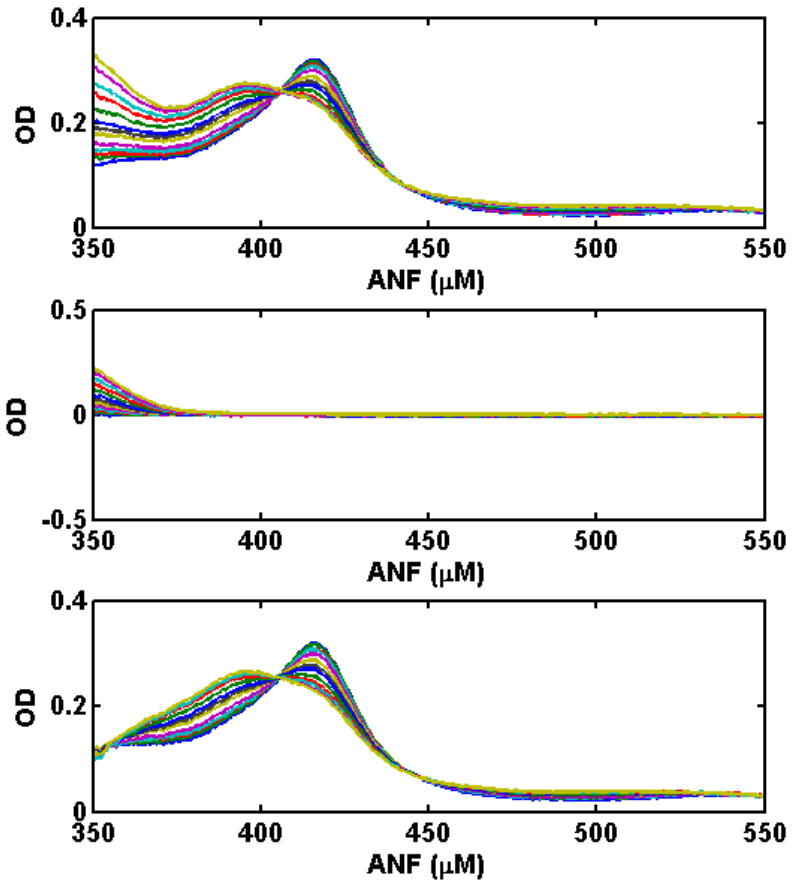

Figure 2.5 Spectral Titration of CYP3A4 Nanodiscs with ANF. Top, ANF titration into CYP3A4 Nanodiscs. Middle, ANF titration into plain Nanodiscs. Bottom, ANF titration into CYP3A4 Nanodiscs with ANF signal subtracted.

Titrations of CYP3A4 Nanodiscs with ANF or TST were monitored by the ability of each substrate to induce a Type I spin conversion (figure 2.6). Fitting to the Hill equation yielded an apparent S_{50} = 44 μM and n = 1.5 for TST, and S_{50} = 15 μM and n = 1.8 for ANF, with maximal high spin conversions of 93% and 85% respectively. A high concentration of CYP3A4 Nanodiscs, 3 μM, was used to stabilize the ANF signal within the Soret region at high substrate concentrations. Spectral binding constants, corrected

for partitioning of ANF and TST into the lipid bilayers of Nanodiscs as discussed in the methods, are 38 µM for TST and 7 µM for ANF.

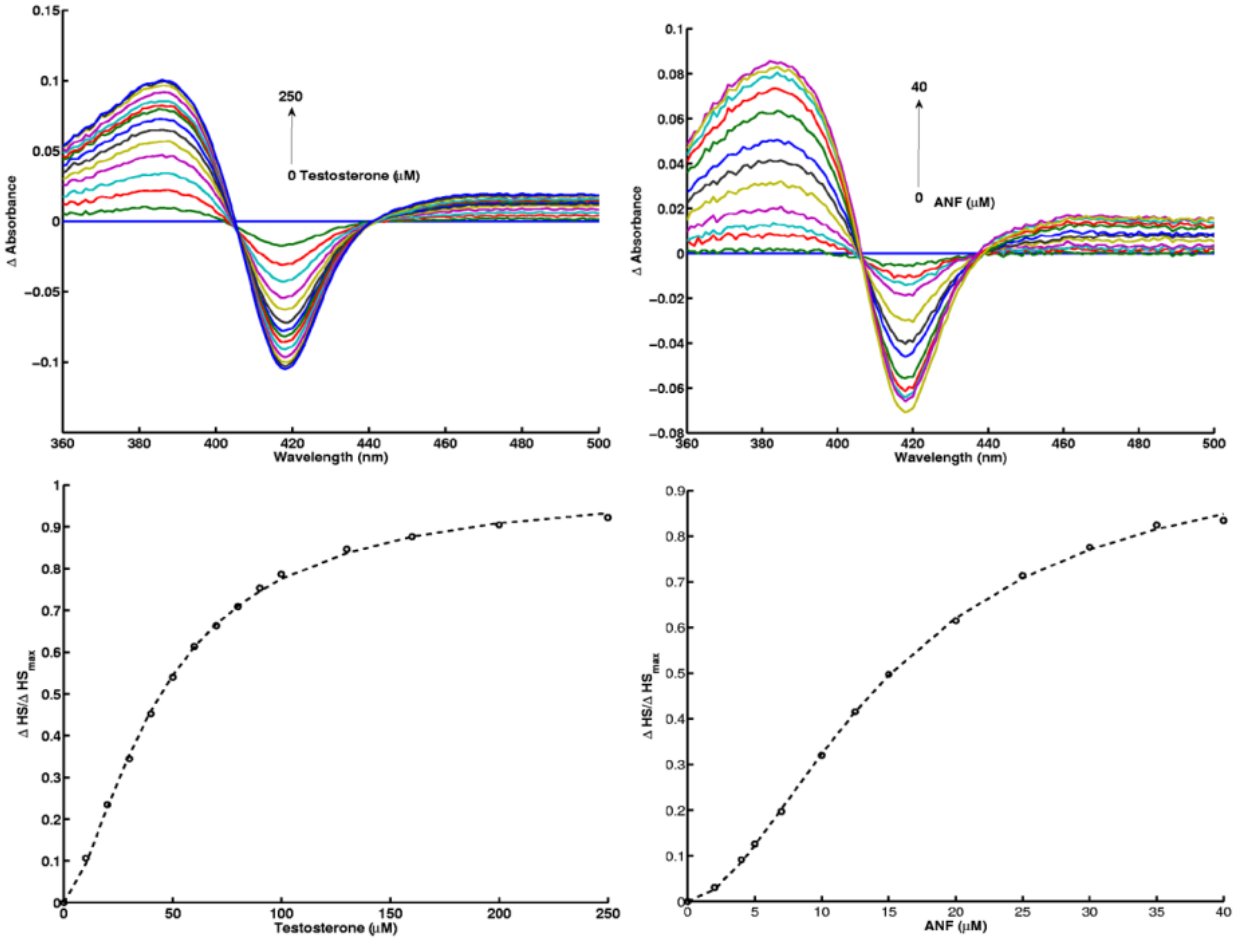

Figure 2.6 Spectral Titration of CYP3A4 Nanodiscs with TST and ANF. Left, The difference spectra and Hill fit of TST. Right, The difference spectra and Hill Fit for ANF.

ANF is often treated as an effector molecule for steroid hydroxylation by CYP3A4, and has been shown to eliminate observed homotropic cooperativity in these reactions (*116, 194*). To probe these effects in relation to spin conversion TST was titrated in the presence of increasing amounts of ANF (Figure 2.7). Due to ANF's own ability to induce a high spin transition the starting fraction of high spin CYP3A4 is larger

at higher ANF concentrations. Fitting of these titration curves to the Hill equation reveals a decrease in TST homotropic cooperativity, as measured by the Hill coefficient, in the presence of ANF and a complete loss of homotropic cooperativity in the presence of 25 µM ANF. While this may suggest that the homotropic cooperativity of TST is being replaced with heterotropic cooperativity between the two different substrates, it is impossible to separate the additive effects of each substrate's own ability to induce a spin transition in this system.

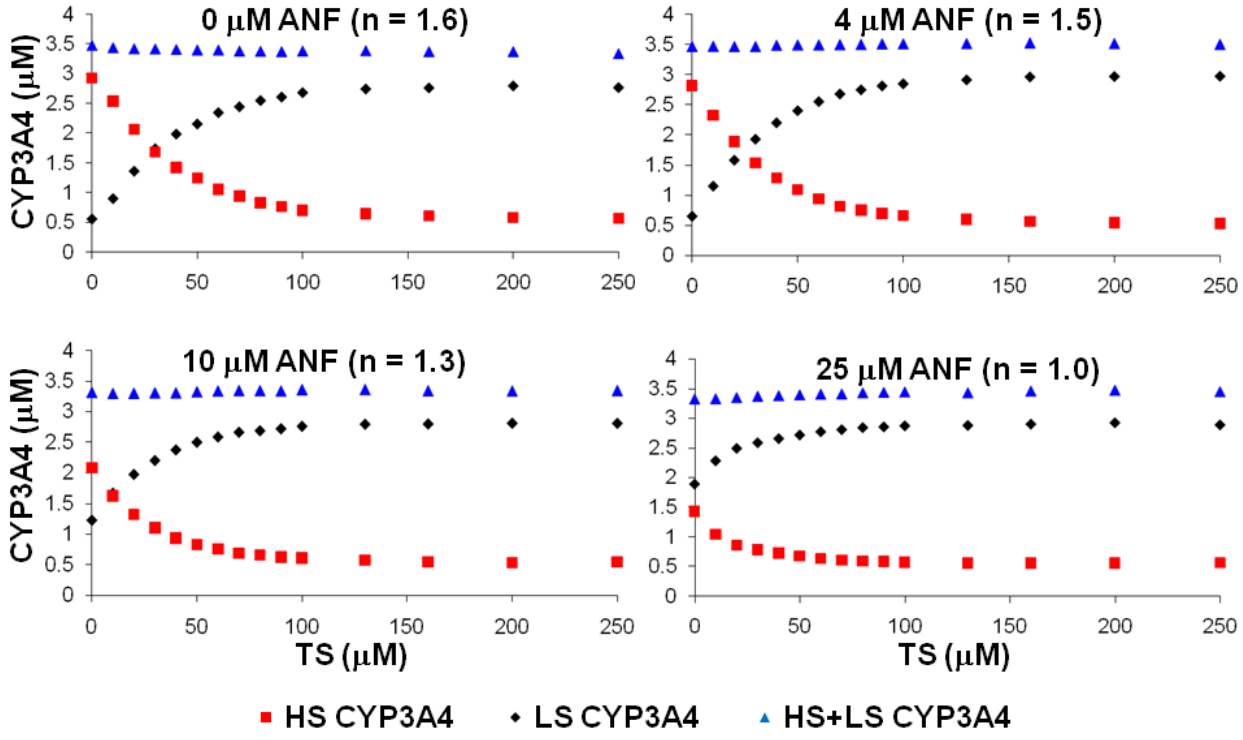

Figure 2.7 Spectral Titration of CYP3A4 Nanodiscs with TST. In the presence of 0 µM (top left), 4 µM (top right), 10 µM (bottom left), and 25 µM (bottom right) ANF.

2.3.2 Mixed Substrate Binding

To deconvolute the additive substrate effects from true heterotropic cooperativity, a series of mixed titrations was performed to examine how the spectral dissociation constant for the total substrate in the system changes as a function of the substrate ratio. In order to account for differences in each substrate's ability to induce a spin transition the concentrations were normalized by their respective S_{50} values, as calculated from single substrate titrations. The three dimensional surface of the high spin fraction was generated from the series of ANF, TST, and mixed titrations, (Figure 2.8). The similar curvature of the surface along the lines defined by equation $([TST]/S_{50,TST} + [ANF]/S_{50,ANF}) = constant$, is revealed by the straight contour lines. The latter indicates that, as the ratio of the substrates changes, the relative (or normalized) amount of two substrates needed to cause 50% spin-shift remains constant. Thus, the apparently observed stimulation caused by addition of the second substrate is entirely due to the higher total substrate concentration in the system and is not the result of any additional synergistic interaction between the substrates.

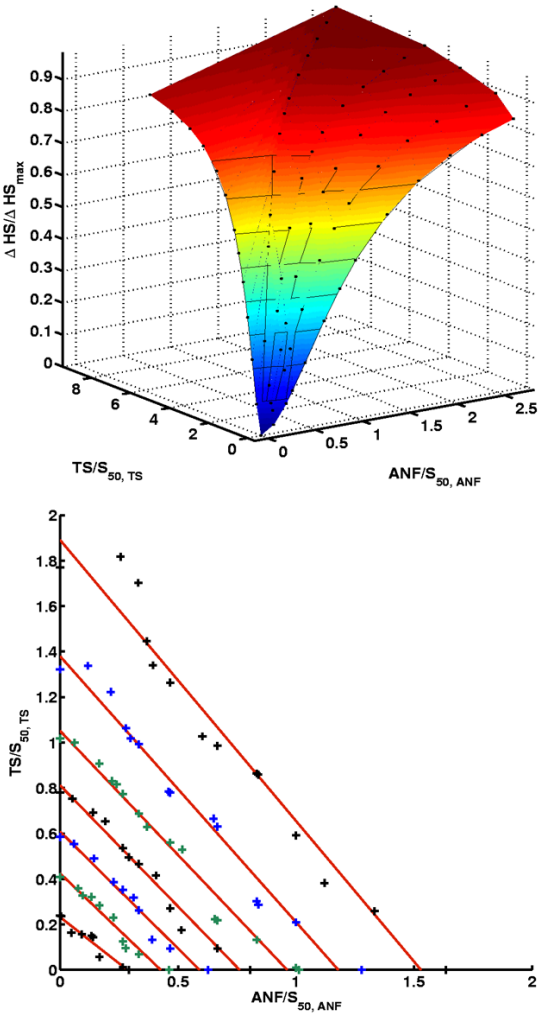

Figure 2.8 Spin Surface and Contour Lines Generated From Single Substrate and Mixed Substrate Spectral Titrations. Adapted from Frank et al. 2009.

2.4 Conclusions

Although heterotropic cooperativity for several CYP3A4 substrate pairs has been reported, typically the signal from one substrate is examined while the other is treated as an effector (*116, 189, 194, 199, 201, 232*) and the stimulatory effects referred to as

“cooperativity.” However, these approaches fail to address the full landscape of interactions, since as in the case of TST, if the first binding event is functionally silent, the distribution between the silent and active enzyme states is a function of the total substrate in the system, the relative affinities of those substrates, and their molar ratio.

The addition of a second substrate will drive the equilibrium towards the functionally competent states based upon its affinity for the enzyme. This must be taken into account to ensure that the observed changes in the equilibrium distribution are due to heterotropic cooperativity and not merely to the trivial additive effect of the presence of additional substrate in the system. We have developed an approach that evaluates the total substrate affinity of the mixed substrate system, allowing for the detection of heterotropic interactions by using mixed titrations of the substrates at various fixed molar ratios. An equation for mixed substrate affinity can be derived which is valid as long as the substrate ratio remains constant. The mixed affinity is specific for a given substrate ratio and also dependent upon the individual affinities of each of the two substrates. Using a series of mixed titrations, a three dimensional binding surface can be generated, which reveals changes in enzyme affinity as a function of substrate ratio. The affinity is measured as a result of simultaneous changes in the concentration of both substrates, allowing for the detection of the presence of additional heterotropic interactions between them, and to separate these interactions from the simple additive effect of the simultaneous binding of two different substrates (*248*).

This method, which estimates the synergistic effect of a combination of individual agents (*248*), is based on the comparison of the observed property as a function of the overall substrate concentration in a mixed titration experiment

(heterotropic titration), in which the ratio of concentrations of two substrates is kept constant, with the normalized results of the same titration experiments using pure substrates (homotropic titrations). Using this method, we have systematically studied the spin shift caused by TST and ANF taken separately and in different mixtures to establish the presence of extra heterotropic interactions between these two substrates. The presence of a secondary substrate, such as ANF, does produce an apparently stimulatory effect upon TST induced high spin shift in CYP3A4. However, this effect can be attributed entirely to the additive effect of ANF's own ability to induce a Type I spin shift, rather than any true additional heterotropic cooperativity. Thus, the well known positive heterotropic effect of ANF on the Type I titration of CYP3A4 by TST (*116, 197, 241*) can be attributed to the additive spin shift caused by ANF binding, and not due to some specific favorable interactions between these two substrates, as it was suggested previously. In addition, this method of analysis of extra heterotropic interactions is not limited to any particular compounds or to the spectral titration method, and can be used also in the studies of steady-state kinetics of product formation.

CHAPTER THREE: CO-INCORPORATION OF CYTOCHROME P450 3A4 AND CYTOCHROME P450 REDUCTASE INTO NANODISCS

3.1 Introduction

Cytochrome P450 3A4 (CYP3A4) plays an important role in the metabolism of xenobiotics and a large number of endogenous compounds in the human liver (*21*), and is the most abundant P450 in this organ (*78*). While detailed biophysical characterization of some of its soluble superfamily relatives has been accomplished, such as cyotochrome P450 101 (CYP101), including the observation of most of its reaction intermediates (*251*), the details of CYP3A4 remain elusive due to its complex behavior, including homotropic and heterotropic cooperativity, and the need for specific additives to *in vitro* reconstitution mixtures, and heterogeneity in CYP3A4 sample preparations (*118, 121-122*). Previous work done to help elucidate the role of substrate binding and thermodynamics with CYP3A4 suffers from a wide variability in techniques and additives used to reconstitute the *in vitro* system, leading to some discrepancy in the reported kinetic parameters in the literature (*124, 129, 140, 155, 186-187, 245*).

Using Nanodisc technology to self-assemble CYP3A4 into a stable lipid bilayer, has allowed for the study of a homogenous monomeric population of the enzyme into a native like state (*155-156, 240*), overcoming many of these previous obstacles. However, incorporation of CYP3A4 alone into Nanodiscs only allows for the study of the early steps in the catalytic cycle, prior to the transfer of the second electron and formation of the peroxo anion intermediate. Recent work has developed a method of

co-incorporation of CYP3A4 and its redox partner cytochrome P450 reductase (CPR) into a single Nanodisc, allowing for the study of the functional interactions of the two proteins in a catalytically active monodisperse environment (*130*). The purification and characterization of this system will be discussed here including the Type I spin-conversion and increase in steady state NADPH consumption rate caused by substrate binding.

3.2 Materials and Methods

3.2.1 Protein Expression and Purification

Cytochrome P450 3A4 (CYP3A4) with a histidine affinity tag was expressed from the NF-14 construct in the pCW Ori+ vector and purified as previously described in section 2.2.1.

Membrane Scaffold Protein 1E3D1 (MSP1E3D1) is an MSP protein that has been extended by three 22 amino acid alpha helices to form Nanodiscs with a larger diameter (*153*). It was designed using two previously described proteins, MSP1E3 and MSP1D1 (*151, 153*). The MSP1E3D1 was cloned into the pET 28 plasmid and expressed in BL-21 (DE3) Gold *E. coli* and purified as previously described in section 2.2.2.

TEV protease with a histidine affinity tag was expressed and purified as previously described in section 2.2.3.

Cytochrome P450 reductase (CPR) was expressed using the rat CPR/pOR262 plasmid, a generous gift from Dr. Todd D. Porter (University of Kentucky, Lexington, KY). Expression and purification of CPR from *E. coli* was performed using a modified procedure previously described (*130, 252-253*). The transformed *E. coli* were plated on LB agar plates containing 50 µg/ml ampicillin and incubated at 37° C overnight. A single colony was added to 10 ml of LB media containing 100 µg/ml ampicillin and shaken at 220 RPM at 37°C, and grown overnight. This was used as the starter culture for growth in 1 L LB media containing 100 µg/ml ampicillin, and 1 µg/ml riboflavin. The culture was grown at 37°C, shaken at 220 RPM until the OD_{600} reached 0.8, and was then induced with the addition of 1 mM IPTG, and grown for an additional 20 hours at 33°C, shaken at 220 RPM. The cells were harvested by centrifugation at 4000 RPM in a JA-10 rotor for 15 minutes at 4°C, resuspended in 50 mM Tris HCl, pH 8.0, 1 mM PMSF, and centrifuged again at 4000 RPM in a JA-10 rotor for 15 minutes, then frozen at -80°C for storage.

The pellet was resuspended in 400 ml/L of culture of 75 mM Tris HCl, pH 8.0, 0.25 M sucrose, 0.25 mM EDTA, 0.02 mg/ml lysozyme at 4°C, then the pellet was collected by centrifugation at 4000 RPM in a JA-10 rotor for 30 minutes. The pellet was resuspended in 50 mM Tris HCl, pH 8.0, 1 mM PMSF, on ice, and sonicated using a Branson Sonifier 450 set to a duty cycle of 80% and an output of 4 for 30 seconds and then allowed to rest on ice for three minutes, for five cycles. The membrane fraction was isolated by centrifugation at 30,000 RPM for 45 minutes in a Ti-45 rotor at 4°C, using a Beckman-Coulter L8-55m preparative ultracentrifuge. The membranes were resuspended at 4°C, with 20 ml/L of culture of 50 mM Tris HCl, pH 7.7, 0.1 mM EDTA,

0.1 mM DTT, 20% (v/v) glycerol for 1 hour, then 10% (v/v) Triton X-100 was added to a final concentration of 0.2% (v/v), and the membranes were stirred at 4°C for an additional hour.

The membrane fraction was then centrifuged at 30,000 RPM for 1 hour in a Ti-45 rotor at 4°C, using a Beckman-Coulter L8-55m preparative ultracentrifuge, and the pellet was discarded. The supernatant was applied to a column of 2'5' ADP agarose, equilibrated in 10 column volumes of 50 mM Tris HCl, pH 7.7, 0.1 mM EDTA, 0.1 mM DTT, 20% (v/v) glycerol, 0.1% (v/v) Triton X-100. The column was washed with 10 column volumes of this equilibration buffer supplemented with 2.5 mM adenosine, and eluted with equilibration buffer supplemented with 2 mM 2' AMP.

For detergent removal a DEAE column was equilibrated with 10 column volumes of 10 mM Tris HCl, pH 7.7, 0.1 mM EDTA, 0.1 mM DTT, 20% (v/v) glycerol. The 2'5' ADP agarose column elution was applied to the column, and the column was then washed with 5 column volumes of the equilibration buffer, and eluted with equilibration buffer supplemented with 0.4 M NaCl. The yellow fractions were collected and the concentration of CPR was determined using an extinction coefficient of 24.1 mM^{-1} cm^{-1} at 456 nm (*254*), and the specific activity was measured using the cytochrome c activity assay as previously described (*255*). The samples were then aliquoted and flash frozen in liquid nitrogen and stored at -80°C until use.

3.2.2 Cleavage of Histidine Tag from MSP1E3D1

TEV protease cleavage of MSP1E3D1 was performed as previously described in section 2.2.4. The final concentration of cleaved MSP1E3D1 was calculated using the

absorbance at 280 nm, and the corresponding extinction coefficient of 26.6 mM^{-1} cm^{-1} (*153*).

3.2.3 Co-Incorporation of CYP3A4 and CPR into Nanodiscs

Assembly of CYP3A4 and CPR in Nanodiscs was accomplished using the larger scaffold protein MSP1E3D1 after removal of its histidine tag by cleavage with TEV protease, following a modified procedure (*130, 252*). The general scheme is shown in figure 3.1. Purified CYP3A4 from the *E. coli* expression system was solubilized by 0.1% Emulgen 913 and mixed with purified CPR in a 1:1.75 molar ratio, and incubated on ice for 30 minutes.

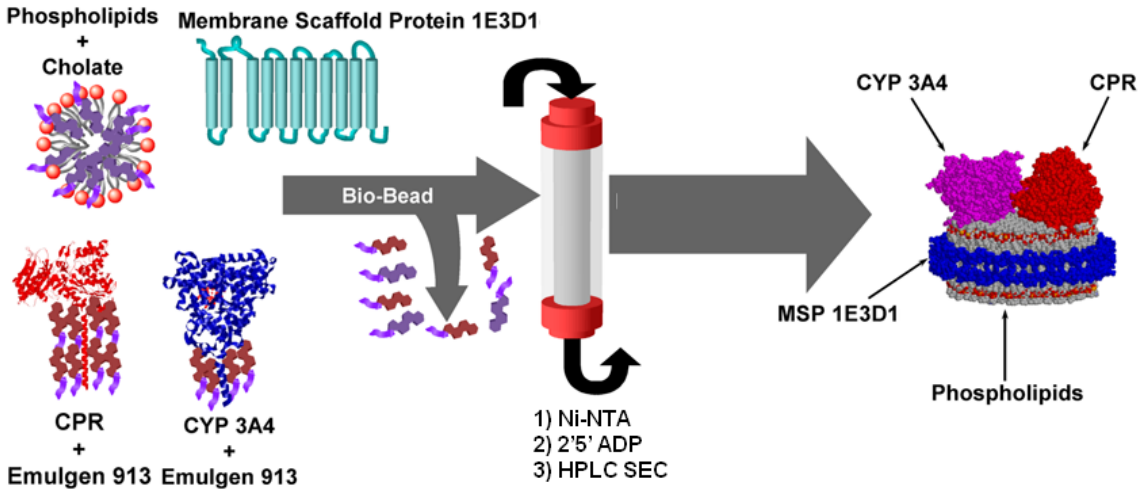

Figure 3.1 Schematic for Co-Incorporation of CYP3A4 and CPR into Nanodiscs. Adapted from Denisov et al. 2007.

A disc reconstitution mixture containing MSP1E3D1, POPC, and sodium cholate present in 1:135:270 molar ratios respectively was added to the CYP3A4-CPR mixture, with a ratio of 10:1 MSP1E3D1 to CYP3A4, yielding an average final ratio of one

CYP3A4 per five Nanodiscs. Detergents were removed by treatment with Amberlite beads (1g/ml of final reconstitution mixture), initiating a self-assembly process which incorporates the CYP3A4 and CPR proteins into a discoidal POPC bilayer ~12 nm in diameter stabilized by the encircling amphipathic MSP1E3D1 belt. The discs were purified over a 5 mL Ni-NTA agarose column, equilibrated in 50 mM potassium phosphate buffer pH = 7.4, 0.3 M NaCl, washed with equilibration buffer plus 15 mM imidazole, and eluted with equilibration buffer plus 250 mM imidazole. This removes any empty Nanodiscs, or discs containing only a CPR as the histidine tag resides on the P450. Red fractions were pooled and applied to a 5 mL 2'5' ADP agarose column equilibrated in 50 mM Tris HCl, pH 7.4, 0.1 M NaCl, which was then washed with 5 column volumes of equilibration buffer and eluted with equilibration buffer supplemented with 2.5 mM 2' AMP, eliminating Nanodiscs which do not contain a CPR protein which will not bind to this column.

The eluted Nanodiscs were concentrated and injected onto a Sephadex G-200 size exclusion column, at a flow rate of 0.5 ml/min, equilibrated in 0.1 M HEPES buffer pH = 7.5, 15 mM $MgCl_2$, 0.1 mM DTT, to remove aggregated proteins. Fractions were individually examined for bromocriptine binding, and those which did not show a ≥85% spin conversion at a saturating concentration were discarded. The remaining pooled fractions showed a minimum 90% spin conversion.

3.2.4 UV-Vis Spectroscopy

Substrate binding was studied at 1 µM CYP3A4 in Nanodiscs using a Carey 300 spectrophotometer. Absorption spectra have been measured at 37°C, in 100 mM

HEPES buffer pH 7.4, containing 7.5mM $MgCl_2$ and 0.1mM DTT. The substrates, testosterone and α-naphthoflavone, were added from stock solutions prepared at the desired molar ratio in methanol, with the final concentration of methanol never more than 1%.

3.2.5 Steady State NADPH Oxidation

Forty-five picomoles of CYP3A4-CPR co-incorporated Nanodiscs were preincubated for 3 minutes at 37˚C, in the presence or absence of substrate, in a 0.6 ml reaction volume in 100 mM HEPES buffer (pH 7.4), 7.5 mM $MgCl_2$, 0.1 mM DTT. The reaction was initiated with the addition of 200 nanomoles of NADPH. NADPH consumption was monitored for 5 minutes and calculated from the absorption changes at 340 nm using the extinction coefficient 6.22 mM^{-1} cm^{-1} for NADPH.

3.3 Results

3.3.1 Characterization of CYP3A4-CPR Nanodiscs

After purification of the CYP3A4-CPR Nanodiscs as described in section 3.2.3, the pooled fractions were characterized by optical spectroscopy to determine the ratio of CYP3A4:CPR in the sample, by comparison to the set of basis spectra for high spin CYP3A4, low spin CYP3A4, and CPR (figures 3.2 and 3.3). The high spin fraction of different sample preparations ranged from 1-7% of the total CYP3A4 with an average of 3%, while the ratio of CYP3A4:CPR varied between 1:2.3 – 1:1, with an average of 1:1.3.

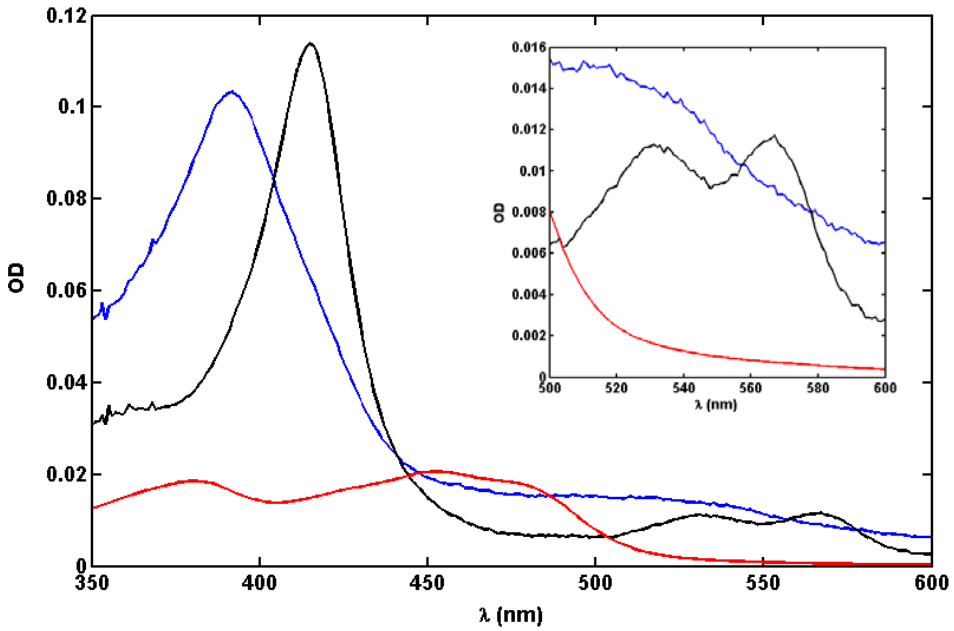

Figure 3.2 Basis Spectra for CYP3A4 and CPR. The basis spectra for low spin ferric CYP3A4 (black) high spin ferric CYP3A4 (blue) and oxidized CPR (red).

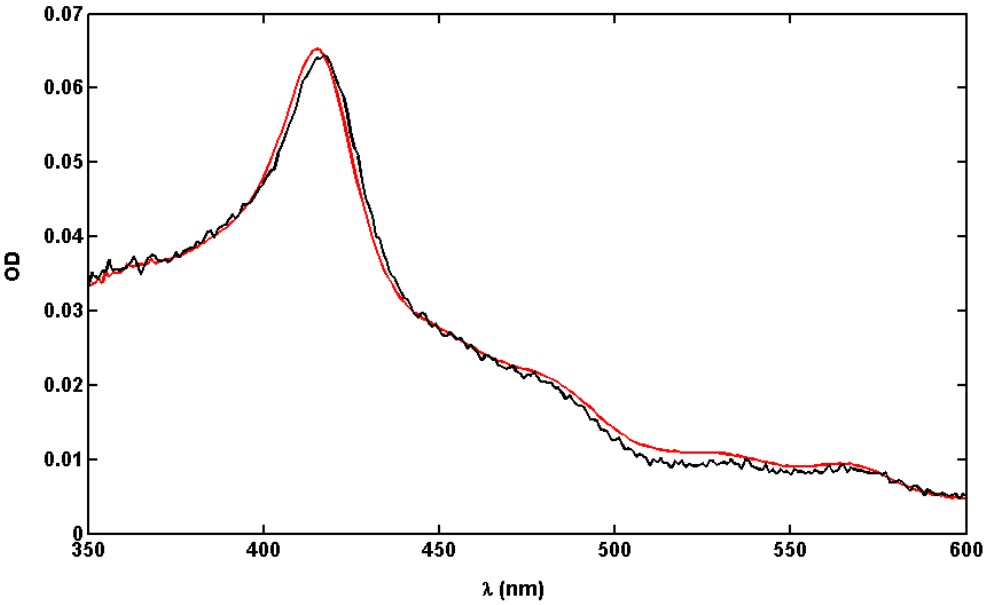

Figure 3.3 Fitting of CYP3A4-CPR Nanodiscs. UV-vis spectrum of CYP3A4-CPR Nanodisc (black), and the fit to the basis spectra of the three proteins (red).

To confirm the CYP3A4-CPR Nanodiscs were catalytically active aliquots of the sample were tested for the ability to oxidize NADPH in the presence and absence of 200 µM TST, as described in section 3.2.5. The presence of a near saturating amount of TST stimulates the activity of the enzyme by a factor of approximately four fold (*130*). A linear fit of the change in absorbance at 340 nm, along with the extinction coefficient of NADPH 6.22 mM^{-1} cm^{-1}, allows for the measurement of the rate of NADPH oxidation by the CYP3A4-CPR Nanodiscs (figure 3.4).

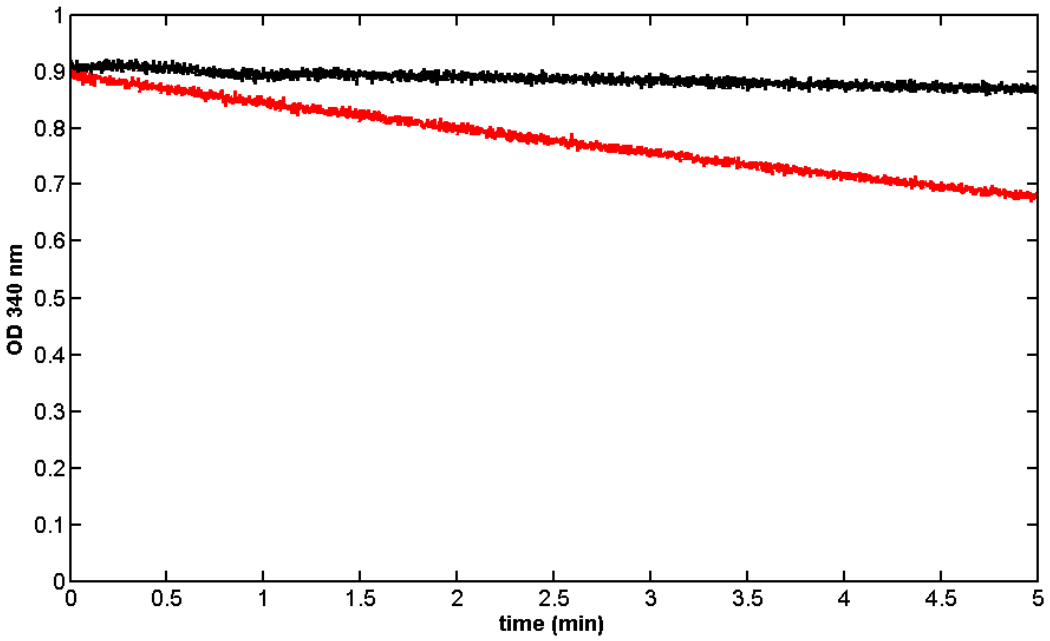

Figure 3.4 Steady State NADPH Oxidation Rate. Steady state NADPH oxidation rate measured by monitoring absorbance at 340 nm for substrate free (black) and 200 µM TST (red) CYP3A4-CPR Nanodiscs.

Substrate free NADPH oxidation rates ranged from 17 – 39 nmol/nmol/min, with an average of 23 nmol/nmol/min, and in the presence of 200 µM TST, they ranged from 77 – 158 nmol/nmol/min with an average of 107 nmol/nmol/min.

3.3.2 ANF Binding to CYP3A4-CPR Nanodiscs

It has been previously shown that CYP3A4-CPR Nanodiscs bind TST identically to CYP3A4 Nanodiscs as monitored by the heme iron spin state (*130*). Spectral analysis of ANF binding to CYP3A4-CPR discs, shown in figure 3.5, was similarly identical to that of CYP3A4 Nanodiscs. Fitting to the Hill equation yielded S_{50} = 9 µM and n = 1.6, for CYP3A4-CPR Nanodiscs compared to S_{50} = 9 µM and n = 1.8, for CYP3A4 Nanodiscs.

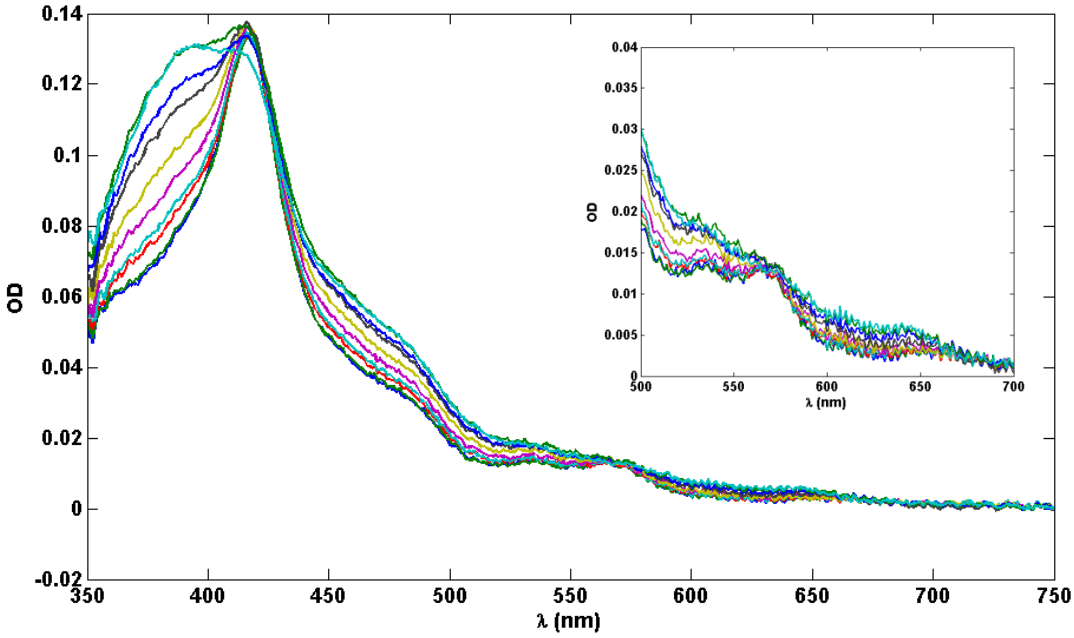

Figure 3.5 ANF Titration. Spectrum of CYP3A4-CPR Nanodiscs shifts from the ferric low spin to the ferric high spin state upon the addition of ANF.

3.3.3 CYP3A4-CPR Nanodisc Steady State NADPH Oxidation

Steady state NADPH oxidation rates were measured for TST and ANF as described in section 3.2.5. For TST the overall trend was similar to previously published results (*130*), but the magnitude was somewhat less, reaching a maximum rate of 188 nmol/nmol/min at 100 µM TST, as seen in figure 3.6. This represents a five-fold increase over the substrate free rate, as measured for this preparation of CYP3A4-CPR Nanodiscs, of 39 nmol/nmol/min. The general trend followed that of a substrate inhibition kinetic model, where later binding events have an inhibitory effect on the kinetic behavior of the enzyme (*167*), as seen by the rapid increase in the oxidation rate followed by the slower decline, to 147 nmol/nmol/min that was still a five-fold increase over the substrate free NADPH oxidation rate.

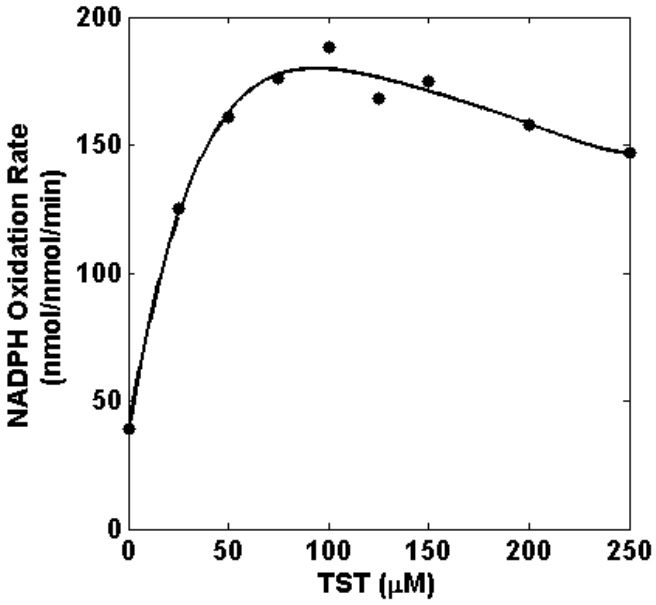

Figure 3.6 Steady State Oxidation of NADPH as a function of TST.

As for TST, ANF followed a similar substrate inhibition type curve, peaking around 5 µM ANF, at a rate of approximately 60 nmol/nmol/min, followed by a decline to 38 nmol/nmol/min, as shown in figure 3.7. However, the response was muted compared to TST, with the peak representing a three-fold increase over the substrate free rate of 20 nmol/nmol/min, and decline only providing a two-fold stimulation of the substrate free oxidation rate.

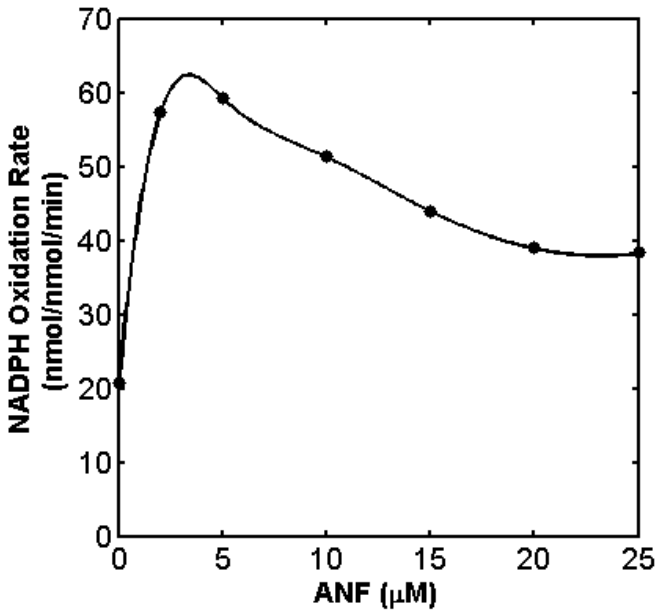

Figure 3.7 Steady State Oxidation of NADPH as a function of ANF.

3.4 Conclusions

Although the co-incorporation of CYP3A4 and its redox partner CPR into a single Nanodisc provides a homogenous monodisperse system for the systematic study of CYP3A4 kinetics the system has several drawbacks. Variability in the CYP3A4:CPR

final ratio made results difficult to replicate. This can be seen in the variability of the substrate free steady state NADPH oxidation rate, which was measured as high as 39 nmol/nmol/min, and as low as 20 nmol/nmol/min. Low yields from the three step purification process (typically <5% of starting CYP3A4), made purifying large quantities of CYP3A4-CPR Nanodiscs in a single sample difficult as well.

In order to overcome the obstacles working with CYP3A4-CPR Nanodiscs, an attempt to add full length CPR to purified CYP3A4 Nanodiscs to reconstitute a catalytically active system was made. Recently Davydov and coworkers have shown that the recombinantly expressed reductase domain from CYP102 can interact with CYP3A4 to deliver electrons (*36*), with a reduction rate of 0.037 ± .01 sec^{-1} for substrate free CYP3A4 Nanodiscs (*37*). Here, the slowest steady state NADPH oxidation rate has been measured at 0.333 sec^{-1} for substrate CYP3A4-CPR Nanodiscs, which represents a lower limit for the reduction rate of CYP3A4 by CPR in the system and is still an order of magnitude higher than that reported by Davydov and coworkers using the soluble CYP102 reductase domain. The work with CYP3A4 Nanodiscs and full length purified CPR will be discussed in chapter four.

CHAPTER FOUR: GLOBAL ANALYSIS OF HETEROTROPIC COOPERATIVITY

4.1 Introduction

In order to circumvent the difficulties working with the CYP3A4-CPR co-incorporated Nanodiscs and still evaluate the entire catalytic cycle of the enzyme purified CPR was mixed with CYP3A4 Nanodiscs to form a functional complex (*252*). This allowed for the observation of spin state, steady state NADPH oxidation, and steady state product formation, as a function of substrate concentration under identical conditions. By simultaneously fitting the three data sets to a three site binding model the individual parameters for the step wise dissociation constants and state specific functional amplitudes can be resolved as has been previously shown with testosterone using CYP3A4-CPR co-incorporated Nanodiscs (*130*).

In order to extend the global analysis to the mixed substrate system, ANF and TST were first independently analyzed for their own kinetic parameters in the CYP3A4 Nanodisc and soluble CPR system. From this analysis it is possible to construct a model based on the linear combination of the two substrates' parameters that yields the interaction surface of the two substrates in the absence of specific heterotropic interactions between them (*247-248*). The model's predictions were then compared to the observed behavior of a mixed substrate system in order to draw conclusions about the presence or absence of heterotropic cooperativity. To examine the effects of heterotropic cooperativity, parameters were introduced into the model that influence the population of the mixed states relative to the non-mixed states. The changes in the

distributions of the enzyme substrate complexes show how heterotropic cooperativity affects the enzyme's overall behavior.

This chapter describes the analysis of the two single substrate systems, the mixed substrate system (using a 1:3 molar ratio of ANF:TST), and the construction of the non-cooperative reference model.

4.2 Materials and Methods

4.2.1 Protein Expression and Purification

Cytochrome P450 3A4 (CYP3A4) with a histidine affinity tag was expressed from the NF-14 construct in the pCW Ori+ vector and purified as previously described in section 2.2.1.

Membrane Scaffold Protein 1D1 (MSP1D1) was cloned into the pET 28 plasmid and expressed in BL-21 (DE3) Gold *E. coli* and purified as previously described in section 2.2.2.

TEV protease with a histidine affinity tag was expressed and purified as previously described in section 2.2.3.

Cytochrome P450 reductase (CPR) was expressed using the rat CPR/pOR262 plasmid, and expressed and purified as previously described in section 3.2.1.

4.2.2 Cleavage of Histidine Tag from MSP1D1

TEV protease cleavage of MSP1D1 was performed as previously described in section 2.2.4.

4.2.3 Incorporation of CYP3A4 into Nanodiscs

Cytochrome P450 3A4 was incorporated into Nanodiscs using the self-assembly process as described in section 2.2.6.

4.2.4 UV-Vis Spectroscopy

Substrate binding was studied at 1 µM CYP3A4 in Nanodiscs using a Carey 300 spectrophotometer. Absorption spectra were measured at 37°C, in 100 mM HEPES buffer pH 7.4, containing 7.5mM $MgCl_2$ and 0.1mM DTT. The substrates, testosterone and α-naphthoflavone, were added from stock solutions prepared at the desired molar ratio in methanol, with the final concentration of methanol never more than 1%.

4.2.5 Counter Flow Job's Titration

The counter flow Job's titration was performed using a modified method as previously described (*256*). Equal volumes, 600 µL, of either 1 µM CYP3A4 Nanodiscs or purified CPR, were placed into the front and rear compartments of a split cell tandem cuvette. The titration was performed by making reciprocal displacements of 20 µL of the solutions between the compartments. Changes in the heme iron spin state were monitored by UV-vis spectroscopy and fit to the equation:

$$F_{1,i} = F_{1,i-1}(1-v_i/V)+(1-F_{1,i-1})(vi/V); \quad F_{1,1} = 0$$

Where $F_{1,i}$ is the fraction of the ligand in the first compartment at the i-th step of the titration, and v_i and V are the volume of the aliquot displaced at the i-th step and the

total volume in each of the compartments, respectively. The fitting program was written in MATLAB using the Nelder-Mead simplex minimization algorithm implemented in the subroutine “fminsearch.m.”

4.2.6 Steady State NADPH Oxidation

Forty-five picomoles of CYP3A4 Nanodiscs were mixed with 157.5 picomoles of CPR and preincubated for 3 minutes at 37˚C, in the presence or absence of substrate, in a 1 ml reaction volume in 100 mM HEPES buffer (pH 7.4), 7.5 mM $MgCl_2$, 0.1 mM DTT. The reaction was initiated with the addition of 200 nanomoles of NADPH. NADPH consumption was monitored for 5 minutes and calculated from the absorption changes at 340 nm using the extinction coefficient 6.22 mM^{-1} cm^{-1} for NADPH. The reaction was quenched with the addition of 10 µl of sulfuric acid, frozen on liquid nitrogen and stored at -80˚ C.

4.2.7 Steady State Product Formation

The frozen samples from the steady state NADPH oxidation experiments were thawed and divided into two 450 µl aliquots to which 6 nmol of cortexolone was added as an internal standard before extraction against 2 ml dichloromethane. The samples were dried under nitrogen gas, resuspended in 70 µl of methanol, and 50 70 µl was loaded onto a Waters Nova-Pak C_{18} column (2.1 x 150 mm), with a flow rate of 0.5 ml/min, and linear gradients of 90% buffer A, 95% water, 5% acetonitrile, 0.1% formic acid and 10% buffer B, 5% water, 95% acetonitrile, 0.1% formic acid to 40% A at 15 min, and 33% A at 17 min, and isocratic flow of 33% A to 40 min. TST and its metabolites were monitored at 240 nm and concentrations were determined using the

extinction coefficient of 18.9 mM^{-1} cm^{-1}, and confirmed by comparison to commercially available standards for 2β-, 6β-, and 15β-OH TST (*130*). ANF and its metabolites were monitored at 290 nm and concentrations were calculated using the extinction coefficient of 23.7 mM^{-1} cm^{-1} (*194*). Standards for the ANF metabolites, the 7,8-dihydrodiol and 5,6-epoxide, were not commercially available, and their identification was surmised from published elution profiles and relative elution times (*194, 257*) (figure 4.1).

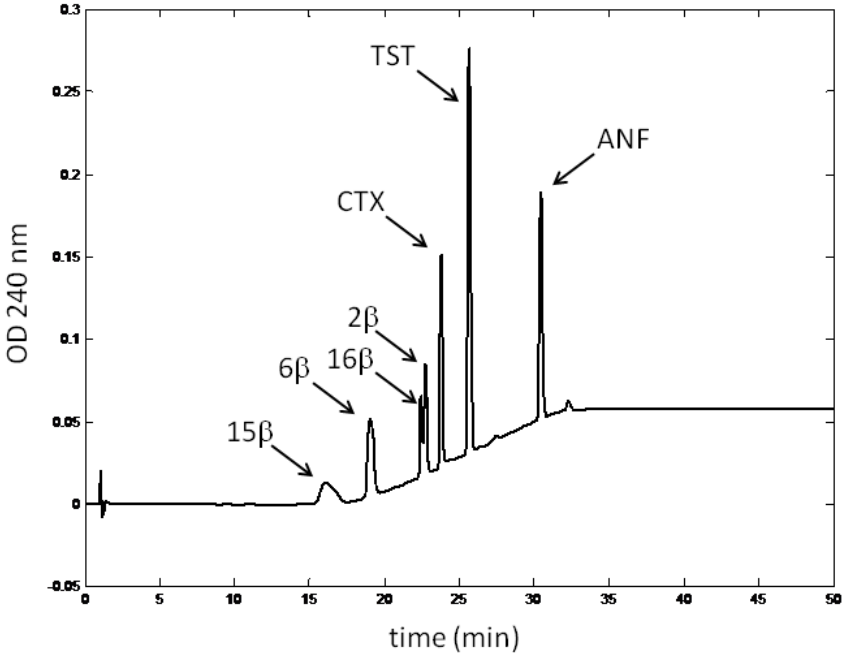

Figure 4.1 Elution Profile for Commercially Available Standards.

4.2.8 Global Analysis Fitting

Global analysis for the three site binding model was performed as previously described (*130*), by simultaneously fitting the experimental data sets to the four state model shown in Scheme 4.1, where E is the concentration of substrate free CYP3A4, S

is the substrate concentration, and ES_i is the concentration of the binding intermediates, complexes of CYP3A4 with i molecules of substrate bound (i = 0,1,2,3):

$$E + S \overset{K_1}{\longleftrightarrow} ES_1 + S \overset{K_2}{\longleftrightarrow} ES_2 + S \overset{K_3}{\longleftrightarrow} ES_3$$

Scheme 4.1

The fractions of the enzyme substrate complexes were expressed using the standard binding polynomials,

$$Y = \frac{\frac{S}{K_1} + \frac{S^2}{K_1K_2} + \frac{S^3}{K_1K_2K_3}}{1 + \frac{S}{K_1} + \frac{S^2}{K_1K_2} + \frac{S^3}{K_1K_2K_3}}$$

and the functional properties at different substrate concentrations were represented as the linear combination of the fractional contributions from binding intermediates. For example, the fraction of the high-spin CYP3A4 in the Type I titrations, Y_S, is calculated as the weighted sum of the signals from the cytochrome P450 molecules with 0, 1, 2, or 3 substrate molecules bound, having a_0, a_1, a_2, and a_3 fractions of high-spin state correspondingly:

$$Y_S = \frac{a_0 + \frac{a_1S}{K_1} + \frac{a_2S^2}{K_1K_2} + \frac{a_3S^3}{K_1K_2K_3}}{1 + \frac{S}{K_1} + \frac{S^2}{K_1K_2} + \frac{S^3}{K_1K_2K_3}}$$

For the two site binding model, the final term of the equations were dropped to represent the three state binding scheme so that the binding polynomials were of the form:

$$Y = \frac{\frac{S}{K_1} + \frac{S^2}{K_1 K_2}}{1 + \frac{S}{K_1} + \frac{S^2}{K_1 K_2}}$$

And the equations for the functional properties were given by:

$$Y_S = \frac{a_0 + \frac{a_1 S}{K_1} + \frac{a_2 S^2}{K_1 K_2}}{1 + \frac{S}{K_1} + \frac{S^2}{K_1 K_2}}$$

The set of such equations for the spectral titration, NADPH consumption, and product formation have been used for the simultaneous fitting of the experimental data obtained under the same conditions, using the same set of dissociation constants which yeilds a total of twelve parameters. The fitting program was written in MATLAB using the Nelder-Mead simplex minimization algorithm implemented in the subroutine "fminsearch.m."

4.2.9 Error Analysis

A Monte Carlo simulation was used to estimate the statistical errors of the fitted parameters. A normally distributed random error was introduced into each fitted data set, using standard deviations of 2% for spin shift, 1 nmol/nmol/min for NADPH oxidation, and 0.1 nmol/nmol/min for product formation. A 67% confidence interval for each parameter value from the fits of 200 error-added data sets was used to estimate the error (*258-259*). The error fitting programs were written in MATLAB using the Nelder-Mead simplex minimization algorithm implemented in the subroutine "fminsearch.m."

4.2.10 Mixed Substrate Modeling

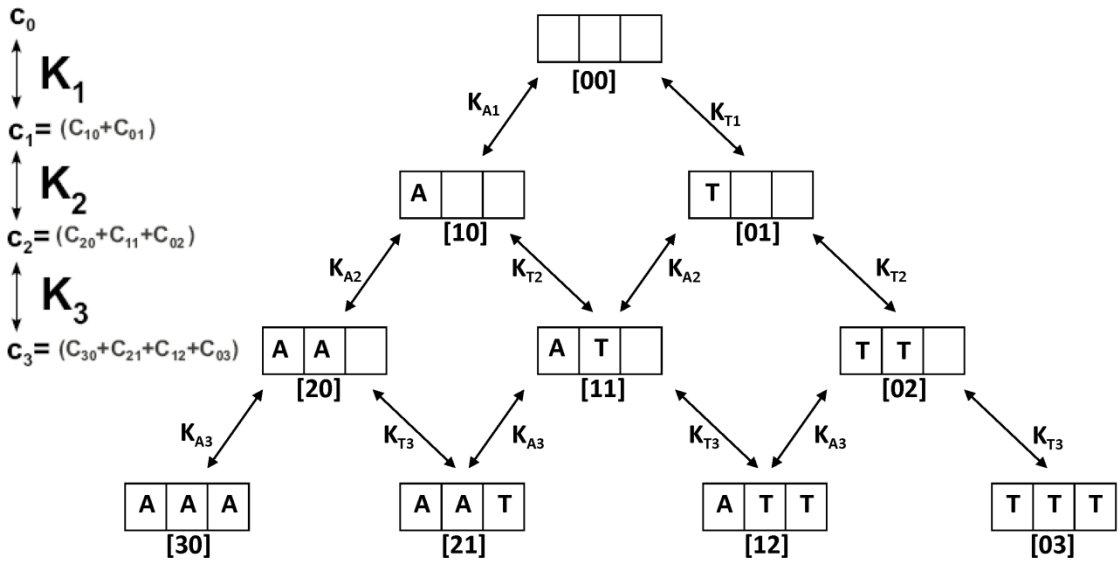

Scheme 4.2

The ten state pyramidal binding model (Scheme 4.2), is used for an enzyme which can bind up to three total molecules of two different substrates. It is an extension of Scheme 1 which is incorporated along the outer pathways of Scheme 4.2. Binding constants K_A and K_T, represent ANF and TST respectively, and are the same for each binding step if there is an absence of intrinsic heterotropic cooperativity, i.e. binding of the next substrate molecule may depend on the presence of previously bound substrates ($K_{A1} \neq K_{A2}$). Scheme 4.2 also includes three mixed states where the enzyme interacts simultaneously with both substrates. In the case of a titration with a mixture of substrates at a constant substrate ratio Scheme 4.2 can be formally represented by Scheme 4.1, where S is the total substrate in the system (here, A + T), and the mixed

binding constants, K_i, are given by the average of the respective K_{Ai} and K_{Ti}, weighted against their molar ratio:

$$K_1 = \mu_A K_{A1} + \mu_T K_{T1}$$

$$K_2 = \mu_A K_{A2} + \mu_T K_{T2}$$

$$K_3 = \mu_A K_{A3} + \mu_T K_{T3}$$

where μ_A and μ_T represent the molar fractions of ANF and TST respectively. Thus each ratio of the two substrates can be represented by its own set of mixed binding constants, and analyzed based upon the global analysis versus total substrate concentration, as if it were a single substrate.

The non-cooperative model for the interactions of ANF and TST was developed in MATLAB and is shown in figure 4.2. In the absence of specific interactions between the two substrates the binding polynomials and functional properties of the enzyme will be equivalent to the linear combination of the two substrates at the given molar ratio.

The total substrate [S] is equal to the sum of the individual substrates, [A] and [T], and μ_A and μ_T represent the molar fractions of A and T respectively.

$$[S] = [A] + [T]$$

$$\mu_A[S] = [A]$$

$$\mu_T[S] = [T]$$

The concentration of enzyme with one substrate bound, c_1, is given by the sum of the concentrations of the two states of the enzyme with a single substrate molecule

bound, c_{01} and c_{10}. Here, K_i's represent association constants for ease of displaying the equations.

$$c_1 = c_{01} + c_{10} = EK_1[S] = EK_{A1}[A] + EK_{T1}[T] = E\mu_A K_{A1}[S] + E\mu_T K_{T1}[S]$$

$$K_1 = \mu_A K_{A1} + \mu_T K_{T1}$$

The concentration of enzyme with two substrates bound, c_2, is given by the sum of the concentrations of the three states of the enzyme with a two substrate molecules bound, c_{02}, c_{20} and c_{11}.

$$c_2 = c_{02} + c_{20} + c_{11} = EK_1K_2[S] = EK_{A1}K_{A2}[A] + EK_{T1}K_{T2}[T] + EK_{T1}K_{A2}[A] + EK_{A1}K_{T2}[T]$$

$$K_1K_2[S] = \mu_A^2 K_{A1}K_{A2}[S] + \mu_T^2 K_{T1}K_{T2}[S] + \mu_T\mu_A(K_{A1}K_{T2} + K_{T1}K_{A2})[S]$$

$$K_2 = (\mu_A K_{A1} + \mu_T K_{T1})(\mu_A K_{A2} + \mu_T K_{T2})/K_1$$

$$K_2 = \mu_A K_{A2} + \mu_T K_{T2}$$

The concentration of enzyme with three substrates bound, c_3, is given by the sum of the concentrations of the four states of the enzyme with a three substrate molecules bound, c_{03}, c_{30}, c_{21} and c_{12}.

$$c_3 = c_{03} + c_{30} + c_{21} + c_{12} = EK_1K_2K_3[S] = EK_{A1}K_{A2}K_{A3}[A] + EK_{T1}K_{T2}K_{T3}[T] +$$
$$EK_{A1}K_{T2}K_{A3}[A] + EK_{A1}K_{A2}K_{T3}[T] + EK_{T1}K_{A2}K_{A3}[A] + EK_{T1}K_{T2}K_{A3}[A] + EK_{T1}K_{A2}K_{T3}[T] +$$
$$EK_{A1}K_{T2}K_{T3}[T]$$

$$K_1K_2K_3[S] = \mu_A^3 K_{A1}K_{A2}K_{A3}[S] + \mu_T^3 K_{T1}K_{T2}\,K_{T3}[S] + \mu_A^2\mu_T(K_{A1}K_{T2}K_{A3} + K_{A1}K_{A2}K_{T3} +$$
$$K_{T1}K_{A2}K_{A3})[S] + \mu_A\mu_T^2(K_{T1}K_{T2}K_{A3} + K_{T1}K_{A2}K_{T3} + K_{A1}K_{T2}K_{T3})[S]$$

$$K_3 = (\mu_A K_{A1} + \mu_T K_{T1})(\mu_A K_{A2} + \mu_T K_{T2})(\mu_A K_{A3} + \mu_T K_{T3})/K_1 K_2$$

$$K_3 = \mu_A K_{A3} + \mu_T K_{T3}$$

This allows for binding constants of the mixed substrate system to be evaluated according to equation 1, by combining the mixed and non-mixed states for a given number of substrates bound into a single state. In order to simulate specific heterotropic interactions, it is necessary to separate the mixed and non-mixed states so that:

$$K_1 = \mu_A K_{A1} + \mu_T K_{T1}$$

$$K_2 = (\mu_A^2 K_{A1} K_{A2} + \mu_T^2 K_{T1} K_{T2} + \gamma_1 \mu_T \mu_A (K_{A1} K_{T2} + K_{T1} K_{A2}))/K_1$$

$$K_3 = (\mu_A^3 K_{A1} K_{A2} K_{A3} + \mu_T^3 K_{T1} K_{T2} K_{T3} + \gamma_2 \mu_A^2 \mu_T (K_{A1} K_{T2} K_{A3} + K_{A1} K_{A2} K_{T3} + K_{T1} K_{A2} K_{A3}) +$$
$$\gamma_3 \mu_A \mu_T^2 (K_{T1} K_{T2} K_{A3} + K_{T1} K_{A2} K_{T3} + K_{A1} K_{T2} K_{T3}))/K_1 K_2$$

and γ_1, γ_2, and γ_3 represent heterotropic parameters, which indicate favorable (or unfavorable) binding for the mixed states relative to the non-mixed states.

To incorporate functional properties, such as spin transition, the mixed and non-mixed states may have different functional amplitudes, it is also necessary to for them to be considered separately:

$$a_1 K_1 = a_{A1} \mu_A K_{A1} + a_{T1} \mu_T K_{T1}$$

$$a_2 K_2 = (a_{A2} \mu_A^2 K_{A1} K_{A2} + a_{T2} \mu_T^2 K_{T1} K_{T2} + a_{M1} \mu_T \mu_A (K_{A1} K_{T2} + K_{T1} K_{A2}))/a_1 K_1$$

$$a_3 K_3 = (a_{A3} \mu_A^3 K_{A1} K_{A2} K_{A3} + a_{T3} \mu_T^3 K_{T1} K_{T2} K_{T3} + a_{M2} \mu_A^2 \mu_T (K_{A1} K_{T2} K_{A3} + K_{A1} K_{A2} K_{T3} +$$
$$K_{T1} K_{A2} K_{A3}) + a_{M3} \mu_A \mu_T^2 (K_{T1} K_{T2} K_{A3} + K_{T1} K_{A2} K_{T3} + K_{A1} K_{T2} K_{T3}))/a_1 K_1 a_2 K_2$$

where a_{Ai} and a_{Ti} represent the functional amplitudes from the non-mixed states of ANF and TST respectively with i substrates bound (I = 0, 1, 2, or 3), and the mixed state amplitudes a_{Mi} are given by the average of the non-mixed amplitudes:

$$a_{M1} = (a_{A2} + a_{T2})/2$$

$$a_{M2} = (2*a_{A3} + a_{T3})/3$$

$$a_{M3} = (a_{A3} + 2*a_{T3})/3$$

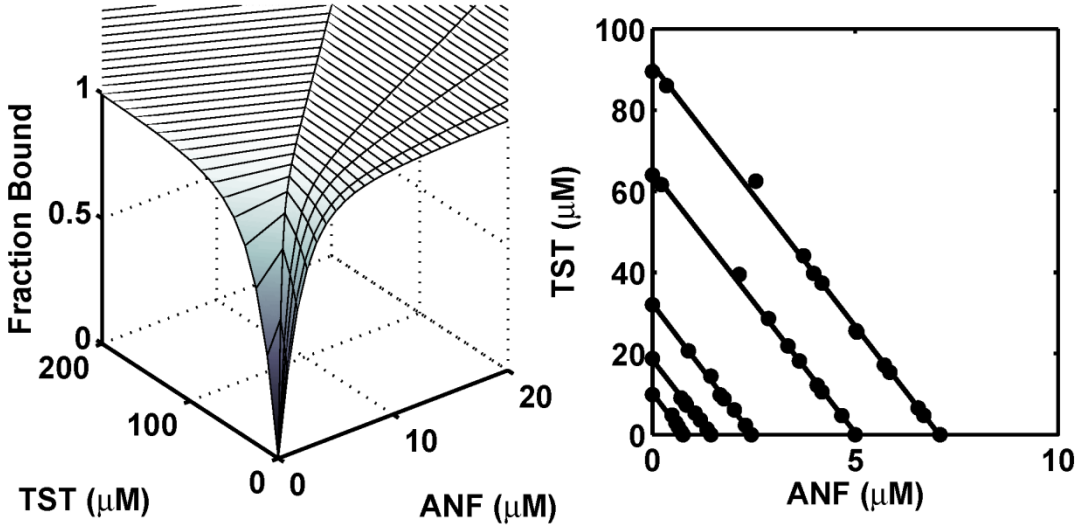

Figure 4.2 Non-Cooperative Surface and Contours. Generated in MATLAB. Adapted from Frank et al. 2011.

4.3 Results

4.3.1 Interactions of CYP3A4 Nanodiscs and Purified CPR

In order to probe the interactions of CYP3A4 in Nanodiscs with purified CPR, a counter flow Job's titration was performed as described in section 4.2.5. This method has been used to show the stoichiometry and affinity for CYP3A4 in Nanodiscs with the soluble reductase domain of CYP102 (*37*), by monitoring the shift to the high spin heme iron state in CYP3A4 induced by association between the reductase and the cytochrome P450. Fitting the changes high spin CYP3A4 amplitude revealed a 1:1 complex formation, revealed by the shape of the curve, which corresponds to the ascending branch of a traditional Job's titration, and peaks at $F_1 = 0.5$, with a K_D of 130 nM (figure 4.3), although due to the small overall change in high spin fraction (<10%), the previously reported K_D of 50 nM measured by size exclusion chromatography may be more accurate (*252*).

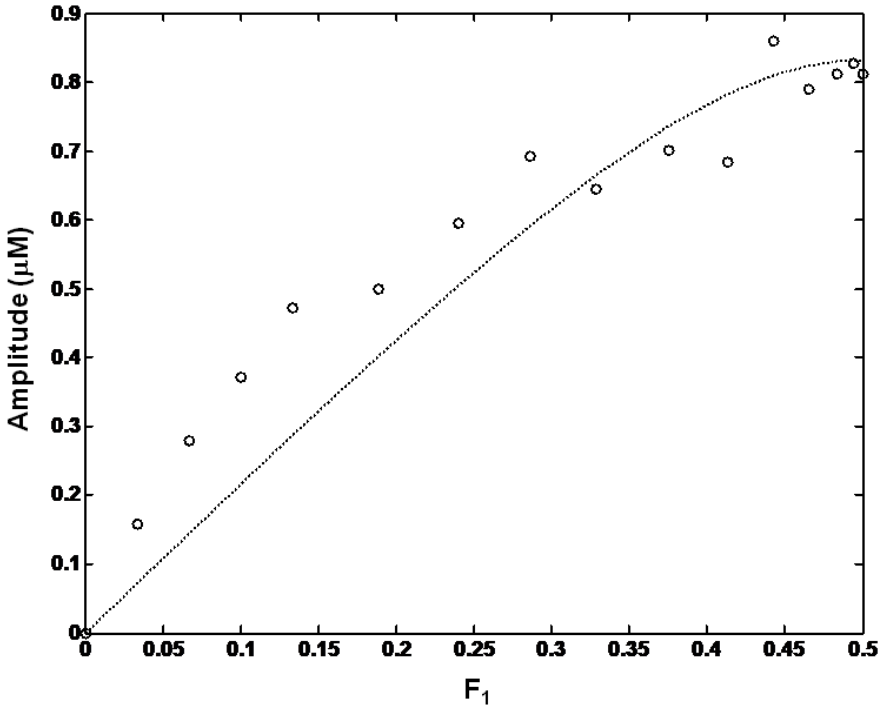

Figure 4.3 Counter Flow Job's Titration Fit of High Spin Amplitude of CYP3A4.

4.3.2 Global Analysis of Testosterone and α-Naphthoflavone

Simultaneous fitting of the three observed enzyme properties, heme iron spin state, NADPH oxidation, and product formation, for each substrate to a three site binding model as described in section 4.2.8, allowed for the deconvolution of the individual stepwise dissociation constants along with resolution of the fractional contributions of the binding intermediates to the overall behavior of the enzyme as a function of substrate concentration (figures 4.5 and 4.6). Attempts to fit the data for either substrate to a two site nonspecific model failed, yielding negative values for two physiological parameters, the spin amplitude and the product formation rate of the ES complex (figure 4.4).

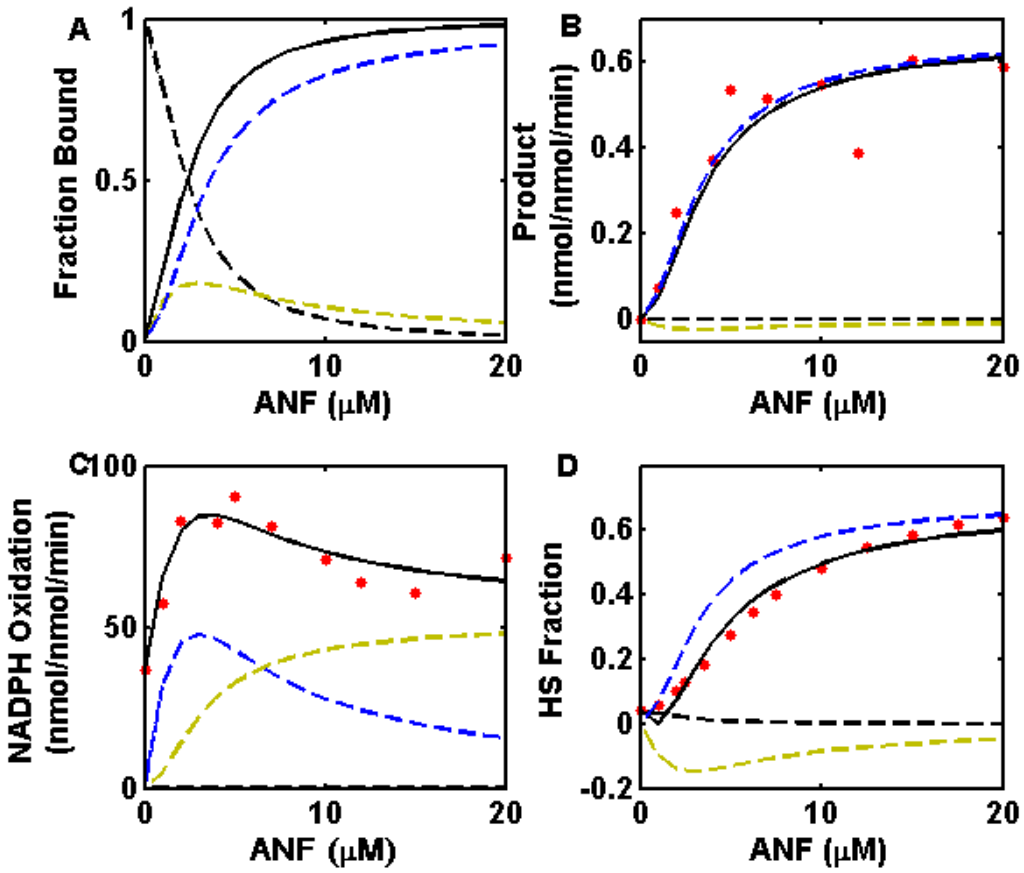

Figure 4.4 Global Fitting of ANF Titrations to a Two Site Binding Model. The experimental data (red circles) for production formation (B), NADPH oxidation (C), and high spin fraction (D), were simultaneously fit to a two site nonspecific binding model, resulting in the global fit for each parameter (black lines), and the overall binding saturation (A). The signal from each intermediate, with 0, 1, or 2, ANF molecules bound is shown by the black, yellow, and blue, dashed lines respectively.

The properties of CYP3A4 follow similar trends for both ANF and TST, such as the fast acceleration and subsequent drop off in steady-state NADPH consumption with increasing substrate concentration. The binding of ANF is approximately one order of magnitude tighter than that of TST, with K_D's of 2, 3, and 7 μM and 27, 46, and 62 μM

respectively (table 1). The binding of the first substrate molecule, forming the ES complex, increases the NADPH oxidation rate by several fold for both substrates, to 182 nmol/nmol/min for TST and 106 nmol/nmol/min for ANF, although it does not induce product formation for either. For TST (22%), but not ANF (4%), this intermediate also provides a small contribution to the spin shift. The binding of the second molecule of substrate forms the ES_2 complex, opens the product forming pathway of the enzyme and further stimulates the NADPH oxidation rate. For TST, both the NADPH oxidation rate and product forming rate are higher than for ANF (344 and 18 nmol/nmol/min for TST and 115 and 0.8 nmol/nmol/min for ANF) and it correlates with a large shift to the high spin state, 83% for TST, but not for ANF (4%). The ES_3 complex is formed with the binding of the third substrate molecule increasing the coupling efficiency (the ratio of the product formation to NADPH consumption) by decreasing NADPH consumption rather than stimulating product forming rates. The third ANF binding also induces the Type I spin transition (89%) which is observed to occur at the second binding event for TST (83%), and is similar upon the formation of the ES_3 complex (84%).

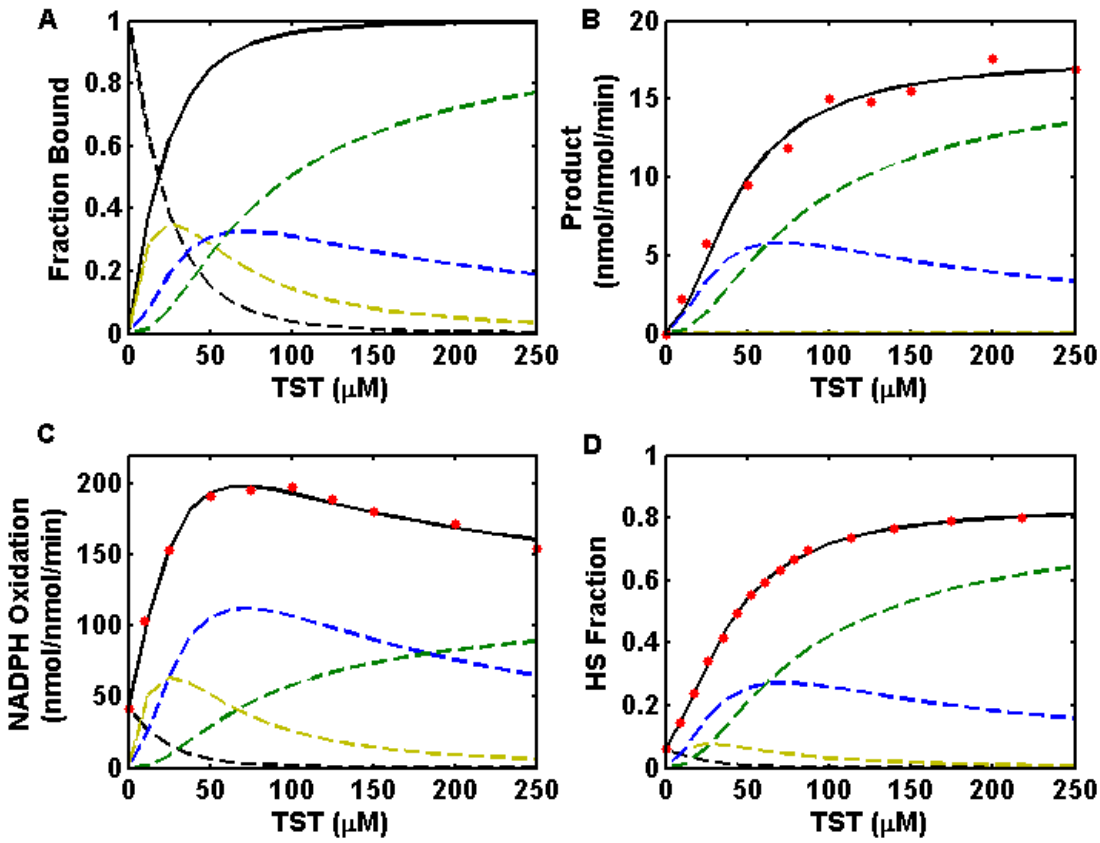

Figure 4.5 Global Fitting of TST Titrations to a Three Site Binding Model. The experimental data (red circles) for production formation (B), NADPH oxidation (C), and high spin fraction (D), were simultaneously fit to a three site nonspecific binding model, resulting in the global fit for each parameter (black lines), and the overall binding saturation (A). The signal from each intermediate, with 0, 1, 2, or 3 TST molecules bound is shown by the black, yellow, blue, and green dashed lines respectively. Adapted from Frank et al. 2011.

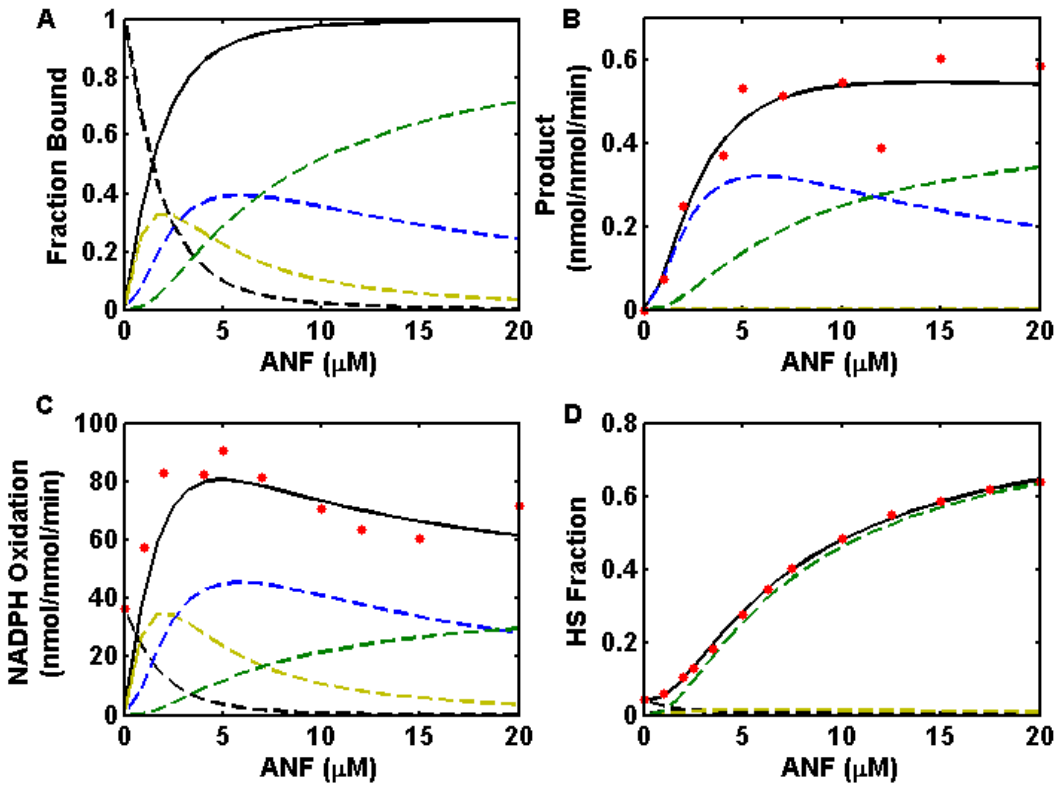

Figure 4.6 Global Fitting of ANF Titrations to a Three Site Binding Model. The experimental data (red circles) for production formation (B), NADPH oxidation (C), and high spin fraction (D), were simultaneously fit to a three site nonspecific binding model, resulting in the global fit for each parameter (black lines), and the overall binding saturation (A). The signal from each intermediate, with 0, 1, 2, or 3 ANF molecules bound is shown by the black, yellow, blue, and green dashed lines respectively. Adapted from Frank et al. 2011.

TST K_D (μM)	27 [23 – 35.5] **Spin Shift (%)**	46 [38 – 52] **NADPH Rate (nmol/nmol/min)**	62 [52 – 77] **Product Forming Rate (nmol/nmol/min)**
E	6±2.0	42±1.0	0±0.1
	-	-	-
ES	22	182	0
	[17 – 32]	[159 – 224]	[0.01 – 0.06]
ES_2	83	344	18
	[71 – 91]	[303 – 375]	[16.6 – 18.7]
ES_3	84	115	18
	[80 – 88]	[112 – 120]	[17.3 – 17.8]
ANF K_D (μM)	2 [1.4 – 3.2] **Spin Shift (%)**	3 [2.3 – 5.1] **NADPH Rate (nmol/nmol/min)**	7 [5 – 8.4] **Product Forming Rate (nmol/nmol/min)**
E	4±2.0	36±1.0	0±0.1
	-	-	-
ES	4	106	0
	[4 – 7.8]	[81 – 140]	[0 – 0.04]
ES_2	4	115	0.8
	[3.8 – 7.0]	[89 – 122]	[0.55 – 1.24]
ES_3	89	41	0.5
	[82 – 94]	[35 – 49]	[0.27 – 0.62]

Table 4.1 Parameters from the Global Fits of ANF and TST. Adapted from Frank et al. 2011.

4.3.3 Global Analysis of α-Naphthoflavone and Testosterone in a 1:3 Molar Ratio

The same trends are followed for the mixed substrate system that were observed for each of the functional properties in both single substrate systems, such as the lack of product formation coming from the ES complex, and the inhibition of NADPH oxidation at higher substrate concentrations (figure 4.7 and table 4.2). While binding of the first substrate triggers an increase in NADPH oxidation rate from 37 nmol/nmol/min to 195 nmol/nmol/min, and it is entirely uncoupled resulting in no product formation. A second substrate molecule must bind for the product forming pathway to open, at a rate

of 4 nmol/nmol/min and the NADPH oxidation rate decreases to 80 nmol/nmol/min. The third binding event does not significantly alter the rate of product formation or NADPH oxidation, but does induce a shift to the high spin state of the heme iron.

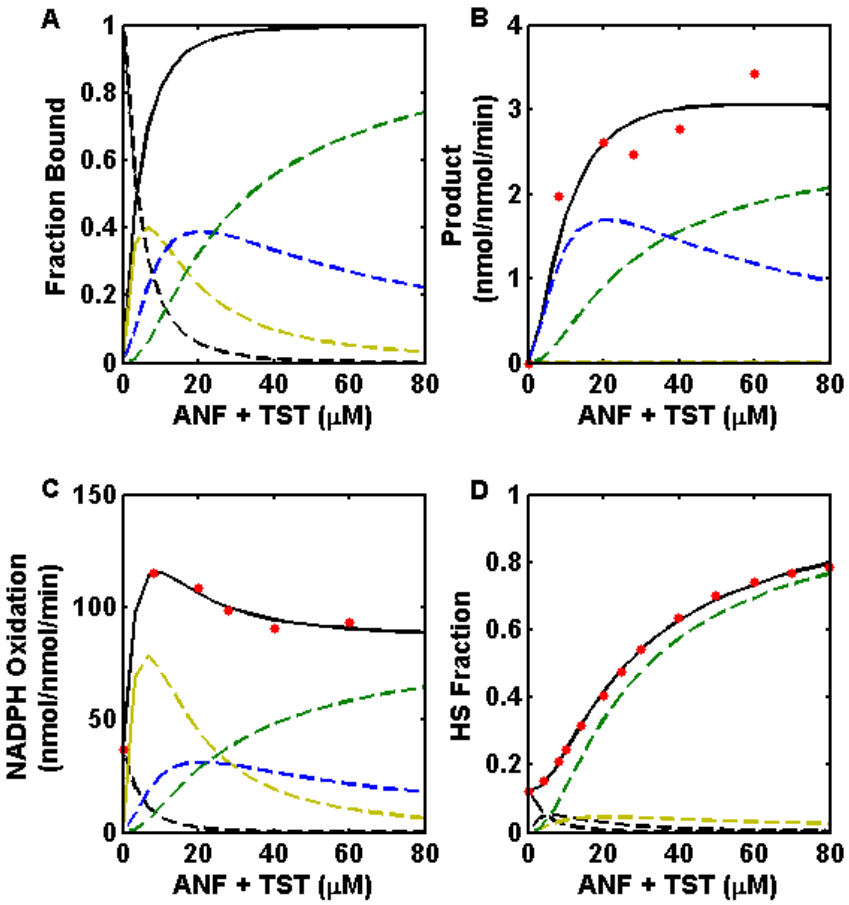

Figure 4.7 Global Fitting of Mixed Substrate Titrations to a Three Site Binding Model. The experimental data (red circles) for production formation (B), NADPH oxidation (C), and high spin fraction (D), were simultaneously fit to a three site nonspecific binding model, resulting in the global fit for each parameter (black lines), and the overall binding saturation (A). The signal from each intermediate, with 0, 1, 2, or 3 substrate molecules bound is shown by the black, yellow, blue, and green dashed lines respectively. Adapted from Frank et al. 2011.

1:3 Mix K_D (μM)	5 [2 – 6] **Spin Shift (%)**	12 [12 – 19] **NADPH Rate (nmol/nmol/min)**	24 [19 – 24] **Product Forming Rate (nmol/nmol/min)**
E	12±2.0 -	37±1.0 -	0±0.1 -
ES	13 [11.7 –14.3]	195 [149 – 205]	0 [0 – 0.01]
ES_2	12 [11.7 -14.1]	80 [54 – 90]	4 [4 – 5.6]
ES_3	103 [100]*	87 [82 – 92]	3 [2.3 – 3]

Table 4.2 Parameters from the Global Fits of the Mixed Substrate System.

Adapted from Frank et al. 2011.

4.3.4 Global Model of α-Naphthoflavone and Testosterone Interactions with CYP3A4

Building upon the linear four state binding models (scheme 4.1) for each substrate, a ten state pyramidal model was developed to account for a mixed substrate system in which CYP3A4 can accommodate up to three molecules of either substrate into the active site (scheme 4.2). The stepwise binding constants for ANF and TST along with functional amplitudes for the outer non-mixed states are given through a global analysis of each substrate (table 4.1). For the three mixed states the average values of the non-mixed amplitudes derived from the homotropic global fits have been used, as it is impossible to directly measure these properties. Since this model is based upon the linear combination of each substrate's global fits, it represents a system without any specific heterotropic cooperativity, but intrinsically includes each substrate's own homotropic cooperativity, if present.

To test the possible effect of heterotropic interactions, a 1:3 ANF:TST titration was simulated with +/-0.6 kcal/mol (at room temperature) of cooperativity for each of the three mixed intermediates and compared to the observed data for each of the three functional properties (figure 4.8). This was accomplished by incorporating a heterotropic parameter for each of the mixed states to increase (for positive cooperativity) or decrease (for negative cooperativity) their populations in the model relative to the non-mixed states. The effect of introduced heterotropic interactions on the spin shift is apparent only at lower substrate concentrations. This is explained by examining the intermediate populations for simulated cooperativity. Positive heterotropic interactions skew the populations of enzyme-substrate complexes towards the more fully saturated mixed states, while negative interactions have the opposite effect. The contribution from the functionally silent ES complex is increased in simulated negative interactions relative to positive ones. The contribution of the ES_2 complex increases at lower substrate concentrations in the presence of the simulated positive heterotropic interactions. Even in the presence of negative interactions, the contribution of the ES_3 complex is so dominant at high substrate concentrations that the effects of simulated heterotropic cooperativity are minimized in this region.

The heterotropic interactions would show the largest effect on product formation if present. This is due to the fact that the product formation is dominated evenly by contributions from the ES_2 and ES_3 complexes, which encompass the mixed substrate complexes where heterotropic interactions are maximized. The effects of the added heterotropic cooperativity for NADPH oxidation are muted due to the larger contribution

of the ES complex and smaller contribution of the ES_3 complex to the overall oxidation rate, relative to product formation.

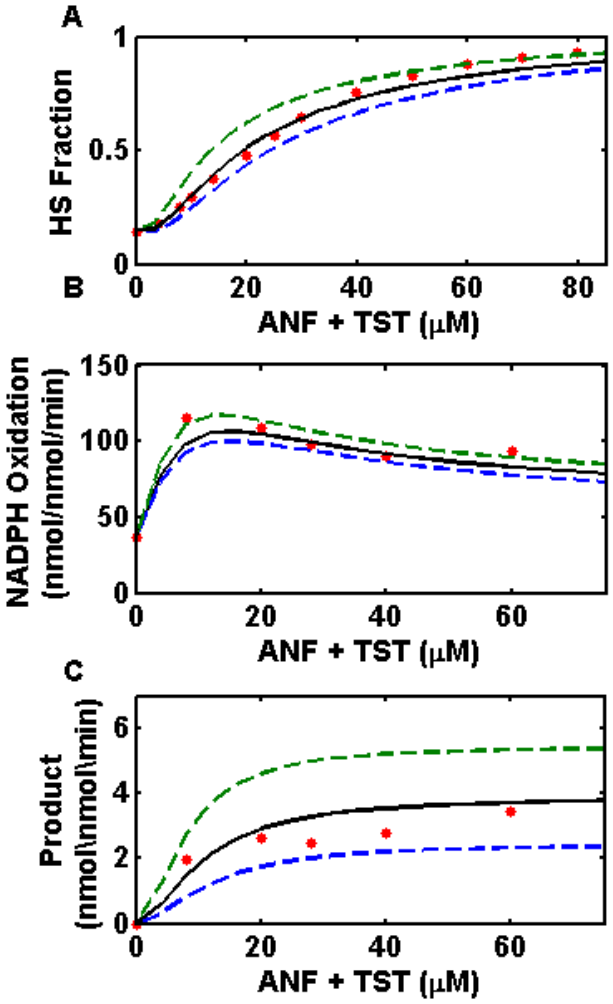

Figure 4.8 Simulations of Functional Properties for the Mixed Substrate System. In the presence of positive (green dashed line), negative (blue dashed line), or no (black solid line) heterotropic cooperativity. Experimental data shown by red circles.

4.4 Conclusions

In the absence of cooperativity the stepwise dissociation constants should conform to the expected statistical ratio for the three site binding model $K_1 = K_2/3 = K_3/9$ (scheme 4.1) (*123*). The ΔΔG's between the sequential binding events can be calculated in comparison to the non-cooperative binding ratio where $\Delta\Delta G_{12} = -RT \cdot \ln(3 \cdot K_1/K_2)$, and $\Delta\Delta G_{23} = -RT \cdot \ln(3 \cdot K_2/K_3)$. For ANF they are -0.4 and -0.2 kcal/mol, and -0.3 and -0.5 kcal/mol for TST (figure 4.9). Similarly for the mixed substrate system, the dissociation constants of 5, 12, and 24 μM (table 4.2) fall in between those of ANF and TST, and calculating the ΔΔG's between the binding events gives -0.2 and 0 kcal/mol of heterotropic cooperativity (figure 4.9), confirming the results of the simulation that there is no heterotropic cooperativity in the system. These values are smaller than RT = 0.6 kcal/mol at room temperature, which means that there is virtually no deviation from purely statistical behavior for binding of these substrates. Because of essentially non-cooperative binding, the observed deviations from Michaelis behavior and apparently cooperative properties of the enzyme arise from differences in the fractional contributions of the enzyme-substrate complexes to their experimentally observed functional properties and are not due to an uneven distribution of the complexes themselves.

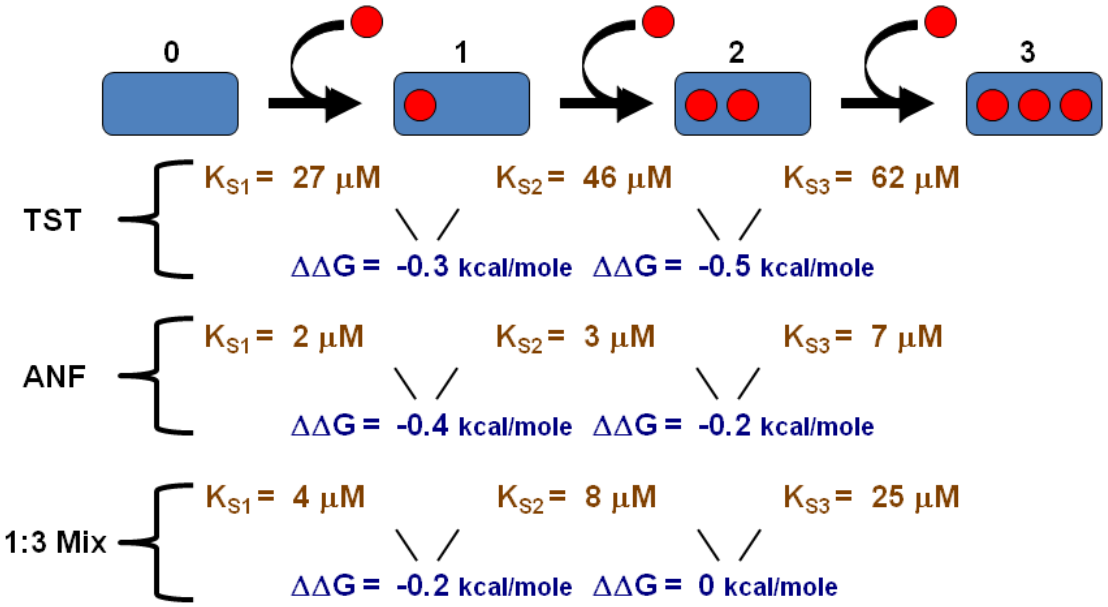

Figure 4.9 Cooperativity of Binding Events in the Single Substrate and Mixed Substrate Systems.

CHAPTER FIVE: CONCLUSIONS AND FUTURE DIRECTIONS

5.1 Conclusions

Cytochrome P450 3A4 (CYP3A4) is the most abundant hepatic P450 (*21*), and capable of metabolizing approximately half of the most commonly prescribed drugs (*87*). Its atypical (non-Michaelis) kinetics have been well established in the literature (*121-122*), as well as its ability to interact with multiple substrates simultaneously (*123, 246*). As a result, CYP3A4 has become an important focus for its potential to mediate drug-drug interactions (*78, 89*). These atypical behaviors fall into two categories; homotropic cooperativity, when molecules of the same substrate interact, and heterotropic cooperativity.

Understanding how homotropic cooperativity arises in this system was recently studied in detail by the Sligar laboratory (*130, 155*). Incorporation of CYP3A4 into Nanodiscs enabled detailed observation of the enzyme's functional properties in a homogenous, monodisperse system, avoiding the ill-defined higher order oligomeric interactions which lead to enzyme heterogeneity in microsomes (*133*), and the detergent effects observed in purified reconstituted systems (*150*). By globally fitting multiple functional properties of the enzyme, including heme iron spin state, NADPH oxidation rate, and product forming rate, to a three site binding model it was possible to resolve the individual step wise dissociation constants and state specific functional amplitudes for testosterone (*130*). Although homotropic cooperativity for TST has been well reported in the literature (*116, 118, 127, 155, 185-187*), it was shown that the

apparent homotropic cooperativity for this substrate was not due to any increase in binding affinity, but rather due to a functionally silent enzyme substrate complex (*123, 130*). The binding of the first molecule of TST to the enzyme fails to open the product forming pathway, nor does it perturb the spin equilibrium, making these properties appear cooperative due to the increased influence of the second and third binding events on the overall dose-response curve.

ANF is another substrate of CYP3A4, which has also been reported to display homotropic cooperativity (*187, 189-190*), as well as heterotropic cooperativity with TST and other substrates (*137, 163, 194*). In the work shown here we have applied the global analysis previously performed for TST to ANF, showing that it too has little binding cooperativity, and the observed apparent cooperativity is likewise derived from a functionally silent first binding event, which shifts the dose-response curve's signal to be more dependent upon the subsequent two binding events.

We further developed the global analysis to incorporate an analysis of the possible heterotropic cooperativity between these two substrates. This model is based upon the fact that in the absence of heterotropic cooperativity the signal from dose-response curve for a given ratio of the two substrates will be equivalent to the linear combination of the two individual dose-response curves for the corresponding ratio (*247-248*). Heterotropic parameters included within the model allow for the simulation of heterotropic cooperativity to examine its effects in the system. By comparing the observed behavior of the enzyme in response to a mixture of ANF and TST to that which is predicted by the model it can be shown that these two substrates do not behave cooperatively.

This method of analysis, the global deconvolution of heterotropic interactions, allows for an easier means of observing heterotropic interactions than previously proposed more complex models (*167*). It is independent of the binding model used, working for two-site, three-site and Hill analyses of the dose-response curves, as well as the observed behavior being modeled: spin state, NADPH oxidation rates, or product forming rates.

5.2 Future Directions

The work presented in this thesis shows that for the specific substrate pairing of ANF and TST there is no heterotropic cooperativity in the system, and homotropic cooperativity is purely the result of different functional amplitudes arising from the various enzyme substrate complexes in solution. However, it remains to be shown if this is a general property for all CYP3A4 substrates which display “drug-drug” interactions or if it is specific to these two. Additionally, it remains to be determined if other cytochromes P450, such as CYP2C9, where heterotropic interactions have been reported (*246*), are also truly cooperative, or if the observed cooperativity is likewise an artifact of the method of the analysis of the system.

It is also well known that the lipid membrane bilayer is heterogeneous in vivo, consisting of a variety of charged and neutral phospholipids which alter the local membrane environment’s properties (*260*). The presence of anionic phospholipids has been observed to stimulate the activity of CYP3A4 (*261-262*), possibly through aiding interactions between CYP3A4 and CPR for efficient electron delivery (*263*). Nanodiscs

provide a method of generating a local membrane environment of controlled lipid content (*264-265*), and would make a useful tool for understanding lipid-protein effects that avoid the complications associated with larger lipid bilayer systems, such as liposomes, which are difficult to prepare with precisely controlled size and lipid stoichiometry.

Work has also been performed to adapt CYP3A4 Nanodiscs into a high throughput screen to test substrate binding by methods such as localized surface plasmon resonance spectroscopy (*266*). Coupling the global deconvolution and mixed substrate analysis techniques described in this work to a high throughput screening system would likely allow for the rapid determination of drug-drug interactions due to heterotropic cooperativity in the various drug metabolizing cytochromes P450, and would be of benefit to the pharmaceutical industry and the development of safer therapeutics.

REFERENCES

1. Klingenberg, M. (1958) Pigments of rat liver microsomes, *Arch. Biochem. Biophys. 75*, 376-386.
2. Garfinkel, D. (1958) Studies on pig liver microsomes. I. Enzymic and pigment composition of different microsomal fractions, *Archives of Biochemistry and Biophysics 77*, 493-509.
3. Omura, T., and Sato, R. (1964) The Carbon Monoxide-Binding Pigment of Liver Microsomes. I. Evidence for its Hemoprotein Nature, *J. Biol. Chem. 239*, 2370-2378.
4. Omura, T., and Sato, R. (1964) The Carbon Monoxide-Binding Pigment of Liver Microsomes: II. Solubilization, Purification, and Properties, *J. Biol. Chem. 239*, 2379-2385.
5. Nelson, D. R., Koymans, L., Kamataki, T., Stegeman, J. J., Feyereisen, R., Waxman, D. J., Waterman, M. R., Gotoh, O., Coon, M. J., Estabrook, R. W., Gunsalus, I. C., and Nebert, D. W. (1996) P450 superfamily: update on new sequences, gene mapping, accession numbers and nomenclature, *Pharmacogenetics 6*, 1-42.
6. Nelson, D. R. (2006) Cytochrome P450 nomenclature, 2004, *Methods Mol Biol 320*, 1-10.
7. Nelson, D. R., Zeldin, D. C., Hoffman, S. M., Maltais, L. J., Wain, H. M., and Nebert, D. W. (2004) Comparison of cytochrome P450 (CYP) genes from the

mouse and human genomes, including nomenclature recommendations for genes, pseudogenes and alternative-splice variants, *Pharmacogenetics 14*, 1-18.

8. Nelson, D. R., Schuler, M. A., Paquette, S. M., Werck-Reichhart, D., and Bak, S. (2004) Comparative genomics of rice and Arabidopsis. Analysis of 727 cytochrome P450 genes and pseudogenes from a monocot and a dicot, *Plant Physiol 135*, 756-772.
9. Nelson, D. R. (1999) Cytochrome P450 and the individuality of species, *Arch Biochem Biophys 369*, 1-10.
10. Nelson, D. R. (2003) Comparison of P450s from human and fugu: 420 million years of vertebrate P450 evolution, *Arch Biochem Biophys 409*, 18-24.
11. Nelson, D. R. (2011) Cytochrome P450 Hompage.
12. Tijet, N., Helvig, C., and Feyereisen, R. (2001) The cytochrome P450 gene superfamily in Drosophila melanogaster: annotation, intron-exon organization and phylogeny, *Gene 262*, 189-198.
13. Ouellet, H., Johnston, J. B., and Ortiz de Montellano, P. R. (2010) The Mycobacterium tuberculosis cytochrome P450 system, *Arch Biochem Biophys 493*, 82-95.
14. Schuler, M. A., and Werck-Reichhart, D. (2003) Functional genomics of P450s, *Annu Rev Plant Biol 54*, 629-667.
15. Paquette, S. M., Bak, S., and Feyereisen, R. (2000) Intron-exon organization and phylogeny in a large superfamily, the paralogous cytochrome P450 genes of Arabidopsis thaliana, *DNA Cell Biol 19*, 307-317.

16. Poulos, T. L., and Johnson, E. F. (2005) Structures of Cytochrome P450 Enzymes, In *Cytochrome P450: Structure, Mechanism, Biochemistry* (Ortiz de Monellano, P. R., Ed.) 3rd ed., pp 87-111, Kluwer Academic, New York.

17. Werck-Reichhart, D., and Feyereisen, R. (2000) Cytochromes P450: a success story, *Genome Biol 1*, REVIEWS3003.

18. Schlichting, I., Berendzen, J., Chu, K., Stock, A. M., Maves, S. A., Benson, D. E., Sweet, R. M., Ringe, D., Petsko, G. A., and Sligar, S. G. (2000) The catalytic pathway of cytochrome p450cam at atomic resolution, *Science 287*, 1615-1622.

19. Hays, A. M. A., Dunn, A. R., Chiu, R., Gray, H. B., Stout, C. D., and Goodin, D. B. (2004) Conformational states of cytochrome P450cam revealed by trapping of synthetic molecular wires, *Journal of Molecular Biology 344*, 455-469.

20. Howe, G. A., and Schilmiller, A. L. (2002) Oxylipin metabolism in response to stress, *Curr Opin Plant Biol 5*, 230-236.

21. Guengerich, F. P. (2005) Human Cytochrome P450 Enzymes, In *Cytochrome P450: Structure, Mechanism, Biochemistry* (Ortiz de Montellano, P. R., Ed.) 3rd ed., pp 377-530, Kluwer Academic, New York.

22. Somerville, C., and Somerville, S. (1999) Plant Functional Genomics, *Science 285*, 380-383.

23. Sligar, S. G. (1975) A kinetic and equilibrium description of camphor hydroxylation by the P-450cam monoxygenase system, University of Illinois, Urbana.

24. Gelb, M. H., Heimbrook, D. C., Mälkönen, P., and Sligar, S. G. (1982) Stereochemistry and Deuterium Isotope Effects in Camphor Hydroxylation by the Cytochrome P-450cam Monooxygenase System, *Biochemistry 21*, 370-377.

25. Fisher, M., and Sligar, S. G. (1995) Control of heme protein redox potential and reduction rate: linear free energy relation between potential and ferric spin state equilibrium, *Journal of American Chemical Society 107*, 5018-5019.

26. Guengerich, F. P. (2001) Common and uncommon cytochrome P450 reactions related to metabolism and chemical toxicity, *Chem Res Toxicol 14*, 611-650.

27. Sono, M., Roach, M. P., Coulter, E. D., and Dawson, J. H. (1996) Heme-Containing Oxygenases, *Chem Rev 96*, 2841-2888.

28. Paine, M. J. I., Scrutton, N. S., Munro, A. W., Gutierrez, A., Roberts, G. C. K., and Wolf, C. R. (2005) Electron Transfer Partners of Cytochrome P450, In *Cytochrome P450: Structure, Mechanism, Biochemistry* (Ortiz de Monellano, P. R., Ed.) 3rd ed., pp 115-148, Kluwer Academic, New York.

29. McLean, K. J., Sabri, M., Marshall, K. R., Lawson, R. J., Lewis, D. G., Clift, D., Balding, P. R., Dunford, A. J., Warman, A. J., McVey, J. P., Quinn, A. M., Sutcliffe, M. J., Scrutton, N. S., and Munro, A. W. (2005) Biodiversity of cytochrome P450 redox systems, *Biochem Soc Trans 33*, 796-801.

30. Shirane, N., Sui, Z., Peterson, J. A., and Ortiz de Montellano, P. R. (1993) Cytochrome P450BM-3 (CYP102): Regiospecificity of Oxidation of w-Unsaturated Fatty Acids and Mechanism-Based Inactivation, *Biochemistry 32*, 13732-13741.

31. Munro, A. W., Lindsay, J. G., Coggins, J. R., Kelly, S. M., and Price, N. C. (1994) Structural and enzymological analysis of the interaction of isolated domains of cytochrome P-450 BM3, *FEBS Letters 343*, 70-74.

32. Davis, S. C., Sui, Z., Peterson, J. A., and Ortiz de Montellano, P. R. (1996) Oxidation of w-Oxo Fatty Acids by Cytochrome P450 BM-3 (CYP102), *Archives of BIochem. Biophys. 328*, 35-42.

33. Anzenbacherova, E., Bec, N., Anzenbacher, P., Hudecek, J., Soucek, P., Jung, C., Munro, A. W., and Lange, R. (2000) Flexibility and stability of the structure of cytochromes P450 3A4 and BM-3, *Eur J Biochem 267*, 2916-2920.

34. Munro, A. W., Leys, D. G., McLean, K. J., Marshall, K. R., Ost, T. W., Daff, S., Miles, C. S., Chapman, S. K., Lysek, D. A., Moser, C. C., Page, C. C., and Dutton, P. L. (2002) P450 BM3: the very model of a modern flavocytochrome, *Trends Biochem Sci 27*, 250-257.

35. Peterson, J. A., Sevrioukova, I., Truan, G., and Graham-Lorence, S. E. (1997) P450BM-3: A tale of two domains - or is it three?, *Steroids 62*, 117-123.

36. Fernando, H., Halpert, J. R., and Davydov, D. R. (2008) Kinetics of electron transfer in the complex of cytochrome P450 3A4 with the flavin domain of cytochrome P450BM-3 as evidence of functional heterogeneity of the heme protein, *Archives of Biochemistry and Biophysics 471*, 20-31.

37. Davydov, D. R., Sineva, E. V., Sistla, S., Davydova, N. Y., Frank, D. J., Sligar, S. G., and Halpert, J. R. (2010) Electron transfer in the complex of membrane-bound human cytochrome P450 3A4 with the flavin domain of P450BM-3: The

effect of oligomerization of the heme protein and intermittent modulation of the spin equilibrium, *Bba-Bioenergetics 1797*, 378-390.

38. Roberts, G. A., Celik, A., Hunter, D. J., Ost, T. W., White, J. H., Chapman, S. K., Turner, N. J., and Flitsch, S. L. (2003) A self-sufficient cytochrome p450 with a primary structural organization that includes a flavin domain and a [2Fe-2S] redox center, *J Biol Chem 278*, 48914-48920.
39. Hunter, D. J., Roberts, G. A., Ost, T. W., White, J. H., Muller, S., Turner, N. J., Flitsch, S. L., and Chapman, S. K. (2005) Analysis of the domain properties of the novel cytochrome P450 RhF, *FEBS Lett 579*, 2215-2220.
40. Shiro, Y., Kato, M., Iizuka, T., Nakahara, K., and Shoun, H. (1994) Kinetics and Thermodynamics of CO Binding to Cytochrome P450nor, *Biochemistry 33*, 8673-8677.
41. Matsumura, H., Matsuda, K., Nakamura, N., Ohtaki, A., Yoshida, H., Kamitori, S., Yohda, M., and Ohno, H. (2011) Monooxygenation by a thermophilic cytochrome P450 via direct electron donation from NADH, *Metallomics*.
42. Puchkaev, A. V., and Ortiz de Montellano, P. R. (2005) The Sulfolobus solfataricus electron donor partners of thermophilic CYP119: an unusual non-NAD(P)H-dependent cytochrome P450 system, *Arch Biochem Biophys 434*, 169-177.
43. Rittle, J., and Green, M. T. (2010) Cytochrome P450 Compound I: Capture, Characterization, and C-H Bond Activation Kinetics, *Science 330*, 933-937.

44. Kellner, D. G., Hung, S. C., Weiss, K. E., and Sligar, S. G. (2002) Kinetic characterization of Compound I formation in the thermostable cytochrome P450 CYP119, *Journal of Biological Chemistry 277*, 9641-9644.

45. Jensen, K., Jensen, P. E., and Moller, B. L. (2011) Light-Driven Cytochrome P450 Hydroxylations, *ACS Chem Biol*.

46. Denisov, I. G., Makris, T. M., Sligar, S. G., and Schlichting, I. (2005) Structure and Chemistry of Cytochrome P450, *Chem Rev 105*, 2253-2278.

47. Guengerich, F. P. (1997) Role of cytochrome P450 enzymes in drug-drug interactions, *Adv Pharmacol 43*, 171-188.

48. Shimada, T., Yamazaki, H., Mimura, M., Inui, Y., and Guengerich, F. P. (1994) Interindividual variations in human liver cytochrome P-450 enzymes involved in the oxidation of drugs, carcinogens and toxic chemicals: studies with liver microsomes of 30 Japanese and 30 Caucasians, *J Pharmacol Exp Ther 270*, 414-423.

49. Kalow, W. (1962) Some aspects of the pharmacology of nicotine, *Appl Ther 4*, 930-932.

50. Smith, R. L., Idle, J. R., Mahgoub, A. A., Sloan, T. P., and Lancaster, R. (1978) Genetically determined defcts of oxidation at carbon centres of drugs, *Lancet 1*, 943-944.

51. Motulsky, A. G. (1957) Drug reactions enzymes, and biochemical genetics, *J Am Med Assoc 165*, 835-837.

52. Gonzalez, F. J., Schmid, B. J., Umeno, M., McBride, O. W., Hardwick, J. P., Meyer, U. A., Gelboin, H. V., and Idle, J. R. (1988) Human P450PCN1:

sequence, chromosome localization, and direct evidence through cDNA expression that P450PCN1 is nifedipine oxidase, *Dna 7*, 79-86.

53. Gaedigk, A., Blum, M., Gaedigk, R., Eichelbaum, M., and Meyer, U. A. (1991) Deletion of the entire cytochrome P450 CYP2D6 gene as a cause of impaired drug metabolism in poor metabolizers of the debrisoquine/sparteine polymorphism, *Am J Hum Genet 48*, 943-950.

54. Woolhouse, N. M., Andoh, B., Mahgoub, A., Sloan, T. P., Idle, J. R., and Smith, R. L. (1979) Debrisoquin hydroxylation polymorphism among Ghanaians and Caucasians, *Clin Pharmacol Ther 26*, 584-591.

55. Nakamura, K., Goto, F., Ray, W. A., McAllister, C. B., Jacqz, E., Wilkinson, G. R., and Branch, R. A. (1985) Interethnic differences in genetic polymorphism of debrisoquin and mephenytoin hydroxylation between Japanese and Caucasian populations, *Clin Pharmacol Ther 38*, 402-408.

56. Daly, A. K. (2003) Pharmacogenetics of the major polymorphic metabolizing enzymes, *Fundam Clin Pharmacol 17*, 27-41.

57. Nagata, K., and Yamazoe, Y. (2002) Genetic polymorphism of human cytochrome p450 involved in drug metabolism, *Drug Metab Pharmacokinet 17*, 167-189.

58. Johansson, I., Lundqvist, E., Bertilsson, L., Dahl, M. L., Sjoqvist, F., and Ingelman-Sundberg, M. (1993) Inherited amplification of an active gene in the cytochrome P450 CYP2D locus as a cause of ultrarapid metabolism of debrisoquine, *Proc Natl Acad Sci U S A 90*, 11825-11829.

59. Neal, R. A., and Halpert, J. (1982) Toxicology of thiono-sulfur compounds, *Annu Rev Pharmacol Toxicol 22*, 321-339.

60. Jollow, D. J., Mitchell, J. R., Potter, W. Z., Davis, D. C., Gillette, J. R., and Brodie, B. B. (1973) Acetaminophen-induced hepatic necrosis. II. Role of covalent binding in vivo, *J Pharmacol Exp Ther 187*, 195-202.

61. Wing, K. D., Glickman, A. H., and Casida, J. E. (1983) Oxidative bioactivation of S-alkyl phosphorothiolate pesticides: stereospecificity of profenofos insecticide activation, *Science 219*, 63-65.

62. Stoilov, I., Akarsu, A. N., Alozie, I., Child, A., Barsoum-Homsy, M., Turacli, M. E., Or, M., Lewis, R. A., Ozdemir, N., Brice, G., Aktan, S. G., Chevrette, L., Coca-Prados, M., and Sarfarazi, M. (1998) Sequence analysis and homology modeling suggest that primary congenital glaucoma on 2p21 results from mutations disrupting either the hinge region or the conserved core structures of cytochrome P4501B1, *Am J Hum Genet 62*, 573-584.

63. Lange, R., Heiber-Langer, I., Bonfils, C., Fabre, I., Negishi, M., and Balny, C. (1994) Activation Volume and Energetic Properies of the Binding of CO to Hemoproteins, *Biophys. J. 66*, 89-98.

64. Ariyoshi, N., Miyamoto, M., Umetsu, Y., Kunitoh, H., Dosaka-Akita, H., Sawamura, Y., Yokota, J., Nemoto, N., Sato, K., and Kamataki, T. (2002) Genetic polymorphism of CYP2A6 gene and tobacco-induced lung cancer risk in male smokers, *Cancer Epidemiol Biomarkers Prev 11*, 890-894.

65. Nebert, D. W. (1989) The Ah locus: genetic differences in toxicity, cancer, mutation, and birth defects, *Crit Rev Toxicol 20*, 153-174.

66. Guengerich, F. P. (1992) Human cytochrome P-450 enzymes, *Life Sci 50*, 1471-1478.

67. Turesky, R. J., Guengerich, F. P., Guillouzo, A., and Langouet, S. (2002) Metabolism of heterocyclic aromatic amines by human hepatocytes and cytochrome P4501A2, *Mutat Res 506-507*, 187-195.

68. Baum, M., Amin, S., Guengerich, F. P., Hecht, S. S., Kohl, W., and Eisenbrand, G. (2001) Metabolic activation of benzo[c]phenanthrene by cytochrome P450 enzymes in human liver and lung, *Chem Res Toxicol 14*, 686-693.

69. Guengerich, F. P., and Liebler, D. C. (1985) Enzymatic activation of chemicals to toxic metabolites, *Crit Rev Toxicol 14*, 259-307.

70. Brian, W. R., Sari, M. A., Iwasaki, M., Shimada, T., Kaminsky, L. S., and Guengerich, F. P. (1990) Catalytic activities of human liver cytochrome P-450 IIIA4 expressed in Saccharomyces cerevisiae, *Biochemistry 29*, 11280-11292.

71. Guengerich, F. P. (1990) Mechanism-based inactivation of human liver microsomal cytochrome P-450 IIIA4 by gestodene, *Chem Res Toxicol 3*, 363-371.

72. Guengerich, F. P., Shimada, T., Iwasaki, M., Butler, M. A., and Kadlubar, F. F. (1990) Activation of carcinogens by human liver cytochromes P-450, *Basic Life Sci 53*, 381-396.

73. de Wildt, S. N., Kearns, G. L., Leeder, J. S., and van den Anker, J. N. (1999) Cytochrome P450 3A: ontogeny and drug disposition, *Clin Pharmacokinet 37*, 485-505.

74. Inoue, K., Inazawa, J., Nakagawa, H., Shimada, T., Yamazaki, H., Guengerich, F. P., and Abe, T. (1992) Assignment of the human cytochrome P-450 nifedipine oxidase gene (CYP3A4) to chromosome 7 at band q22.1 by fluorescence in situ hybridization, *Jpn J Hum Genet 37*, 133-138.

75. Remmer, H. (1958) Acceleration of evipan degradation by glycocorticoids., *Naunyn Schmiedebergs Arch Exp Pathol Pharmakol 233*, 184-191.

76. Molowa, D. T., Schuetz, E. G., Wrighton, S. A., Watkins, P. B., Kremers, P., Mendez-Picon, G., Parker, G. A., and Guzelian, P. S. (1986) Complete cDNA sequence of a cytochrome P-450 inducible by glucocorticoids in human liver, *Proc Natl Acad Sci U S A 83*, 5311-5315.

77. Bork, R. W., Muto, T., Beaune, P. H., Srivastava, P. K., Lloyd, R. S., and Guengerich, F. P. (1989) Characterization of mRNA species related to human liver cytochrome P-450 nifedipine oxidase and the regulation of catalytic activity, *J Biol Chem 264*, 910-919.

78. Guengerich, F. P. (1999) Cytochrome P-450 3A4: regulation and role in drug metabolism, *Annu Rev Pharmacol Toxicol 39*, 1-17.

79. Coumoul, X., Diry, M., and Barouki, R. (2002) PXR-dependent induction of human CYP3A4 gene expression by organochlorine pesticides, *Biochem Pharmacol 64*, 1513-1519.

80. Lehmann, J. M., McKee, D. D., Watson, M. A., Willson, T. M., Moore, J. T., and Kliewer, S. A. (1998) The human orphan nuclear receptor PXR is activated by compounds that regulate CYP3A4 gene expression and cause drug interactions, *J Clin Invest 102*, 1016-1023.

81. Thummel, K. E., Brimer, C., Yasuda, K., Thottassery, J., Senn, T., Lin, Y., Ishizuka, H., Kharasch, E., Schuetz, J., and Schuetz, E. (2001) Transcriptional control of intestinal cytochrome P-4503A by 1alpha,25-dihydroxy vitamin D3, *Mol Pharmacol 60*, 1399-1406.

82. Takeshita, A., Taguchi, M., Koibuchi, N., and Ozawa, Y. (2002) Putative role of the orphan nuclear receptor SXR (steroid and xenobiotic receptor) in the mechanism of CYP3A4 inhibition by xenobiotics, *J Biol Chem 277*, 32453-32458.

83. Wang, J. S., Backman, J. T., Wen, X., Taavitsainen, P., Neuvonen, P. J., and Kivisto, K. T. (2000) Fluvoxamine is a more potent inhibitor of lidocaine metabolism than ketoconazole and erythromycin in vitro, *Drug Metab Dispos 28*, 51-57.

84. Danan, G., Descatoire, V., and Pessayre, D. (1981) Self-induction by erythromycin of its own transformation into a metabolite forming an inactive complex with reduced cytochrome P-450, *J Pharmacol Exp Ther 218*, 509-514.

85. Murray, B. P., and Correia, M. A. (2001) Ubiquitin-dependent 26S proteasomal pathway: a role in the degradation of native human liver CYP3A4 expressed in Saccharomyces cerevisiae?, *Arch Biochem Biophys 393*, 106-116.

86. Lamba, J. K., Lin, Y. S., Thummel, K., Daly, A., Watkins, P. B., Strom, S., Zhang, J., and Schuetz, E. G. (2002) Common allelic variants of cytochrome P4503A4 and their prevalence in different populations, *Pharmacogenetics 12*, 121-132.

87. Wienkers, L. C., and Heath, T. G. (2005) Predicting in vivo drug interactions from in vitro drug discovery data, *Nat Rev Drug Discov 4*, 825-833.

88. Rendic, S. (2002) Summary of information on human CYP enzymes: human P450 metabolism data, *Drug Metab Rev 34*, 83-448.

89. Bachmann, K. A., Ring, B.J., Wrighton, S.A. (2003) Drug-Drug Interactions and the Cytochromes P450, In *Drug Metabolizing Enzymes. Cytochrome P450 and Other Enzymes in Drug Discovery and Development* (Lee, J. S., Obach, R.S., Fisher, M.B., Ed.), pp 311-336, CRC Press, Boca Raton, FL.

90. Silvers, K. J., Chazinski, T., McManus, M. E., Bauer, S. L., Gonzalez, F. J., Gelboin, H. V., Maurel, P., and Howard, P. C. (1992) Cytochrome P-450 3A4 (nifedipine oxidase) is responsible for the C-oxidative metabolism of 1-nitropyrene in human liver microsomal samples, *Cancer Res 52*, 6237-6243.

91. Sattler, M., Guengerich, F. P., Yun, C. H., Christians, U., and Sewing, K. F. (1992) Cytochrome P-450 3A enzymes are responsible for biotransformation of FK506 and rapamycin in man and rat, *Drug Metab Dispos 20*, 753-761.

92. Fleming, C. M., Branch, R. A., Wilkinson, G. R., and Guengerich, F. P. (1992) Human liver microsomal N-hydroxylation of dapsone by cytochrome P-4503A4, *Mol Pharmacol 41*, 975-980.

93. Halvorson, M., Greenway, D., Eberhart, D., Fitzgerald, K., and Parkinson, A. (1990) Reconstitution of testosterone oxidation by purified rat cytochrome P450p (IIIA1), *Arch Biochem Biophys 277*, 166-180.

94. Halpert, J., Jaw, J. Y., and Balfour, C. (1989) Specific inactivation by 17 beta-substituted steroids of rabbit and rat liver cytochromes P-450 responsible for progesterone 21-hydroxylation, *Mol Pharmacol 35*, 148-156.

95. Wolff, T., Distlerath, L. M., Worthington, M. T., Groopman, J. D., Hammons, G. J., Kadlubar, F. F., Prough, R. A., Martin, M. V., and Guengerich, F. P. (1985) Substrate specificity of human liver cytochrome P-450 debrisoquine 4-hydroxylase probed using immunochemical inhibition and chemical modeling, *Cancer Res 45*, 2116-2122.

96. Shimada, T., and Guengerich, F. P. (1989) Evidence for cytochrome P-450NF, the nifedipine oxidase, being the principal enzyme involved in the bioactivation of aflatoxins in human liver, *Proc Natl Acad Sci U S A 86*, 462-465.

97. Lemoine, A., Gautier, J. C., Azoulay, D., Kiffel, L., Belloc, C., Guengerich, F. P., Maurel, P., Beaune, P., and Leroux, J. P. (1993) Major pathway of imipramine metabolism is catalyzed by cytochromes P-450 1A2 and P-450 3A4 in human liver, *Mol Pharmacol 43*, 827-832.

98. Harvison, P. J., Guengerich, F. P., Rashed, M. S., and Nelson, S. D. (1988) Cytochrome P-450 isozyme selectivity in the oxidation of acetaminophen, *Chem Res Toxicol 1*, 47-52.

99. Brian, W. R., Srivastava, P. K., Umbenhauer, D. R., Lloyd, R. S., and Guengerich, F. P. (1989) Expression of a human liver cytochrome P-450 protein with tolbutamide hydroxylase activity in Saccharomyces cerevisiae, *Biochemistry 28*, 4993-4999.

100. Gillam, E. M., Baba, T., Kim, B. R., Ohmori, S., and Guengerich, F. P. (1993) Expression of modified human cytochrome P450 3A4 in Escherichia coli and purification and reconstitution of the enzyme, *Arch Biochem Biophys 305*, 123-131.

101. Imaoka, S., Imai, Y., Shimada, T., and Funae, Y. (1992) Role of phospholipids in reconstituted cytochrome P450 3A form and mechanism of their activation of catalytic activity, *Biochemistry 31*, 6063-6069.

102. Yamazaki, H., Yune-Fang Ueng, Tsutomu Shimada, and F. Peter Guengerich. (1995) Roles of Divalent Metal Ions in Oxidations Catalyzed by Recombinant Cytochrome P450 3A4 and Replacement of NADPH-Cytochrome P450 Reductase with Other Flavoproteins, Ferredoxin, and Oxygen Surrogates, *Biochemistry 34*, 8380-8389.

103. Yamazaki, H., Johnson, W. W., Ueng, Y.-F., Shimada, T., and Guengerich, F. P. (1996) Lack of Electron Transfer from Cytochrome b5 in Stimulation of Cayalytic Activities of Cytochrome P450 3A4, *J. Biol. Chem. 271*, 27438-22744?

104. Yamazaki, H., Nakano, M., Imai, Y., Ueng, Y. F., Guengerich, F. P., and Shimada, T. (1996) Roles of cytochrome b5 in the oxidation of testosterone and nifedipine by recombinant cytochrome P450 3A4 and by human liver microsomes, *Arch Biochem Biophys 325*, 174-182.

105. Yamazaki, H., and Shimada, T. (1997) Progesterone and testosterone hydroxylation by cytochromes P450 2C19, 2C9, and 3A4 in human liver microsomes, *Arch Biochem Biophys 346*, 161-169.

106. Yamazaki, H., Gillam, E. M., Dong, M. S., Johnson, W. W., Guengerich, F. P., and Shimada, T. (1997) Reconstitution of recombinant cytochrome P450 2C10(2C9) and comparison with cytochrome P450 3A4 and other forms: effects of cytochrome P450-P450 and cytochrome P450-b5 interactions, *Arch Biochem Biophys 342*, 329-337.

107. Shet, M. S., Fisher, C. W., Arlotto, M. P., Shackleton, C. H., Holmans, P. L., Martin-Wixtrom, C. A., Saeki, Y., and Estabrook, R. W. (1994) Purification and enzymatic properties of a recombinant fusion protein expressed in Escherichia coli containing the domains of bovine P450 17A and rat NADPH-P450 reductase, *Arch Biochem Biophys 311*, 402-417.

108. Shet, M. S., Faulkner, K. M., Holmans, P. L., Fisher, C. W., and Estabrook, R. W. (1995) The Effects of Cytochrome b5, NADPH-P450 Reductase, and Lipid on the Rate of 6b-Hydroxylation of Testosterone as Catalyzxed by a Human P450 3A4 Fusion Protein, *Archives of Biochemistry and Biophysics 318*, 314-321.

109. Fisher, C. W., Shet, M. S., and Estabrook, R. W. (1996) Construction of plasmids and expression in Escherichia coli of enzymatically active fusion proteins containing the heme-domain of a P450 linked to NADPH-P450 reductase, *Methods Enzymol 272*, 15-25.

110. Gilep, A. A., Guryev, O. L., Usanov, S. A., and Estabrook, R. W. (2001) Apo-cytochrome b5 as an indicator of changes in heme accessability: preliminary studies with cytochrome P450 3A4, *J Inorg Biochem 87*, 237-244.

111. Gilep, A. A., Guryev, O. L., Usanov, S. A., and Estabrook, R. W. (2001) An enzymatically active chimeric protein containing the hydrophilic form of NADPH-cytochrome P450 reductase fused to the membrane-binding domain of cytochrome b5, *Biochem Biophys Res Commun 284*, 937-941.

112. Gilep, A. A., Guryev, O. L., Usanov, S. A., and Estabrook, R. W. (2001) Reconstitution of the enzymatic activities of cytochrome P450s using recombinant flavocytochromes containing rat cytochrome b(5) fused to NADPH--

cytochrome P450 reductase with various membrane-binding segments, *Arch Biochem Biophys 390*, 215-221.

113. Guryev, O. L., Gilep, A. A., Usanov, S. A., and Estabrook, R. W. (2001) Interaction of apo-cytochrome b5 with cytochromes P4503A4 and P45017A: relevance of heme transfer reactions, *Biochemistry 40*, 5018-5031.

114. Fraser, D. J., Feyereisen, R., Harlow, G. R., and Halpert, J. R. (1997) Isolation, heterologous expression and functional characterization of a novel cytochrome P450 3A enzyme from a canine liver cDNA library, *J Pharmacol Exp Ther 283*, 1425-1432.

115. Harlow, G. R., and Halpert, J. R. (1997) Alanine-scanning mutagenesis of a putative substrate recognition site in human cytochrome P450 3A4. Role of residues 210 and 211 in flavonoid activation and substrate specificity, *J Biol Chem 272*, 5396-5402.

116. Harlow, G. R., and Halpert, J. R. (1998) Analysis of human cytochrome P450 3A4 cooperativity: construction and characterization of a site-directed mutant that displays hyperbolic steroid hydroxylation kinetics, *Proc. Natl. Acad. Sci. U.S.A. 95*, 6636-6641.

117. Guengerich, F. P. (2003) Cytochrome P450 oxidations in the generation of reactive electrophiles: epoxidation and related reactions, *Arch Biochem Biophys 409*, 59-71.

118. Isin, E. M., and Guengerich, F. P. (2006) Kinetics and thermodynamics of ligand binding by cytochrome P450 3A4, *J Biol Chem 281*, 9127-9136.

119. Guengerich, F. P. (2002) Rate-limiting steps in cytochrome P450 catalysis, *Biol Chem 383*, 1553-1564.

120. Guengerich, F. P. (1983) Oxidation-reduction properties of rat liver cytochromes P-450 and NADPH-cytochrome p-450 reductase related to catalysis in reconstituted systems, *Biochemistry 22*, 2811-2820.

121. Davydov, D. R., and Halpert, J. R. (2008) Allosteric P450 mechanisms: multiple binding sites, multiple conformers or both?, *Expert Opinion on Drug Metabolism & Toxicology 4*, 1523-1535.

122. Atkins, W. M. (2005) Non-Michaelis-Menten kinetics in cytochrome P 450-catalyzed reactions, *Annu. Rev. Pharmacol. Toxicol. 45*, 291-310.

123. Sligar, S. G., and Denisov, I. G. (2007) Understanding Cooperativity in Human P450 Mediated Drug-Drug Interactions, *Drug Metab. Rev. 39*, 567-579.

124. Domanski, T. L., Liu, J., Harlow, G. R., and Halpert, J. R. (1998) Analysis of four residues within substrate recognition site 4 of human cytochrome P450 3A4: role in steroid hydroxylase activity and alpha-naphthoflavone stimulation, *Arch Biochem Biophys 350*, 223-232.

125. Ekroos, M., and Sjogren, T. (2006) Structural basis for ligand promiscuity in cytochrome P450 3A4, *Proc Natl Acad Sci U S A 103*, 13682-13687.

126. Williams, P. A., Cosme, J., Vinkovic, D. M., Ward, A., Angove, H. C., Day, P. J., Vonrhein, C., Tickle, I. J., and Jhoti, H. (2004) Crystal structures of human cytochrome P450 3A4 bound to metyrapone and progesterone, *Science 305*, 683-686.

127. Cameron, M. D., Wen, B., Allen, K. E., Roberts, A. G., Schuman, J. T., Campbell, A. P., Kunze, K. L., and Nelson, S. D. (2005) Cooperative binding of midazolam with testosterone and alpha-naphthoflavone within the CYP3A4 active site: a NMR T1 paramagnetic relaxation study, *Biochemistry 44*, 14143-14151.

128. Cameron, M. D., Wen, B., Roberts, A. G., Atkins, W. M., Campbell, A. P., and Nelson, S. D. (2007) Cooperative binding of acetaminophen and caffeine within the P450 3A4 active site, *Chem. Res. Toxicol. 20*, 1434-1441.

129. Dabrowski, M. J., Schrag, M. L., Wienkers, L. C., and Atkins, W. M. (2002) Pyrene.pyrene complexes at the active site of cytochrome P450 3A4: evidence for a multiple substrate binding site, *J Am Chem Soc 124*, 11866-11867.

130. Denisov, I. G., Baas, B. J., Grinkova, Y. V., and Sligar, S. G. (2007) Cooperativity in cytochrome P450 3A4: linkages in substrate binding, spin state, uncoupling, and product formation, *J. Biol. Chem. 282*, 7066-7076.

131. Fernando, H., Halpert, J. R., and Davydov, D. R. (2006) Resolution of multiple substrate binding sites in cytochrome P450 3A4: the stoichiometry of the enzyme-substrate complexes probed by FRET and Job's titration, *Biochemistry 45*, 4199-4209.

132. Davydov, D. R., Halpert, J. R., Renaud, J. P., and Hui Bon Hoa, G. (2003) Conformational heterogeneity of cytochrome P450 3A4 revealed by high pressure spectroscopy, *Biochem Biophys Res Commun 312*, 121-130.

133. Davydov, D. R., Fernando, H., Baas, B. J., Sligar, S. G., and Halpert, J. R. (2005) Kinetics of Dithionite-Dependent Reduction of Cytochrome P450 3A4:

Heterogeneity of the Enzyme Caused by Its Oligomerization, *Biochemistry. 44*, 13902-13913.

134. Denisov, I. G., and Sligar, S. G. (2011) Cytochromes P450 in nanodiscs, *Biochim Biophys Acta 1814*, 223-229.

135. Popot, J. L. (2010) Amphipols, nanodiscs, and fluorinated surfactants: three nonconventional approaches to studying membrane proteins in aqueous solutions, *Annu Rev Biochem 79*, 737-775.

136. Phillips, I. R., and Shephard, E. A. (2006) *Cytochrome P450 protocols*, 2nd ed., Humana Press, Totowa, N.J.

137. Shou, M., Grogan, J., Mancewicz, J. A., Krausz, K. W., Gonzalez, F. J., Gelboin, H. V., and Korzekwa, K. R. (1994) Activation of CYP3A4: Evidence for the Simultaneous Binding of Two Substrates in a Cytochorme P450 Active Site, *Biochemistry 33*, 6450-6455.

138. Lown, K. S., Kolars, J. C., Thummel, K. E., Barnett, J. L., Kunze, K. L., Wrighton, S. A., and Watkins, P. B. (1994) Interpatient heterogeneity in expression of CYP3A4 and CYP3A5 in small bowel. Lack of prediction by the erythromycin breath test [published erratum appears in Drug Metab Dispos 1995 Mar;23(3):following table of contents], *Drug Metab Dispos 22*, 947-955.

139. George, J., Liddle, C., Murray, M., Byth, K., and Farrell, G. C. (1995) Pre-translational regulation of cytochrome P450 genes is responsible for disease-specific changes of individual P450 enzymes among patients with cirrhosis, *Biochem Pharmacol 49*, 873-881.

140. Hosea, N. A., and Guengerich, F. P. (1998) Oxidation of nonionic detergents by cytochrome P450 enzymes, *Arch Biochem Biophys 353*, 365-373.

141. Reed, J. R., Kelley, R. W., and Backes, W. L. (2006) An evaluation of methods for the reconstitution of cytochromes P450 and NADPH P450 reductase into lipid vesicles, *Drug Metabolism and Disposition 34*, 660-666.

142. Schwarz, D., Gast, K., Meyer, H. W., Lachmann, U., Coon, M. J., and Ruckpaul, K. (1984) Incorporation of the cytochrome P-450 monooxygenase system into large unilamellar liposomes using octylglucoside, especially for measurements of protein diffusion in membranes, *Biochem Biophys Res Commun 121*, 118-125.

143. Bayburt, T., Carlson, J., Godfrey, B., Shank-Retzlaff, M., and Sligar, S. G. (2000) Structure, behavior, and manipulation of nanoscale biological assemblies, In *Handbook of Nanostructured Materials and Nanotechnology*, pp 637-710.

144. Bayburt, T. H., Carlson, J. W., and Sligar, S. G. (1998) Reconstitution and imaging of a membrane protein in a nanometer-size phospholipid bilayer, *J Struct Biol 123*, 37-44.

145. Durbin, D. M., and Jonas, A. (1999) Lipid-free apolipoproteins A-I and A-II promote remodeling of reconstituted high density lipoproteins and alter their reactivity with lecithin:cholesterol acyltransferase, *J Lipid Res 40*, 2293-2302.

146. Phillips, J. C., Wriggers, W., Li, Z., Jonas, A., and Schulten, K. (1997) Predicting the Structure of Apolipoprotein A-1 in Reconstituted High-Density Lipoprotein Disks, *Biophys. J. 73*, 2337-2346.

147. Jonas, A., Kezdy, K. E., and Wald, J. H. (1989) Defined Apolipoprotein A-I Conformations in Reconstituted High Density Lipoprotein Discs, *J. Biol. Chem. 264*, 4818-4824.

148. Jonas, A. (1986) Reconstitution of high-density lipoproteins, *Methods Enzymol 128*, 553-582.

149. Bayburt, T. H., Grinkova, Y. V., and Sligar, S. G. (2002) Self-assembly of discoidal phospholipid bilayer nanoparticles with membrane scaffold proteins, *Nano Letters 2*, 853-856.

150. Bayburt, T. H., and Sligar, S. G. (2010) Membrane protein assembly into Nanodiscs, *FEBS Lett 584*, 1721-1727.

151. Denisov, I. G., McLean, M. A., Shaw, A. W., Grinkova, Y. V., and Sligar, S. G. (2005) Thermotropic Phase Transition in Soluble Nanoscale Lipid Bilayers, *Journal of Physical Chemistry B 109*, 15580-15588.

152. Shih, A. Y., Denisov, I. G., Phillips, J. C., Sligar, S. G., and Schulten, K. (2004) Molecular Dynamics Simulations of Discoidal Bilayers Assembled from Truncated Human Lipoproteins, *Biophys J 8*, 8.

153. Denisov, I. G., Grinkova, Y. V., Lazarides, A. A., and Sligar, S. G. (2004) Directed Self-Assembly of Monodisperse Phospholipid Bliayer Nanodiscs with Controlled Size, *J. Amer. Chem. Soc. 126*, 3477-3487.

154. Grinkova, Y. V., Denisov, I. G., and Sligar, S. G. (2010) Engineering extended membrane scaffold proteins for self-assembly of soluble nanoscale lipid bilayers, *Protein Eng Des Sel 23*, 843-848.

155. Baas, B. J., Denisov, I. G., and Sligar, S. G. (2004) Homotropic cooperativity of monomeric cytochrome P450 3A4 in a nanoscale native bilayer environment, *Arch. Biochem. Biophys. 430*, 218-228.

156. Denisov, I. G., Grinkova, Y. V., Baas, B. J., and Sligar, S. G. (2006) The ferrous-dioxygen intermediate in human cytochrome P450 3A4. Substrate dependence of formation and decay kinetics, *J Biol Chem 281*, 23313-23318.

157. Kijac, A. Z., Li, Y., Sligar, S. G., and Rienstra, C. M. (2007) Magic-angle spinning solid-state NMR spectroscopy of nanodisc-embedded human CYP3A4, *Biochemistry 46*, 13696-13703.

158. Di Cera, E. (1998) Site-Specific Thermodynamics: Understanding Cooperativity in Molecular Recognition, *Chem. Rev. 98*, 1563-1591.

159. Ingelman-Sundberg, M., and Johansson, I. (1980) Catalytic properties of purified forms of rabbit liver microsomal cytochrome P-450 in reconstituted phospholipid vesicles, *Biochemistry 19*, 4004-4011.

160. Schwab, G. E., Raucy, J. L., and Johnson, E. F. (1988) Modulation of rabbit and human hepatic cytochrome P-450-catalyzed steroid hydroxylations by alpha-naphthoflavone, *Mol Pharmacol 33*, 493-499.

161. Johnson, E. F., Schwab, G. E., and Dieter, H. H. (1983) Allosteric regulation of the 16 alpha-hydroxylation of progesterone as catalyzed by rabbit microsomal cytochrome P-450 3b, *J Biol Chem 258*, 2785-2788.

162. Tang, W., and Stearns, R. A. (2001) Heterotropic cooperativity of cytochrome P450 3A4 and potential drug-drug interactions, *Curr Drug Metab 2*, 185-198.

163. Niwa, T., Murayama, N., and Yamazaki, H. (2008) Heterotropic cooperativity in oxidation mediated by cytochrome P450, *Curr. Drug Metab. 9*, 453-462.

164. Zhang, Z., Li, Y., Shou, M., Zhang, Y., Ngui, J. S., Stearns, R. A., Evans, D. C., Baillie, T. A., and Tang, W. (2004) Influence of different recombinant systems on the cooperativity exhibited by cytochrome P4503A4, *Xenobiotica 34*, 473-486.

165. Oda, Y., and Kharasch, E. D. (2001) Metabolism of levo-.alpha.-acetylmethadol (LAAM) by human liver cytochrome p450: involvement of CYP3A4 characterized by atypical kinetics with two binding sites, *Journal of Pharmacology and Experimental Therapeutics 297*, 410-422.

166. Di Marco, A., Marcucci, I., Verdirame, M., Perez, J., Sanchez, M., Pelaez, F., Chaudhary, A., and Laufer, R. (2005) Development and validation of a high-throughput radiometric CYP3A4/5 inhibition assay using tritiated testosterone, *Drug Metab Dispos 33*, 349-358.

167. Tracy, T. S. (2006) Atypical cytochrome p450 kinetics : implications for drug discovery, *Drugs R D 7*, 349-363.

168. Houston, J. B., Kenworthy, K.E., Galetin, A. (2003) Typical and Atypical Enzyme Kinetics, In *Drug Metabolizing Enzymes. Cytochrome P450 and Other Enzymes in Drug Discovery and Development* (Lee, J. S., Obach, R.S., Fisher, M.B., Ed.), pp 211-254, CRC Press, Boca Raton, FL.

169. Houston, J. B., and Galetin, A. (2005) Modelling atypical CYP3A4 kinetics: principles and pragmatism, *Arch Biochem Biophys 433*, 351-360.

170. Cupp-Vickery, J., Anderson, R., and Hatziris, Z. (2000) Crystal structures of ligand complexes of P450eryF exhibiting homotropic cooperativity, *Proc Natl Acad Sci U S A 97*, 3050-3055.

171. Davydov, D. R., Kumar, S., and Halpert, J. R. (2002) Allosteric mechanisms in P450eryF probed with 1-pyrenebutanol, a novel fluorescent substrate, *Biochem Biophys Res Commun 294*, 806-812.

172. Locuson, C. W., Gannett, P. M., and Tracy, T. S. (2006) Heteroactivator effects on the coupling and spin state equilibrium of CYP2C9, *Arch Biochem Biophys 449*, 115-129.

173. Hummel, M. A., Gannett, P. M., Aguilar, J. S., and Tracy, T. S. (2004) Effector-mediated alteration of substrate orientation in cytochrome P450 2C9, *Biochemistry 43*, 7207-7214.

174. Konecny, J., Jurica, J., Tomandl, J., and Glatz, Z. (2007) Study of recombinant cytochrome P450 2C9 activity with diclofenac by MEKC, *Electrophoresis 28*, 1229-1234.

175. Sohl, C. D., Isin, E. M., Eoff, R. L., Marsch, G. A., Stec, D. F., and Guengerich, F. P. (2008) Cooperativity in Oxidation Reactions Catalyzed by Cytochrome P450 1A2: Highly cooperative pyrene hydroxylation and multiphasic kinetics of ligand binding, *J. Biol. Chem. 283*, 7293-7308.

176. Harrelson, J. P., Atkins, W. M., and Nelson, S. D. (2008) Multiple-ligand binding in CYP2A6: probing mechanisms of cytochrome P450 cooperativity by assessing substrate dynamics, *Biochemistry 47*, 2978-2988.

177. Scott, E. E., He, Y. Q., and Halpert, J. R. (2002) Substrate routes to the buried active site may vary among cytochromes P450: mutagenesis of the F-G region in P450 2B1, *Chem Res Toxicol 15*, 1407-1413.

178. Spatzenegger, M., Liu, H., Wang, Q., Debarber, A., Koop, D. R., and Halpert, J. R. (2003) Analysis of differential substrate selectivities of CYP2B6 and CYP2E1 by site-directed mutagenesis and molecular modeling, *J Pharmacol Exp Ther 304*, 477-487.

179. Gustafsson, M. C. U., Roitel, O., Marshall, K. R., Noble, M. A., Chapman, S. K., Pessegueiro, A., Fulco, A. J., Cheesman, M. R., von Wachenfeldt, C., and Munro, A. W. (2004) Expression, Purification, and Characterization of Bacillus subtilis Cytochromes P450 CYP102A2 and CYP102A3: Flavocytochrome Homologues of P450 BM3 from Bacillus megaterium, *Biochemistry 43*, 5474-5487.

180. Ouellet, H., Podust, L. M., and Ortiz de Montellano, P. R. (2008) Mycobacterium tuberculosis CYP130: crystal structure, biophysical characterization, and interactions with antifungal azole drugs, *J Biol Chem 283*, 5069-5080.

181. Zhao, B., Guengerich, F. P., Bellamine, A., Lamb, D. C., Izumikawa, M., Lei, L., Podust, L. M., Sundaramoorthy, M., Kalaitzis, J. A., Reddy, L. M., Kelly, S. L., Moore, B. S., Stec, D., Voehler, M., Falck, J. R., Shimada, T., and Waterman, M. R. (2005) Binding of two flaviolin substrate molecules, oxidative coupling, and crystal structure of Streptomyces coelicolor A3(2) cytochrome P450 158A2, *J Biol Chem 280*, 11599-11607.

182. Ding, Y., Seufert, W. H., Beck, Z. Q., and Sherman, D. H. (2008) Analysis of the Cryptophycin P450 Epoxidase Reveals Substrate Tolerance and Cooperativity, *J. Am. Chem. Soc. 130*, 5492-5498.

183. Aburto, J., Correa-Basurto, J., and Torres, E. (2008) Atypical kinetic behavior of chloroperoxidase-mediated oxidative halogenation of polycyclic aromatic hydrocarbons, *Arch Biochem Biophys 480*, 33-40.

184. Torres, E., and Aburto, J. (2005) Chloroperoxidase-catalyzed oxidation of 4,6-dimethyldibenzothiophene as dimer complexes: evidence for kinetic cooperativity, *Arch Biochem Biophys 437*, 224-232.

185. Hosea, N. A., Miller, G. P., and Guengerich, F. P. (2000) Elucidation of distinct ligand binding sites for cytochrome P450 3A4, *Biochemistry 39*, 5929-5939.

186. Roberts, A. G., Campbell, A. P., and Atkins, W. M. (2005) The thermodynamic landscape of testosterone binding to cytochrome P450 3A4: ligand binding and spin state equilibria, *Biochemistry 44*, 1353-1366.

187. Tsalkova, T. N., Davydova, N. Y., Halpert, J. R., and Davydov, D. R. (2007) Mechanism of interactions of alpha-naphthoflavone with cytochrome P450 3A4 explored with an engineered enzyme bearing a fluorescent probe, *Biochemistry 46*, 106-119.

188. Davydov, D. R., Davydova, N. Y., Tsalkova, T. N., and Halpert, J. R. (2008) Effect of glutathione on homo- and heterotropic cooperativity in cytochrome P450 3A4, *Arch. Biochem. Biophys. 471*, 134-145.

189. Domanski, T. L., He, Y. A., Harlow, G. R., and Halpert, J. R. (2000) Dual role of human cytochrome P450 3A4 residue Phe-304 in substrate specificity and cooperativity, *J Pharmacol Exp Ther 293*, 585-591.

190. Nath, A., Grinkova, Y. V., Sligar, S. G., and Atkins, W. M. (2007) Ligand binding to cytochrome P450 3A4 in phospholipid bilayer nanodiscs: the effect of model membranes, *J. Biol. Chem. 282*, 28309-28320.

191. Kapelyukh, Y., Paine, M. J. I., Marechal, J.-D., Sutcliffe, M. J., Wolf, C. R., and Roberts, G. C. K. (2008) Multiple substrate binding by cytochrome P450 3A4: estimation of the number of bound substrate molecules, *Drug Metab. Dispos. 36*, 2136-2144.

192. Nath, A., Fernandez, C., Lampe, J. N., and Atkins, W. M. (2008) Spectral resolution of a second binding site for Nile Red on cytochrome P4503A4, *Arch. Biochem. Biophys. 474*, 198-204.

193. Carr, B. A., Norcross, R., Fang, Y., Lu, P., Rodrigues, A. D., Shou, M., Rushmore, T., and Booth-Genthe, C. (2006) Characterization of the rhesus monkey CYP3A64 enzyme: Species comparisons of CYP3A substrate specificity and kinetics using baculovirus-expressed recombinant enzymes, *Drug Metab Dispos*.

194. Ueng, Y.-F., Kuwabara, T., Chun, Y.-J., and Guengerich, F. P. (1997) Cooperativity in Oxidations Catalyzed by Cytochrome P450 3A4, *Biochemistry 36*, 370-381.

195. Andersson, T., Miners, J. O., Veronese, M. E., and Birkett, D. J. (1994) Diazepam metabolism by human liver microsomes is mediated by both S-

mephenytoin hydroxylase and CYP3A isoforms, *Br J Clin Pharmacol 38*, 131-137.

196. Kerr, B. M., Thummel, K. E., Wurden, C. J., Klein, S. M., Kroetz, D. L., Gonzalez, F. J., and Levy, R. H. (1994) Human liver carbamazepine metabolism. Role of CYP3A4 and CYP2C8 in 10,11-epoxide formation, *Biochem Pharmacol 47*, 1969-1979.

197. Emoto, C., Yamazaki, H., Iketaki, H., Yamasaki, S., Satoh, T., Shimizu, R., Suzuki, S., Shimada, N., Nakajima, M., and Yokoi, T. (2001) Cooperativity of .alpha.-naphthoflavone in cytochrome P450 3A-dependent drug oxidation activities in hepatic and intestinal microsomes from mouse and human, *Xenobiotica 31*, 265-275.

198. Shou, M., Dai, R., Cui, D., Korzekwa, K. R., Baillie, T. A., and Rushmore, T. H. (2001) A kinetic model for the metabolic interaction of two substrates at the active site of cytochrome P450 3A4, *Journal of Biological Chemistry 276*, 2256-2262.

199. Wang, R. W., Newton, D. J., Liu, N., Atkins, W. M., and Lu, A. Y. (2000) Human cytochrome P-450 3A4: in vitro drug-drug interaction patterns are substrate-dependent, *Drug Metab Dispos 28*, 360-366.

200. Atkins, W. M. (2006) Current views on the fundamental mechanisms of cytochrome P450 allosterism, *Expert Opin Drug Metab Toxicol 2*, 573-579.

201. Korzekwa, K. R., Krishnamachary, N., Shou, M., Ogai, A., Parise, R. A., Rettie, A. E., Gonzalez, F. J., and Tracy, T. S. (1998) Evaluation of atypical cytochrome P450 kinetics with two-substrate models: evidence that multiple substrates can

simultaneously bind to cytochrome P450 active sites, *Biochemistry 37*, 4137-4147.

202. Houston, J. B. (1994) Utility of in vitro drug metabolism data in predicting in vivo metabolic clearance, *Biochem Pharmacol 47*, 1469-1479.

203. Houston, J. B., and Carlile, D. J. (1997) Prediction of hepatic clearance from microsomes, hepatocytes, and liver slices, *Drug Metab Rev 29*, 891-922.

204. Tracy, T. S. (2003) Atypical enzyme kinetics: their effect on in vitro-in vivo pharmacokinetic predictions and drug interactions, *Curr Drug Metab 4*, 341-346.

205. Woodbury, C. P. (2008) *Introduction to Macromolecular Binding Equilibria*, CRC Press, Boca Raton.

206. Connors, K. A. (1987) *Binding constants : the measurement of molecular complex stability*, Wiley Interscience, New York.

207. Winzor, D. J., Sawyer, W.H. (1995) *Quantitative Characterization of Ligand Binding*, Wiley-Liss,, New York.

208. Klotz, I. M., and Hunston, D. L. (1975) Protein interactions with small molecules. Relationships between stoichiometric binding constants, site binding constants, and empirical binding parameters, *J Biol Chem 250*, 3001-3009.

209. Klotz, I. M. (1997) *Ligand-Receptor Energetics: A Guide for the Perplexed*, Wiley and Sons, New York.

210. Hill, A. V. (1913) The combinations of haemoglobin with oxygen and with carbon monoxide., *Biochemical Journal 7*, 471-480.

211. Pauling, L. (1935) The Oxygen Equilibrium of Hemoglobin and Its Structural Interpretation, *Proc Natl Acad Sci U S A 21*, 186-191.

212. Coryell, C. D. (1939) Existence of chemical interactions between the hemes (hemins) in ferrihemoglobin (methemoglobin) and the role of interactions in the interpretation of ferro-ferrihemoglobin electrode potential measurements, *Journal of Physical Chemistry 43*, 841-852.

213. Hinz, H. J., and Sturtevant, J. M. (1972) Calorimetric studies of dilute aqueous suspensions of bilayers formed from synthetic L-a-lecithins, *J Biol Chem 247*, 6071-6075.

214. Jones, M. N. (1979) The thermal behavior of lipids and biological membranes, In *Biochemical Thermodynamics* (Jones, M. N., Ed.), pp 185-223, Elsevier Scientific, Amsterdam.

215. Zimm, B. H., Bragg, J.K. (1959) Theory of the Phase Transition between Helix and Random Coil in Polypeptide Chains, *J Chem Phys 31*, 526.

216. Tracy, T. S., and Hummel, M. A. (2004) Modeling kinetic data from in vitro drug metabolism enzyme experiments, *Drug Metab Rev 36*, 231-242.

217. Bardsley, W. G., and Wyman, J. (1978) Concerning the thermodynamic definition and graphical manifestations of positive and negative co-operativity, *J Theor Biol 72*, 373-376.

218. Di Cera, E. (1990) Thermodynamics of local linkage effects. Contracted partition functions and the analysis of site-specific energetics, *Biophysical Chemistry 37*, 147-164.

219. Di Cera, E. (1995) *Thermodynamic Theory of Site-Specific Binding Processes in Biological Macromolecules*, Cambridge University Press, Cambridge.

220. Ben-Naim, A. (2001) *Cooperativity and Regulation in Biochemical Processes*, Kluwer Academic / Plenum Publishers, New York.

221. Cornish-Bowden, A., and Koshland, D. E., Jr. (1975) Diagnostic uses of the Hill (Logit and Nernst) plots, *Journal of Molecular Biology 95*, 201-212.

222. Bardsley, W. G. (1977) Factorability of the allosteric binding polynomial and graphical manifestations of cooperativity in third degree saturation functions, *J Theor Biol 67*, 407-431.

223. Hill, T. L. (1985) *Cooperativity Theory in Biochemistry. Steady-State and Equilibrium Systems*, Springer-Verlag, New York.

224. Di Cera, E., Page, M. J., Bah, A., Bush-Pelc, L. A., and Garvey, L. C. (2007) Thrombin allostery, *Phys Chem Chem Phys 9*, 1291-1306.

225. Di Cera, E. (2008) Thrombin, *Mol Aspects Med 29*, 203-254.

226. Wei, L., Locuson, C. W., and Tracy, T. S. (2007) Polymorphic variants of CYP2C9: mechanisms involved in reduced catalytic activity, *Mol Pharmacol 72*, 1280-1288.

227. Davydov, D. R., Botchkareva, A. E., Davydova, N. E., and Halpert, J. R. (2005) Resolution of two substrate-binding sites in an engineered cytochrome P450eryF bearing a fluorescent probe, *Biophys J 89*, 418-432.

228. Brown, H. S., Galetin, A., Hallifax, D., and Houston, J. B. (2006) Prediction of in vivo drug-drug interactions from in vitro data : factors affecting prototypic drug-drug interactions involving CYP2C9, CYP2D6 and CYP3A4, *Clin Pharmacokinet 45*, 1035-1050.

229. Miller, G. P., and Guengerich, F. P. (2001) Binding and Oxidation of Alkyl 4-Nitrophenyl Ethers by Rabbit Cytochrome P450 1A2: Evidence for Two Binding Sites, *Biochemistry 40*, 7262-7272.

230. Khan, K. K., Liu, H., and Halpert, J. R. (2003) Homotropic versus heterotopic cooperativity of cytochrome P450eryF: A substrate oxidation and spectral titration study, *Drug Metabolism and Disposition 31*, 356-359.

231. Li, Q. S., Ogawa, J., Schmid, R. D., and Shimizu, S. (2005) Indole hydroxylation by bacterial cytochrome P450 BM-3 and modulation of activity by cumene hydroperoxide, *Biosci Biotechnol Biochem 69*, 293-300.

232. Shou, M., Lin, Y., Lu, P., Tang, C., Mei, Q., Cui, D., Tang, W., Ngui, J. S., Lin, C. C., Singh, R., Wong, B. K., Yergey, J. A., Lin, J. H., Pearson, P. G., Baillie, T. A., Rodrigues, A. D., and Rushmore, T. H. (2001) Enzyme kinetics of cytochrome P450-mediated reactions, *Curr Drug Metab 2*, 17-36.

233. Segel, I. H. (1975) *Enzyme Kinetics. Behavior and Analysis of Rapid Equilibrium and Steady-State Enzyme Systems*, Wiley Interscience, New York.

234. Galetin, A., Clarke, S. E., and Houston, J. B. (2002) Quinidine and haloperidol as modifiers of CYP3A4 activity: multisite kinetic model approach, *Drug Metab Dispos 30*, 1512-1522.

235. Galetin, A., Clarke, S. E., and Houston, J. B. (2003) Multisite kinetic analysis of interactions between prototypical CYP3A4 subgroup substrates: midazolam, testosterone, and nifedipine, *Drug Metab Dispos 31*, 1108-1116.

236. Kenworthy, K. E., Clarke, S. E., Andrews, J., and Houston, J. B. (2001) Multisite kinetic models for CYP3A4: simultaneous activation and inhibition of diazepam and testosterone metabolism, *Drug Metab Dispos 29*, 1644-1651.

237. Sligar, S. G. (1976) Coupling of spin, substrate, and redox equilibria in cytochrome P450, *Biochemistry 15*, 5399-5406.

238. Sligar, S. G., and Gunsalus, I. C. (1976) A thermodynamic model of regulation: modulation of redox equilibria in camphor monoxygenase, *Proc Natl Acad Sci U S A 73*, 1078-1082.

239. Fisher, M. T., and Sligar, S. G. (1985) Control of heme protein redox potential and reduction rate: linear free energy relation between potential and ferric spin state equilibrium, *Journal of the American Chemical Society 107*, 5018-5019.

240. Das, A., Grinkova, Y. V., and Sligar, S. G. (2007) Redox potential control by drug binding to cytochrome P450 3A4, *J Am Chem Soc 129*, 13778-13779.

241. Roberts, A. G., and Atkins, W. M. (2007) Energetics of heterotropic cooperativity between alpha-naphthoflavone and testosterone binding to CYP3A4, *Arch Biochem Biophys 463*, 89-101.

242. Nath, A., Atkins, W. M., and Sligar, S. G. (2007) Applications of phospholipid bilayer nanodiscs in the study of membranes and membrane proteins, *Biochemistry 46*, 2059-2069.

243. Nath, A., Koo, P. K., Rhoades, E., and Atkins, W. M. (2008) Allosteric effects on substrate dissociation from cytochrome P450 3A4 in nanodiscs observed by ensemble and single-molecule fluorescence spectroscopy, *J Am Chem Soc 130*, 15746-15747.

244. Boek-Dohalská, L., Hodek, P., Sulc, M., and Stiborová, M. (2001) [alpha]-Naphthoflavone acts as activator and reversible or irreversible inhibitor of rabbit microsomal CYP3A6, *Chemico-Biological Interactions 138*, 85-106.

245. Domanski, T. L., He, Y. A., Khan, K. K., Roussel, F., Wang, Q., and Halpert, J. R. (2001) Phenylalanine and tryptophan scanning mutagenesis of CYP3A4 substrate recognition site residues and effect on substrate oxidation and cooperativity, *Biochemistry 40*, 10150-10160.

246. Denisov, I. G., Frank, D. J., and Sligar, S. G. (2009) Cooperative properties of cytochromes P450, *Pharmacol. Ther. 124*, 151-167.

247. Greco, W. R., Bravo, G., and Parsons, J. C. (1995) The search for synergy: a critical review from a response surface perspective, *Pharmacol Rev 47*, 331-385.

248. Berenbaum, M. C. (1985) The expected effect of a combination of agents: the general solution, *J Theor Biol 114*, 413-431.

249. Kapust, R. B., Tözsér, J., Copeland, T. D., and Waugh, D. S. (2002) The P1' specificity of tobacco etch virus protease, *Biochemical and Biophysical Research Communications 294*, 949-955.

250. Heap, R. B., Symons, A. M., and Watkins, J. C. (1970) Steroids and their interactions with phospholipids: Solubility, distribution coefficient and effect on potassium permeability of liposomes, *Biochim. Biophys. Acta 218*, 482-495.

251. Makris, T. M., Denisov, I. G., Schlichting, I., and Sligar, S. G. (2005) Activation of Molecular Oxygen by Cytochrome P450, In *Cytochrome P450: Structure, Mechanism, Biochemistry* (Ortiz de Montellano, P. R., Ed.) 3rd ed., pp 149-182, Kluwer Academic, New York.

252. Grinkova, Y. V., Denisov, I. G., and Sligar, S. G. (2010) Functional reconstitution of monomeric CYP3A4 with multiple cytochrome P450 reductase molecules in Nanodiscs, *Biochem Biophys Res Commun 398*, 194-198.

253. Shen, A. L., Porter, T. D., Wilson, T. E., and Kasper, C. B. (1989) Structural analysis of the FMN binding domain of NADPH-cytochrome P-450 oxidoreductase by site-directed mutagenesis, *J Biol Chem 264*, 7584-7589.

254. Porter, T. D., Wilson, T. E., and Kasper, C. B. (1987) Expression of a functional 78,000 dalton mammalian flavoprotein, NADPH-cytochrome P-450 oxidoreductase, in Escherichia coli, *Archives of Biochemistry and Biophysics 254*, 353-367.

255. Yasukochi, Y., and Masters, B. S. (1976) Some properties of a detergent-solubilized NADPH-cytochrome c(cytochrome P-450) reductase purified by biospecific affinity chromatography, *J. Biol. Chem. 251*, 5337-5344.

256. Davydov, D. R., Fernando, H., and Halpert, J. R. (2006) Variable path length and counter-flow continuous variation methods for the study of the formation of high-affinity complexes by absorbance spectroscopy. An application to the studies of substrate binding in cytochrome P450, *Biophys Chem 123*, 95-101.

257. Borek-Dohalska, L., and Stiborova, M. (2010) Cytochrome P450 3A activities can their modulation by alpha-naphthoflavone in vitro are dictated by the efficiencies of model experimental systems, *Collect Czech Chem C 75*, 201-220.

258. Straume, M., and Johnson, M. L. (1992) Monte Carlo method for determining complete confidence probability distributions of estimated model parameters, *Methods Enzymol. 210*, 117-129.

259. Tellinghuisen, J. (2009) The least-squares analysis of data from binding and enzyme kinetics studies weights, bias, and confidence intervals in usual and unusual situations, *Methods Enzymol. 467*, 499-529.

260. van Meer, G., Voelker, D. R., and Feigenson, G. W. (2008) Membrane lipids: where they are and how they behave, *Nat Rev Mol Cell Biol 9*, 112-124.

261. Kim, K. H., Ahn, T., and Yun, C. H. (2003) Membrane properties induced by anionic phospholipids and phosphatidylethanolamine are critical for the membrane binding and catalytic activity of human cytochrome P450 3A4, *Biochemistry 42*, 15377-15387.

262. Ingelman-Sundberg, M., Hagbjork, A. L., Ueng, Y. F., Yamazaki, H., and Guengerich, F. P. (1996) High rates of substrate hydroxylation by human cytochrome P450 3A4 in reconstituted membranous vesicles: influence of membrane charge, *Biochem Biophys Res Commun 221*, 318-322.

263. Wu, E. S., and Yang, C. S. (1984) Lateral diffusion of cytochrome P-450 in phospholipid bilayers, *Biochemistry 23*, 28-33.

264. Boettcher, J. M., Davis-Harrison, R. L., Clay, M. C., Nieuwkoop, A. J., Ohkubo, Y. Z., Tajkhorshid, E., Morrissey, J. H., and Rienstra, C. M. (2011) Atomic View of Calcium-Induced Clustering of Phosphatidylserine in Mixed Lipid Bilayers, *Biochemistry*.

265. Shaw, A. W., Pureza, V. S., Sligar, S. G., and Morrissey, J. H. (2007) The local phospholipid environment modulates the activation of blood clotting, *J Biol Chem 282*, 6556-6563.

266. Das, A., Zhao, J., Schatz, G. C., Sligar, S. G., and Van Duyne, R. P. (2009) Screening of type I and II drug binding to human cytochrome P450-3A4 in nanodiscs by localized surface plasmon resonance spectroscopy, *Anal Chem 81*, 3754-3759.

AUTHOR'S BIOGRAPHY

Daniel was born June 30, 1981 to Sally and Michael Frank in Milwaukee, WI. At the age of five he moved to Westchester, NY where he later graduated from Mamaroneck High School in 1999. He then attended Johns Hopkins University in Baltimore, MD, earning a Bachelor of Science degree in biomedical engineering, with minors in computer science and mathematical science in 2003. He went on to intern at a mesenchymal stem cell company, Osiris Therapeutics located in Baltimore, MD before taking a job as an immunology laboratory technician under Drs. Anne Davidson and Betty Diamond at the Albert Einstein College of Medicine in the Bronx, NY. In 2005 he moved with them to Columbia University Medical Center in Manhattan, NY and began the post-baccalaureate program at Columbia University. He earned a certificate in the premedical sciences in 2006, and continued on to the University of Illinois at Urbana-Champaign to pursue his Ph.D. in biochemistry in Dr. Stephen Sligar's laboratory. His work under Dr. Sligar has resulted in this thesis. Daniel has accepted a postdoctoral position with Dr. Paul Ortiz de Montellano at the University of California San Francisco, where he plans to continue his research into cytochromes P450.